NASA TECHNICAL MEMORANDUM

NASA TM SX-3444

Joint Program
with U.S. Air Force
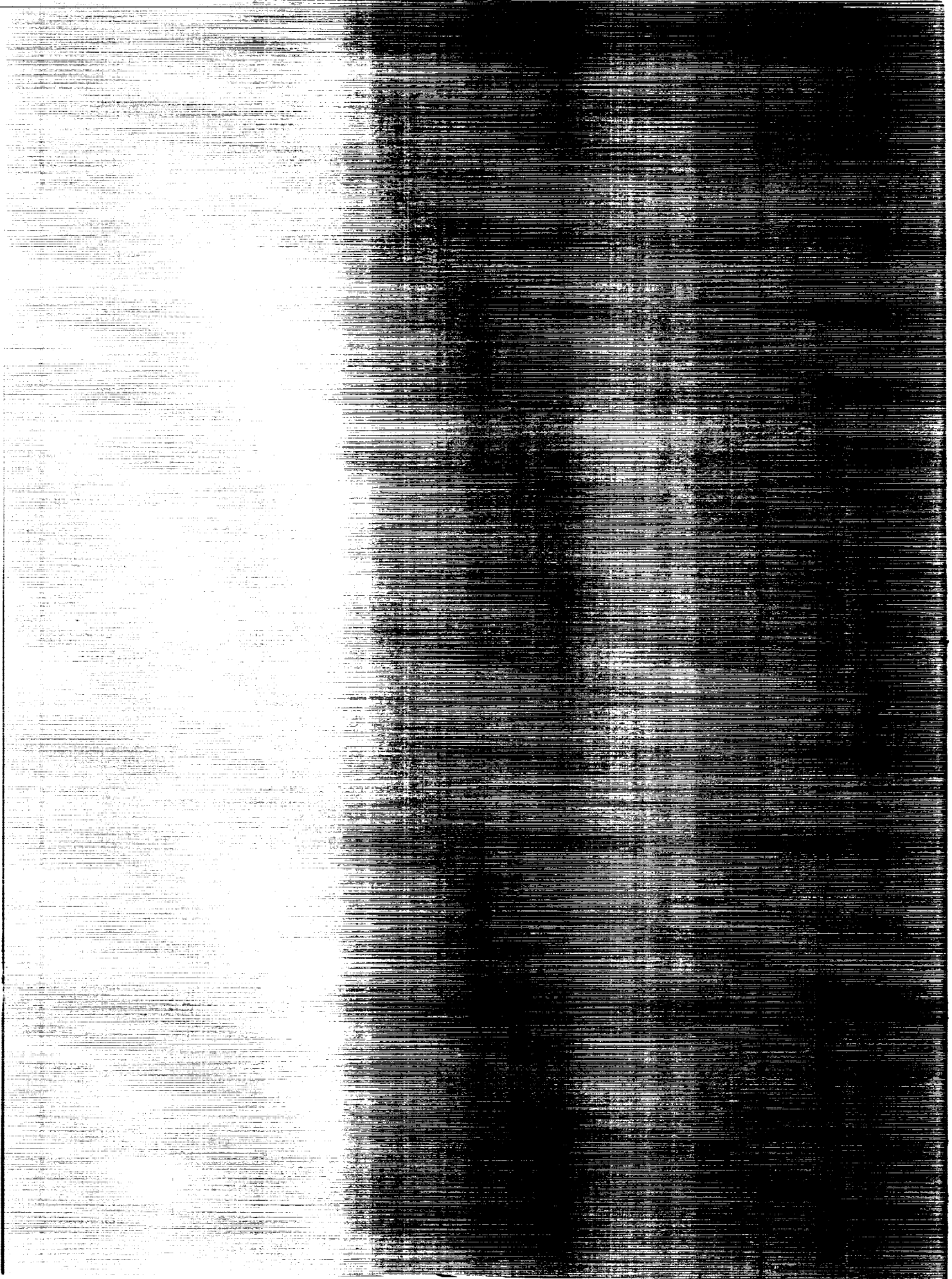
/N-07

3 8/ 3 06

CASE
COPY

EXPERIMENTAL RESULTS AND DATA
FORMAT OF PRELIMINARY FAN FLUTTER
INVESTIGATION USING YF100 ENGINE

by Charles M. Mehalic, Herbert G. Hurrell, John H. Dicus,
Joseph F. Lubomski, Anatole P. Kurkov, and David G. Evans
Lewis Research Center
Cleveland, Ohio 44135

1. Report No. NASA TM SX-3444	2. Government Accession No.	3. Recipient's Catalog No.
4. Title and Subtitle EXPERIMENTAL RESULTS AND DATA FORMAT OF PRELIMINARY FAN FLUTTER INVESTIGATION USING YF100 ENGINE		5. Report Date
		6. Performing Organization Code
7. Author(s) Charles M. Mehalic, Herbert G. Hurrell, John H. Dicus, Joseph F. Lubomski, Anatole P. Kurkov, and David G. Evans		8. Performing Organization Report No. E-8877
		10. Work Unit No. 505-05
9. Performing Organization Name and Address National Aeronautics and Space Administration Lewis Research Center Cleveland, Ohio 44135		11. Contract or Grant No.
		13. Type of Report and Period Covered Technical Memorandum
12. Sponsoring Agency Name and Address National Aeronautics and Space Administration Washington, D.C. 20546		14. Sponsoring Agency Code

15. Supplementary Notes

16. Abstract

A preliminary investigation was conducted to determine the conditions which can cause flutter to occur in the first-stage rotor of the fan of a turbofan engine. Strain gages and stagewise aerodynamic instrumentation were installed in the fan of a YF100 engine. The engine was operated over the low corrected speed range of the fan map, from below its normal operating line to near stall, and over a range of inlet guide vane angles, pressures, and temperatures. Flutter was encountered, and the characteristics of the six flutter points and the associated aerodynamic conditions were recorded. Comparisons with the 97 nonflutter points recorded were made. The data format is presented to assist in future data transmittals and analysis. A companion report, NASA TM X-3508, describes the engine modifications, strain-gage instrumentation, and data acquisition system used in the investigation.

17. Key Words (Suggested by Author(s)) Turbofan engine; Subsonic stall flutter; Compressor performance; Aeroelastic instability	18. Distribution Statement Unclassified - limited. All requests should be referred to the U.S. Air Force, Deputy for F-15/Joint Engine Project Office, ASD/YFJ, Wright-Patterson AFB, Ohio 45433.		
19. Security Classif. (of this report) Unclassified	20. Security Classif. (of this page) Unclassified	21. No. of Pages 99	22. Price*

EXPERIMENTAL RESULTS AND DATA FORMAT OF PRELIMINARY FAN

FLUTTER INVESTIGATION USING YF100 ENGINE*

by Charles M. Mehalic, Herbert G. Hurrell, John H. Dicus, Joseph F. Lubomski, Anatole P. Kurkov, and David G. Evans

Lewis Research Center

SUMMARY

A preliminary investigation of fan flutter was performed by using the YF100 turbofan engine. The investigation was the initial phase of a flutter research program wherein full-scale, advanced turbine engines are to be used as the research facilities. The preliminary phase had two objectives: (1) to establish testing techniques consistent with both research goals and engine safety and (2) to define generally, for later investigation, the operating conditions associated with fan flutter in the YF100 engine. The results of this preliminary phase, along with a description of the data format to assist in future data transmittals and analysis, are included in this report. A companion report, NASA TM X-3508 describes the details of the engine modifications, strain-gage instrumentation, and data acquisition system used in the investigation.

The investigation covered a range of subsonic operating points of the fan. Corrected rotor speeds ranged from 62 to 93 percent of design, and fan pressure ratio was varied from 1.2 to 2.7. Fan inlet conditions covered a pressure range of 5.2 to 17.2 newtons per square centimeter (7.5 to 25.0 psia) and a temperature range of 4.4° to 171° C (40° to 340° F). The blade vibratory conditions associated with flutter were monitored and recorded by means of strain gages installed on the fan rotor blades and stators. Aerodynamic information was acquired from overall fan performance and from interstage pressure and temperature measurements.

The two objectives were accomplished. Fan flutter was encountered under certain operating conditions. The test procedures and monitoring techniques employed permitted the safe acquisition of research data under flutter conditions. The flutter encountered was identified as predominantly above-shroud torsion of the first-stage rotor blades. The vibratory frequency varied from 1067 to 1095 hertz for the flutter data acquired. Flutter was observed only when the fan inlet temperature was raised to 171° C (340° F); however, detailed investigation of the temperature effect was deferred to the next test phase. With the inlet temperature at 171° C (340° F), steady-state and high-frequency data measurements were obtained in or near flutter conditions for inlet pressures from 10.3 to 17.2 newtons per square centimeter (15.0 to 25.0 psia).

INTRODUCTION

This report presents the results of a preliminary aeromechanical investigation of the fan flutter characteristics of a typical advanced airbreathing turbofan engine. Flutter is the dynamic aeroelastic instability caused by the interaction of aerodynamic forces and structural deformations (ref. 1). It has become a problem of concern in advanced fan and compressor designs for both commercial and military engines because of the emphasis on improved performance and lighter weight. The resulting combination of high aerodynamic loading and thin, elastic blades provides fertile conditions for flutter, which manifests itself in large vibratory stresses. Advanced design techniques, therefore, must include accurate methods for predicting and correcting conditions causing flutter. Although progress has been made in developing analytical methods for the prediction of certain types of flutter (refs. 2 to 4), the diversity of flutter-inducing conditions which can exist in advanced fans and compressors warrants further research in this problem area.

For this reason, flutter research has become a part of the Full-Scale Engine Research (FSER) program at the Lewis Research Center. This is a cooperative program between the Air Force and NASA, intended to strengthen the technology base for the future development of airbreathing engines. Fan flutter was chosen as the starting point of this program. The large dimensions and good accessibility of fans provide relative ease of instrumentation for both structural and aerodynamic measurements. The F100 Series I engine, referred to in this report as the YF100, was selected to be the research vehicle for the investigation. This is an early prototype model of the current F100 engine, which is an advanced afterburning, twin-spool, turbofan engine. It had exhibited fan first-stage blade flutter under certain fan subsonic operating conditions. The basic goal of the YF100 investigation was to gain increased understanding of this flutter phenomenon through detailed measurements on an engine operating in flutter and nonflutter conditions.

The YF100 flutter program is being conducted in two phases. The first phase was exploratory and had two specific purposes: (1) to gain experience in the monitoring techniques and procedures required for this potentially hazardous mode of engine testing and (2) to locate general flutter regions for later investigation. The second phase is planned to be a more thorough, parametric investigation with increased aerodynamic and structural instrumentation.

The purpose of this report is to present the experimental data obtained in the first phase, including the overall performance and operating characteristics of the engine, fan, and compressor; the fan first-stage performance; and rotor flutter characteristics. Also, the data format is described to assist in future data transmittals and analysis. A companion report (ref. 5) contains information on the engine installation, monitoring

devices, the Phase I instrumentation, the method of strain-gage application, durability of the strain gages, and data acquisition systems.

The Phase I flutter investigation covered a range of the fan subsonic operating points from below the normal operating line to near stall. Corrected speeds ranged from 62 to 93 percent of design. Pressure ratio ranged from 1.2 to 2.7 as a result of the corrected speed changes and exhaust-nozzle area variations. Fan inlet conditions were varied over a range of pressure from 5.2 to 17.2 newtons per square centimeter (7.5 to 25.0 psia) and of temperature from 4.4° to 171° C (40° to 340° F). The airflow direction relative to the first rotor blade, an important flutter consideration, was manipulated by changing the angular setting of the inlet guide vanes. The tests were conducted in the PSL-1 altitude chamber of the Lewis Propulsion Systems Laboratory.

DESCRIPTION OF ENGINE AND INSTALLATION

The YF100 engine used in this investigation was a Series I engine (serial no. FX213-15) retired from the F100 development program. The engine was rebuilt for the flutter program with new or refurbished parts where necessary. It is a twin-spool, high-thrust-weight-ratio, afterburning turbofan engine. The low-pressure rotor has a three-stage fan driven by a two-stage turbine. The high-pressure rotor has a 10-stage compressor driven by a two-stage, high-pressure turbine through a shaft that is concentric and corotating with the fan shaft. The overall fan and compressor total-pressure ratio is nominally 23 to 1, with the nominal fan pressure ratio being 2.8 to 1 for sea-level static standard day conditions. The ratio of fan airflow bypassed around the high-pressure compressor to the airflow entering the compressor is nominally 0.7 to 1 at sea-level static standard day conditions (with both fan and core values corrected to fan inlet conditions). The design corrected speed and the corrected airflow of the fan are 9650 rpm and 98.43 kilograms per second (217.0 lbm/sec), respectively. The corresponding values for the high-pressure compressor are 10 070 rpm and 24.69 kilograms per second (54.44 lbm/sec) (corrected to conditions at the core inlet, station 2.5). It should be noted, however, that the actual corrected speeds and flows at intermediate throttle (maximum nonafterburning) may vary according to engine trim and fan inlet conditions.

The fan has an inlet guide vane assembly with variable angular positioning of the trailing edges of the 21 vanes. Each stage of the fan has a part-span shroud to increase both rotor blade damping and system stiffness and thus avoid resonance and flutter. In the first stage, the shroud is located at midchord at approximately 65 percent span. The first-stage blade is a multiple circular arc series airfoil designed for high-tip-speed operation. The blade thickness-chord ratio is 9 percent at the root, tapering to

3

3 percent at the tip. The chord length is 11.315 centimeters (2.874 in.) at the root and 13.657 centimeters (3.469 in.) at the tip. The hub-tip ratio of the first-stage rotor blade is 0.4, and the aspect ratio is 2.83. The blade span is 41.579 centimeters (20.561 in.) measured from root to tip along the average stacking line. The radius from the fan centerline to the tip of the first-stage blade is 68.374 centimeters (17.367 in.). The material of the 38 first-stage rotor blades is a - 8-percent-aluminum - 1-percent-molybdenum - 1-percent-vanadium alloy. The first-stage stator assembly has 52 vanes. Flow path dimensions for various axial stations in the fan are given in table I.

Manual control systems were provided on the engine for positioning the fan inlet guide vanes and exhaust nozzle. For the flutter investigation, a 100-channel slipring assembly was installed in the bullet nose of the engine, and leadout wires were routed through the stationary leading edges of the inlet guide vanes. A more detailed description of the installation of the slipring assembly and the manual control systems is included in reference 5. An exhaust-nozzle plug to provide areas smaller than obtainable with the standard nozzle was also included in the installation. The plug was 36.8 centimeters (14.5 in.) in diameter and extended upstream of the nozzle primary throat.

The engine was installed in an altitude chamber of the Propulsion Systems Laboratory at the Lewis Research Center. Figure 1 shows the engine installed in the test chamber. A schematic drawing showing the engine installed in the test cell is presented in figure 2(a). The relative locations of the bellmouth and inlet duct, the slipring, and the exhaust-nozzle plug can be seen. Distances from various points in the inlet duct to the engine inlet flange are listed.

INSTRUMENTATION

Aerodynamic

The aerodynamic instrumentation stations and station designations are shown relative to the inlet system and the internal engine components in figure 2(a). The interstage instrumentation installed in each stage of the fan is shown in figure 2(b). Because of blockage considerations, the first- and second-stage fan stator instrumentation was built into the stator leading edges.

The cross-sectional layout of instrumentation at each measuring station is shown in figure 2(c). The temperature probes, which were designed to measure steady-state temperatures only, utilized Chromel-Alumel thermocouples. High-response pressures were measured with closely coupled miniature pressure transducers. The pressure probes were designed to have a frequency response of 500 hertz.

Table I lists all the aerodynamic instrumentation shown in figure 2 and gives detailed information pertaining to each measuring station, such as probe radial positions and rake circumferential locations.

Strain Gages

For the first phase of the YF100 program, the engine had 114 strain gages mounted on the fan rotor and stator blades. There were a total of 90 strain gages installed on the rotor blades, 40 on the first rotor, 28 on the second rotor, and 22 on the third rotor. The remaining 24 strain gages were installed on the stators with 12 being on the first-stage stators and 12 on the second-stage stators. The locations of the strain gages on the blades and the circumferential locations of the blades with strain gages are shown in figure 3. The strain-gage locations on each blade were chosen to give the best possible determination of maximum vibratory stress for any particular mode of vibration known to exist. The manufacturer's shaker bench tests and holography were used to determine the most advantageous positions for locating the strain gages.

The following rotor strain gages (fig. 3(a)) were used:

(1) Tip gages designated as TIP and located at the rotor blade tip between the leading edge and midchord on rotors 1 to 3. These gages were active for any of the above-shroud coupled modes, for torsional modes, and for all tip modes.

(2) ASMT gages located above the shrouds at the maximum chordwise thickness. These gages were installed on all three fan rotors and were most active for above-shroud bending, first coupled, and second coupled modes.

(3) ASTE gages located above the shroud at the trailing edge on rotors 1 and 2. These gages were most active for above-shroud torsion and for the third coupled mode.

(4) SHRD-CC and SHRD-CX gages located on the underside of the shroud adjacent to either the concave (CC) surface or the convex (CX) surface of the airfoil on all three fan rotors. These gages were moderately active for the coupled modes, above-shroud bending, and some of the tip modes.

(5) RMT gages located at the root of the airfoil at the maximum chordwise thickness of all three rotors. These gages were moderately active for the second coupled mode.

(6) FILLET gages located at the fillet of the blade platform and dovetail near the leading edges on the first-stage rotor only. These gages were installed to determine the vibratory stress levels during engine resonances and flutter in the fillet area, which is a high-steady-state-stress location.

(7) D-WEB gages on the web of the fan disks on all three rotors. These gages were installed to determine if the rotor disks were involved in either resonance- or flutter-induced vibrations.

5

The following stator gages (fig. 3(a)) were used:

(1) ODMT gages located at the root at the maximum thickness on the first- and second-stage stators

(2) ODLE gages located at the root at the leading edge on the first-stage stator

(3) ODTE gages located at the root at the trailing edge on the second-stage stator

(4) MSMT gages located at midspan at the maximum thickness on the first- and second-stage stators

The details of the strain-gage application technique and the data acquisition and monitoring system are set forth in reference 5.

DATA FORMAT

Appendix B describes the printout format for the steady-state data (from the Central Automatic Digital Data Encoder (CADDE)) and for the digital transient data, describes the recording format for the analog transient data, and defines the symbols used. (Additional symbols are defined in appendix A.) These formats are described to assist in future data transmittals and analysis.

TEST CONDITIONS AND METHOD OF OPERATION

The initial engine tests were run to determine baseline altitude performance. These tests were carried out before the fan strain gages and slipring assembly were installed. Performance data were obtained at engine inlet Reynolds number indices of 0.42, 0.30, and 0.25 at several points along the normal (part power) operating line. No attempt was made during these tests to obtain data at off-design operating conditions.

For the fan flutter tests, the engine was run at several inlet conditions with pressures ranging from 5.2 to 17.2 newtons per square centimeter (7.5 to 25.0 psia) at temperatures of 4.4° to 171° C (40° to 340° F) over a corrected speed range of 6000 to 9000 rpm (62.2 to 93.3 percent of design corrected speed). A summary of the fan flutter testing is presented in table II. As shown in the table, fan inlet variable vane (CIVV) angles of -25° to 5° and exhaust-nozzle areas of 0.237 to 0.319 square meter (2.55 to 3.43 ft^2), or 89.5 to 120.4 percent of design, were investigated during the course of the testing. The table also indicates the type of instability encountered during the engine tests (rotating stall or flutter, determined by spectral analysis of strain-gage signals).

Three methods of transient engine operation were used to attempt to induce fan flutter: decelerations, CIVV excursions, and exhaust-nozzle area reductions. During

6

each attempt to induce fan flutter, the engine inlet pressure and temperature were held constant. For decelerations, the CIVV angle and exhaust-nozzle area were manually set to constant values during the transient. The tests involving CIVV excursions were carried out with a constant exhaust-nozzle area. Engine speed decreased when the CIVV angles were moved toward the axial or positive angle direction, so throttle movements were used to hold speed constant during these tests. During exhaust-nozzle area reductions the CIVV angles were set to a constant value, and speed was held constant by adjusting the throttle during the transient.

Steady-state data were recorded before the beginning of each transient excursion toward the flutter region. During the transient, high-speed digital and analog data were recorded, and the output of the fan rotor strain gages was simultaneously monitored to detect the onset of flutter. When a predetermined safe dynamic stress level was reached, steady-state data were again recorded. The transient excursion was then reversed to move the engine out of the instability. A log of the steady-state and analog data points recorded during the flutter tests showing the primary engine variables is included in table III. As noted in the table, 3 high-response (analog) and 3 steady-state (CADDE) data points were recorded during fan flutter, 20 analog and 77 CADDE data points were recorded at nonflutter conditions, and 3 analog and 2 CADDE data points were recorded during fan stalls and rotating stalls.

RESULTS

Baseline Performance

The results of the baseline altitude performance tests are presented in figures 4 and 5. Both overall engine and fan and compressor performance are shown for engine inlet Reynolds number indices of 0.42, 0.30, and 0.25, and comparisons are made with the manufacturer's check run results. The check run was carried out on a sea-level stand before the engine was delivered to Lewis.

Overall engine part power operating line pressure ratios and bypass ratios are shown in figures 4(a) and (b). The comparison with the sea-level check run data shows good agreement. Figure 4(c) presents the normal exhaust-nozzle area schedule (without a plug) that was used to obtain the data during both the sea-level check run and the baseline altitude tests.

The operating characteristics of the core compressor are presented in figure 5(a). The nominal operating line shows good agreement between the sea-level check run and the baseline altitude tests. The core compressor variable inlet guide vane and stator (RCVV) schedule is shown in figure 5(b) along with data verifying proper operation of the variable vanes.

7

Data obtained on the normal part power operating line of the fan during the baseline tests are presented in figure 5(c). Also shown is the operating line obtained during the manufacturer's initial check run. The fan variable inlet guide vane (CIVV) schedule is included as figure 5(d). The data from both the check run and the baseline tests indicate the vanes were about 2° outside the normal tolerance band from 92 to 100 percent corrected fan speed. Since the CIVV angles were to be controlled manually during the flutter testing, adjustments were not made to correct the error during the baseline tests.

Flutter Mapping

Previous experience of the engine manufacturer with the YF100 fan was used as a guideline in determining the areas of the fan performance map to be explored in the flutter mapping tests. First-stage rotor blade flutter with a frequency of 800 hertz had been experienced in a fan rig with sea-level ambient fan inlet conditions at a corrected rotor speed of approximately 82 percent design and a CIVV angle setting of -20°. Although this flutter region had been observed very near the surge line, it was thought that higher density inlet conditions or different CIVV settings would bring the region sufficiently close to the normal part power operating line to be reached with small exhaust-nozzle area reductions. Also, fan first-stage rotor blade flutter experienced during engine tests indicated the existence of an 1100 hertz flutter region. This region crossed the normal intermediate power operating line of the fan at a corrected speed of about 70 percent at fan inlet pressures and temperatures simulating a high Mach number flight condition. In these engine tests, fan inlet pressures ranged from less than 13.8 newtons per square centimeter (20.0 psia) to more than 20.7 newtons per square centimeter (30.0 psia), and inlet temperatures varied from approximately 93° C (200° F) to more than 205° C (400° F). There were indications that the size and existence of the 1100-hertz region were influenced by both inlet pressure and temperature; that is, increased pressure or temperature enlarged the flutter region.

Mapping of both the 800- and 1100-hertz regions and the transitional area between the two was an objective of the Lewis tests. It was believed logical to conduct low-temperature runs first and thus avoid subjecting the strain gages to the high temperatures until later in the program. However, no flutter was observed in the runs with low inlet temperatures of 4.4° to 93° C (40° to 200° F). The 800-hertz region was not close enough to the operating line to be reached with the exhaust areas afforded by the engine nozzle. (The nozzle plug had not yet been installed.)

When the inlet temperature was brought to 171° C (340° F), flutter in the 1100-hertz mode was encountered. By this time, however, the strain-gage coverage was at a

8

minimum because of the many hours expended on the low-temperature runs. Therefore, there was no real opportunity to investigate the temperature effect in any detail. Rather, it was deemed advisable to retain the original first-phase plan of making only enough excursions into flutter to locate the general region and conducting further investigations during the second phase of the program.

The specific results of the flutter mapping tests are shown in figure 6. The map shown in figure 6(a) is the manufacturer's design performance map showing fan pressure ratio as a function of corrected flow for various corrected rotor speeds. The indicated surge line is for the normal schedule of CIVV angle settings (fig. 5(c)). Also shown in figure 6(a) are the normal part power and intermediate power operating lines. (In normal operation, the fan operates along the intermediate power operating line as flight Mach number increases.) The cross-hatched area indicates the approximate region of the performance map covered in the search for flutter. The points indicated as flutter points represent steady-state data readings taken when the fan first-stage rotor was either in flutter or on the verge of flutter. They are all points near the boundary of the flutter region for the particular condition of inlet temperature and pressure and CIVV angle setting indicated in the figure.

The excursions in CIVV angle and the rotor decelerations made during the flutter mapping tests are shown in figures 6(b) and (c), respectively, as plots of CIVV angle against corrected speed. Points where flutter, or near-flutter, conditions occurred are also located in these figures; however, except for the 10.3-newton-per-square-centimeter (15.0-psia) inlet condition, the flutter was actually encountered during excursions in exhaust-nozzle area, rather than during excursions in CIVV angle or rotor speed.

Stage Performance

The fan first-stage characteristic curves obtained during the flutter tests are presented in figure 7. The average stage pressure coefficient as a function of flow coefficient is shown in figure 7(a) for fan variable inlet guide vane settings of -25°, -15°, -7.5°, and 5°. For the speeds at which the data were recorded, the normal schedule value of CIVV was -25° (fully cambered position). An increase in the pressure coefficient is noted as the CIVV are moved toward the axial direction (toward stall). At a CIVV angle of 5° there is also a change in slope of the characteristic curve that indicates operation near stall.

Similarly, the fan first-stage temperature coefficient and efficiency are presented in figures 7(b) and (c). The temperature coefficient curves shift with CIVV angle, but the slopes remain negative for all CIVV angles investigated. The efficiency of the fan

first stage (fig. 7(c)) shows high values with the CIVV at -25° (design). The efficiency is greatly reduced for a CIVV angle of 5° (30° from design in the axial direction).

The data obtained during first-stage stall flutter (solid symbols in figs. 7(a) to (c)) do not indicate anything unusual when compared with the flutter-free data. The ratio of the radial variation of stage efficiency during flutter to the efficiency when the stage was flutter-free (ratio of CADDE data point 213 to 210) is shown in figure 7(d). Both points were taken at approximately equal fan corrected operating conditions. In this figure the local efficiency across the stage appears somewhat higher during flutter. The efficiencies were calculated by using local measurements at the first-stage exit and average values at the engine inlet, so that radial variations in the streamline may have influenced the level of the efficiencies used in the ratio. The largest increase in efficiency, approximately 5.5 percent, occurred in the tip region, where, as shown in the section Rotor Dynamic Characteristics, the largest blade excursions occurred during flutter, and thus where the largest unsteady work effects may have been present. This was also the spanwise region of the blading which was most influenced by the tip wall boundary-layer profile entering the engine, as shown at station 2 in figure 7(e). The profile shape shown did not change significantly for the ranges of corrected speeds, corrected air-flows, and inlet Reynolds numbers covered in this test program.

Flutter Correlations

During the search for flutter in the Phase I testing, a considerable amount of the data collected was used for a parametric study of the stability criteria. In this study the data were processed by using a relatively simple method of analysis. In order to obtain the first-stage rotor relative inlet diagram conditions, a simplified radial equilibrium analysis was used. (See appendix C.) Also, changes in blade metal angles due to either centrifugal or pressure loading (required to determine blade incidence angles) were neglected. Thus, it is possible that some of the conclusions reached in this section will be modified when a more complete analysis is performed; however, the results should be useful as a guide for future testing.

Most flutter boundary correlations are based on the relation between the reduced frequency k (or, alternatively, the reduced velocity) and the incidence angle. However, since the data were obtained for only one flutter region, and since blade deformations were neglected, these parameters were replaced by the relative velocity W and the relative inlet air angle β for the present study. In addition to W and β, temperature and pressure were included in the parametric investigation. The temperature in combination with W determines the relative inlet Mach number and in combination with P the density. The relative inlet Mach number is always an important cascade performance parameter, whereas the density dependence is expected only whenever the mechan-

10

ical damping is nonzero (ref. 2). It is noted that W, P, and T also fix the inlet Reynolds number, so that no other variable need be considered to describe the Reynolds number dependence. The experimental results presented in this section demonstrate that these four variables are indeed necessary for the description of the flutter boundary.

Figure 8 illustrates the positions on the fan map of the data points included in the parametric study. Also indicated are the approximate CIVV angles and temperature levels. The flutter condition is identified by tailed symbols. The fan map was supplied by the manufacturer and applies for the design CIVV setting of -25°. Consequently, the stall line and the speed lines are not applicable for the points with the off-design CIVV angles. Rotating stall was detected during the recording of CADDE point 195 and might have affected its position on the fan map (its corrected flow is lower than expected). During the recording of point 199, the engine stalled; however, no rotating stall was detected in the fan during the recording.

Figure 8(b) presents the relative inlet velocities and air angles. Also indicated are the approximate pressure and temperature for each data point. The relative velocities and inlet air angles were computed at 85 percent blade span, a point considered representative of the flow conditions midway between the damper and tip shroud. These variables are not sufficient to define the flutter boundary. For example, the inlet air angle is lower (corresponds to a higher incidence), and the relative velocity is higher for point 171 than for flutter points 212, 213, and 215. Since the pressures for points 171 and 212 are the same, the addition of P to W and β to separate the flutter from the nonflutter points is not sufficient, and the effect of temperature must be considered. The temperature for point 171 was lower than that for point 212. On the other hand, if values of W, β, and T for points 210 and 213 are considered, it may be seen that P cannot be left out, since otherwise point 210 would correspond to flutter. There are also other pairs of points which could have been selected to illustrate the necessity of including P and T.

Relative inlet Mach numbers for the same set of data points are presented in figure 8(c). Flutter occurs at the relatively lower Mach numbers. However, the importance of the relative velocity for the definition of the flutter boundary may be seen by comparing points 175 and 215 in figures 8(b) and (c). The absence of flutter for point 175 is attributed to the lower relative velocity for this point.

Considering the amount of flutter data and the spread in the engine inlet conditions for the flutter points recorded, prediction of the location of the stability boundaries in figure 8(b) is probably not warranted at this time. However, it is clear that the flutter boundary corresponding to $P_{T,2} = 14$ newtons per square centimeter (20 psia) and $T_{T,2} = 171^O$ C (340° F) should pass somewhat below points 215 and 213. Since point 207 was close to flutter (A_8 at flutter onset was within 5 percent of A_8 for point 207), the $P_{T,2} = 17$ newtons per square centimeter (25 psia), $T_{T,2} = 171^O$ C (340° F)

boundary should be somewhat to the left of or above points 207 and 208. The peak vibratory stresses at the flutter frequency for CADDE points 213, 212, and 215 for strain gage 117 (ASTE) were approximately 4, 5, and 6 kilonewtons per square centimeter (5.8, 7.1, and 8.7 ksi), respectively.

Rotor Dynamic Characteristics

The vibratory modes of the fan first-stage rotor blades are shown in the Campbell diagram in figure 9. This diagram was constructed from data supplied by the manufacturer's bench tests, which used a shaker and holography on the blades alone supplemented by holography on the fully assembled rotor, and from the Lewis engine test data. Strain-gage data were also obtained on the other fan rotor and stator rows; however, no dynamic activity was found over the range of inlet and engine operating conditions covered.

The portion of the blade of interest is the area above the shroud. From blade-alone bench tests at room temperature and zero speed, the first mode observed was the first normal mode, or first bending, which occurs at or near 405 hertz. The second mode observed was the first torsion at or near 1098 hertz, and the third mode observed was a coupling between first torsion and second bending at about 1316 hertz. A coupled mode between first bending and first torsion could also be anticipated, although it did not show up in the blade bench tests or holographs. Holography of the full assembled rotor showed a coupling of first bending and first torsion at about 756 hertz, and some engine order excitations were observed during the test program at frequencies between 800 and 900 hertz. Thus, it is assumed that in this rotor assembly the blade coupled mode between the first bending and first torsion can be excited, and it is included in the Campbell diagram.

Flutter data were obtained rather late in the program; thus, the number of active strain gages was limited because of strain-gage mortality (ref. 5). During analog data points 49 and 50 (table III) rotating stall was recorded in the first-stage rotor at an inlet temperature of 4.4° C (40° F), an inlet pressure of 17.2 newtons per square centimeter (25.0 psia), and a fan mechanical speed of approximately 7600 rpm. The rotating stall occurred during a CIVV excursion from -15° to 4°. Figure 10 shows a high-speed oscillograph trace of six first-stage rotor strain gages during rotating stall (fig. 10(a)) and flutter (fig. 10(b) to (d)). Figures 11(a) to (c) illustrate the frequency spectrum of several of these strain gages recorded during the rotating stall. Figures 11(a) and (c) show that the rotating stall cell appears at a frequency of 45 hertz (36 percent of fan rotor speed). The ASMT gage (fig. 10(a)) shows this rather clearly and also shows a strong first bending mode around 450 hertz. The first bending condition is plotted in the Campbell diagram (fig. 9).

12

When the noise spikes from several magnetic speed pickups are ignored, the tip gage traces in figure 10(a) indicate a frequency component around 2700 hertz. This is due to a 21E excitation tip mode being generated by rotor blades passing the 21 CIVV vanes. This mode was the most common engine order resonance observed throughout the test program. The spectrum plot of the tip gage, figure 11(c), which indicates a sizable component of the rotating stall cell at 45 hertz, also shows a component between 850 and 900 hertz. This component may be a 7E excitation of the first bending and first torsion coupled mode noted previously in figure 9, or it may be interference from the speed pickup signal, since it was dependent on speed. It was independent of the stall cell because it was present before the stall cell was encountered (fig. 11(b)) but did not show up on any other gages in any measurable quantity.

The ASTE gages were the least active gages observed during rotating stall. Figure 11(a) shows that only a moderate excitation at 45 hertz and a trace of excitation at 450 hertz were present. A data point (analog reading 52) was also taken at a lower speed with the same inlet conditions as used when rotating stall was encountered. In this run at a speed near 6600 rpm, a CIVV excursion was made by starting at 0° and going to a positive angle. At a CIVV angle of 1.4° stall (surge) occurred. No evidence of rotating stall or of any aeroelastic instability was observed.

Stall flutter data were recorded during analog data points 53, 54, and 56. For these points the inlet temperature was 171° C (340° F) and the inlet pressures were 17.2, 13.8, and 10.3 newtons per square centimeter (25.0, 20.0, and 15.0 psia), respectively. For data points 53 and 54 the CIVV angle was set at -15°, and stall flutter was induced by closing down the exhaust-nozzle area. For data point 56 closing down the exhaust-nozzle area was insufficient to induce flutter, and it was necessary to open the CIVV angle to increase the rotor incidence angle to induce flutter. In a CIVV excursion from -15° to -7.5° stall flutter was obtained, but the oscillation fluctuated between a stable condition and an unstable condition. There was a beat frequency present of about 4.5 hertz. The three flutter points are shown plotted in figure 9. The frequencies were nonintegral order (between 7E and 8E), as would be expected for flutter.

Oscillograph traces of the strain-gage signals recorded during the flutter runs are shown in figures 10(b) to (d). The data shown in figure 10(b) were obtained during analog data point 53, and the data in figure 10(c) during point 54. Both of these traces were obtained at a paper speed of 406.4 centimeters per second (160 in./sec). These traces are similar; however, the amplitude of point 53 is slightly higher. The ASTE gages, notably strain gage 117, were the most active, and the ASMT gages the least active. Some amplitude modulation was observed. No frequency modulation was observed. The predominant frequency of the oscillations recorded during point 53 was about 1067 hertz, while for point 54 the principal frequency was 1080 hertz. This is shown in the spectrum plots in figures 11(d) to (r). Figure 10(d) is a slow speed oscillograph trace of some of

the data obtained during point 56. The feature to note in this data is the beat type oscillation of strain gage 117 (ASTE). As noted previously, the beat frequency was between 4.5 and 5 hertz, while the principal frequency of the flutter instability was about 1095 hertz.

In table IV the results from spectrum plots 11(d) to (r) are listed as well as the blade second mode (above-shroud) torsional natural frequencies obtained during bench testing on the rotor blades prior to engine buildup. Also shown is the ratio of vibratory stress to maximum vibratory stress on the blade in slot 16 where all three of the above-shroud strain gages were still active. In addition, this same stress ratio for blade above-shroud torsion obtained during the bench testing is also shown. From the table several conditions can be noted. The frequencies of the two data points are consistent. Note also that the flutter frequency of analog data point 53 and the blade bench test torsional frequency were nearly coincident. For any one blade the stress was highest at the ASTE strain gage, lower at the TIP strain gage, and lowest at the ASMT strain gage. From the stress ratio results it may be inferred that the blade in slot 20 had the highest stress of those observed. No conclusion could be drawn between the stress ratios obtained in bench testing and those for points 53 and 54.

From the data shown in table IV, it is possible to determine the approximate mode shape of the aeroelastic oscillations on the fan first-stage rotor blade in slot 16. This determination is limited to the portion of the blade above the shroud and is shown in figure 12(a). The strain-gage data indicate that the node line starts at the blade tip, either at midchord or between the leading edge and the midchord. The node runs down the span and then moves toward and terminates at the trailing edge near the part-span shroud. Referring back to the Campbell diagram for this rotor, figure 9, for the range of frequencies observed and noted in table IV, one would assume that the portion of the blade above the shroud was oscillating in the second mode (above-shroud torsion), although the node line constructed from the data is more indicative of a coupled mode. Figure 12(b) shows a time-averaged holograph taken during the bench tests of the rotor assembly at a frequency of 1077 hertz with an exciting force of 22.24 newtons (5.00 lb). From these data, it is apparent that the majority of the above-shroud portions of the blades were oscillating in the second or torsional mode, although there is some evidence of coupled modes. However, it is assumed that the principal mode of oscillations observed during flutter testing was the second or torsional mode.

Figure 13 shows a plot of the principal frequency of the unstable flutter oscillations as a function of inlet pressure for analog data points 53, 54, and 56. The frequency decreases linearly as the pressure increases. This frequency shift with pressure results from the aerodynamic contribution to the instability. With increasing pressure, the destabilizing effect of the aerodynamics should be greater at a given frequency and result in the instability occurring at lower frequencies (even with a constant structural natural frequency).

14

Table V shows the results of a further analysis of these three flutter data points to determine the interblade phase angles. These results were obtained by using the analog data recorded on the Central Analog Facility (ref. 5) and a fast Fourier transformer (FFT) Digital Signal Analyzer. The FFT was made from 16 averages from which the transfer function, magnitude, and phase and the coherence function were obtained. The flutter frequencies obtained in this analysis were within 1 percent of the values shown in table IV, which were obtained with the on-line data reduction equipment during flutter testing. The phase angles obtained were those between strain gage 103 (TIP, slot 16) and strain gage 104 (TIP, slot 20) and between strain gage 116 (ASTE, slot 16) and strain gage 117 (ASTE, slot 19). For analog data point 53, the results obtained indicate that the interblade phase angle was of the order of -19.25° to -19.33°. This angle was for an inlet pressure of 17.2 newtons per square centimeter (25.0 psia). Analog data point 54 was obtained at an inlet pressure of 13.8 newtons per square centimeter (20.0 psia), and for this point the interblade phase angle had been reduced to -16°. For the data reduced from points 53 and 54 the coherence function had a value ranging from 0.99 to 0.995. This indicates that the interblade phase angle was remaining constant within each data point. For these two points the motion of the blade in slot 16 (fig. 3(b)) was leading the motion of the blades in slots 19 and 20. In other words, the interblade phase angle indicated a trailing relation between successive blades in the direction of rotation (clockwise looking upstream). For analog point 56 with an inlet pressure of 10.3 newtons per square centimeter (15.0 psia) this was not the case. For this point the blade in slot 16 was trailing the motion of the other two blades with an interblade phase angle varying from 36° to 45°. The value of the coherence function for this point varied from 0.70 to 0.89, which indicated that the angle was varying. This behavior supports the previous interpretation of the data, that there was fluctuation between a stable and an unstable condition.

The four strain gages used in this analysis were the only meaningful active gages available. Thus, the analysis and results are limited and, as such, insufficient for forming any firm conclusions. The trends observed, however, were anticipated. It was anticipated that an interblade phase angle would be such that the angle would conform to the relation $\beta_I = 2\pi I/\eta$, where I is an integer of value 1 or greater. This relation can be deduced from a strictly geometric argument. Lane in reference 6 shows the applicability of this relation in determining the mode shape in the linear rotor flutter problem and has also implied the validity of it in the nonlinear problem. The results shown in table V indicate that for analog data point 53 the relation is valid with the value of I being 2.

For data point 54 the inlet pressure was reduced, and as a result the interblade phase angle also, as noted previously. The facts that the value for the phase angle was obtained from three blades and four strain gages, that the stress levels of these gages

were high, that the values obtained coincided well, and that the coherence was nearly unity indicate that the results obtained are valid. Therefore, the geometry requirements (I = 2) for this data point would indicate that some of the blades in the blade row may have been fluttering at larger interblade phase angles or were not involved in the instability.

SUMMARY OF RESULTS

A preliminary investigation was conducted to determine the operating conditions and aeromechanical relations required to cause subsonic stall flutter in the fan first-stage rotor of the YF100 engine. The following results were obtained:

1. Tests covering the baseline performance of the engine, fan, and compressor and the preliminary investigation of flutter in the fan were completed and documented. During fan flutter 3 high-response and 3 steady-state data points were recorded, during nonflutter conditions 20 and 77 data points, respectively, and during conditions of fan stall and rotating stall 3 and 2 data points, respectively.

2. Flutter could only be induced at the highest inlet temperature investigated, 171° C (340° F), at inlet pressures of 10.3 newtons per square centimeter (15.0 psia) and above, at corrected fan speeds from 64 to 75 percent design, and at inlet guide vane camber angles less than normal. Flutter was encountered with the fan on or near the normal operating line.

3. Flutter frequencies were nonintegral order (between 7E and 8E, where E is the dimensionless ratio of vibratory frequency to rotor speed) and ranged in frequency from approximately 1067 to 1095 hertz. The flutter had the characteristics of being an above-shroud first torsion mode. Engine order excitations of the rotor blading at 21E and 7E were also observed, the latter occurring at between 800 and 900 hertz as a coupled first bending and first torsional mode.

4. The interblade phase angle relation between successive blades in the direction of rotor rotation during flutter changed from a leading phase angle of approximately 40° at an inlet pressure of 10.3 newtons per square centimeter (15.0 psia) to a trailing phase angle of approximately 16° and 19.5° as inlet pressure was increased to 13.8 and 17.2 newtons per square centimeter (20.0 and 25.0 psia), respectively.

5. The performance of the fan as a whole and the fan first stage was unaffected by flutter. However, the local efficiency across the tip region of the first stage increased approximately 5.5 percent during flutter.

6. Correlation of the steady-state data points taken during and near flutter demonstrated that in addition to reduced velocity and flow angle, parameters such as inlet pressure and temperature are required to define the flutter condition. Inclusion of

16

these parameters, however, was not sufficient to predict the exact location of the flutter boundaries for the simplified correlations presented in this report.

Lewis Research Center,
    National Aeronautics and Space Administration,
        Cleveland, Ohio, October 14, 1976,
            505-05.

APPENDIX A

SYMBOLS

A   area

a   speed of sound

b   one-half of blade chord

CIVV   fan variable inlet guide vane setting (negative angle denotes preswirl conditions)

E   dimensionless ratio of vibratory frequency to rotor speed

FTIT   fan turbine inlet temperature

g   acceleration due to gravity

I   integer

k   reduced frequency, $\omega b/W$

M   Mach number

N   rotative speed

n   number of blades in row

P   pressure

R   gas constant

RCVV   setting of compressor variable inlet guide vanes and first two stator rows (negative angle denotes preswirl conditions)

RNI   Reynolds number index, $\delta/\varphi\sqrt{\theta}$

T   temperature

u   absolute viscosity

W   relative flow velocity

w   mass flow

β relative flow angle from tangential

β_I interblade phase angle

γ ratio of specific heats

δ $P_T/P_{T,SL}$

η adiabatic efficiency

18

θ	$T_T/T_{T,SL}$
σ	vibratory stress amplitude
Φ, FC	flow coefficient, axial velocity/tip velocity
φ	u/u_{SL}
ψp, PC	pressure coefficient, ideal enthalpy change/(tip velocity)^2
ψT, TC	temperature coefficient, ψp/η
ω	flutter frequency

Subscripts:

a	air
b	bypass duct
c	core compressor
F	fan or fan duct
m	mixed (fan and core stream combined)
r	ratio
S	static
SL	standard sea-level conditions
T	total
1	fan airflow measuring station (see fig. 2(c))
2	engine inlet (13.7 cm (5.4 in.) upstream of engine front flange)
2.05	fan first-stage rotor inlet
2.1	fan first-stage stator inlet
2.5	compressor inlet
3	compressor exit
4.5	fan turbine inlet
8	primary nozzle throat

Superscript:

$(\overline{})$	station average

APPENDIX B

DATA FORMATS

A sample computer printout for the steady-state (CADDE) data is shown in table VI. The printout consists of option 1 and options 3 to 7. Questionable values are followed by an H on the printouts. The engineering parameters displayed in option 1 are defined in table VII. The headings used in the remaining options are defined as follows:

Option 3 - general performance parameters:

TO	total temperature at bellmouth inlet, ^{O}R
PT2	total pressure at engine inlet, psia
C2WA2	engine inlet mass flow corrected to engine inlet conditions, lbm/sec
WA2	engine inlet mass flow, a numerical integration at station 1, lbm/sec
C2.5W2.5	core mass flow corrected to core inlet conditions, lbm/sec
WA2.5	core mass flow, lbm/sec
PCN1	corrected fan speed, percent of design (9650 rpm)
PCN2	corrected core speed, percent of design (10 070 rpm)
PC2WA2	corrected fan mass flow, percent of design (217 lbm/sec)
PC2.5W2.5	corrected compressor mass flow measured at station 2.5, percent of design (54.44 lbm/sec)
EPR	engine pressure ratio, PT6M/PT2
ETR	engine temperature ratio, T6M/T2
BPR	bypass ratio, ratio of fan duct mass flow to core mass flow, based on energy balance
C2N1	fan speed corrected to engine inlet conditions, rpm
C2.5N2	core speed corrected to core inlet conditions, rpm
N1	fan speed, rpm
N2	core speed, rpm
T4.5	rake measured total temperature at fan turbine inlet, ^{O}R
C2T4.5	T4.5 corrected to engine inlet conditions, $T4.5/\theta 2$, ^{O}R
C2T4	T4 corrected to engine inlet conditions, $T4/\theta 2$, ^{O}R

FTIT, R	harness measured fan turbine inlet temperature, ^{O}R
C2FTIT, R	FTIT corrected to engine inlet conditions, ^{O}R
PT3	total pressure at core compressor discharge, psia
T3	total temperature at core compressor discharge, psia
FTIT, F	harness measured fan turbine inlet temperature, ^{O}F
C2FTIT, F	FTIT corrected to engine inlet conditions, ^{O}F
RCVV	angle of variable vanes at entrance to core compressor (rear compressor variable vanes) (negative angle denotes preswirl), deg
CIVV	angle of fan inlet variable vanes (compressor inlet variable vanes) (negative angle denotes preswirl), deg
PLA	power lever angle, deg
A8	nozzle throat area, ft^2
WFE	engine fuel flow, lbm/hr
C2WFE	WFE corrected to engine inlet conditions, $WFE\sqrt{\theta 2}/\delta 2$
PT2.5M/PT2	ratio of mixed (mass flow weighted) fan exit total pressure to engine inlet total pressure
PT3/PT2.5	ratio of core compressor discharge total pressure to core compressor inlet total pressure
TTC-5	turbine cooling chamber 5 measured temperature, ^{O}F
TCO5	turbine cooling chamber 5 allowable temperature, ^{O}F
TOL	tolerance on allowable temperature
TTC-11	turbine cooling chamber 11 measured temperature, ^{O}F
TC11	turbine cooling chamber 11 allowable temperature, ^{O}F
TTC-22	turbine cooling chamber 22 measured temperature, ^{O}F
TC22	turbine cooling chamber 22 allowable temperature, ^{O}F
TTC-90	turbine cooling chamber 90 measured temperature, ^{O}F
TC90	turbine cooling chamber 90 allowable temperature, ^{O}F
PSTC-5	turbine cooling chamber 5 measured pressure, psia
PCO5	turbine cooling chamber 5 allowable pressure, psia
PSTC-11	turbine cooling chamber 11 measured pressure, psia
PC11	turbine cooling chamber 11 allowable pressure, psia

PSTC-22	turbine cooling chamber 22 measured pressure, psia
PS22	turbine cooling chamber 22 allowable pressure, psia
PSTC-90	turbine cooling chamber 90 measured pressure, psia
PB	burner pressure, psia
PSBR	burner exit static pressure, psia

Option 4 - energy balance parameters:

T4	turbine inlet temperature, $^{\circ}$R
WA2.5	core airflow, lbm/sec
DELPB	combustor delta P, psi
WG4	combustor exit gas flow (air and fuel), lbm/sec
WA4	combustor exit airflow, lbm/sec
FAE	combustor fuel-air ratio, WFE/WA4

Option 5 - measured total pressure, static pressure, and total temperature at each engine instrumentation station:

PT	total pressure
PS	static pressure
T	total temperature
L, R, M	left side, right side (looking upstream), mixed
F	fan duct

Option 6 - flow properties at various engine instrumentation stations:

GAMMA	ratio of specific heats
H	specific enthalpy, Btu/lbm
M	Mach number
DELTA	ratio of total pressure to sea-level standard pressure
THETA	ratio of total temperature to sea-level standard temperature
RNI	Reynolds number index
F/A	fuel-air ratio

Option 7 - stage and stage group performance parameters:

I	station number of stage or stage group entrance
J	station number of stage or stage group exit
PT(J)/PT(I)	pressure ratio across stage or stage group
T(J)/T(I)	temperature ratio across stage or stage group
ETA(I-J)	stage or stage group isentropic efficiency
TC(I-J)	temperature coefficient for stage or stage group
PC(I-J)	pressure coefficient for stage or stage group
FC(I-J)	flow coefficient for stage or stage group

A portion of a sample computer printout for the digital transient data is shown in table VIII. The lineup consists of 200 channels and the relation between channel number and instrumentation identification is shown in table IX. The time interval between successive samples of a given channel is 42 milliseconds. Pressures listed are in psia and temperatures listed are in ^{O}R.

Transient data were also recorded in analog format on a 180-channel multiplexed magnetic-tape system. A 14-channel FM tape handler running at 304.8 centimeters per second (120 in./sec) recorded data onto 12 of the tracks (tracks 1 to 6 and 8 to 13), while a separate track (track 7) was used to record time. Fifteen signals were frequency multiplexed onto each of the 12 data tracks to give the 180-channel recording capability. Each channel had an input filter with an 8-kilohertz bandwidth, and the transmission lines from the test cell to the central recording facility were limited to an 8-kilohertz transmission capability. Table X shows specifications for each of the 15 channels multiplexed onto each track.

The analog data lineup, table XI, shows the strain gages used and the high-response pressures recorded on the analog tape.

APPENDIX C

CALCULATION PROCEDURE

The efficiency of a fan or compressor stage or stage group ETA(η) is given by

$$ETA = \frac{H_{j,is} - H_i}{H_j - H_i}$$

where

$H_{j,is}$ specific enthalpy at exit of stage or stage group if compression process is isentropic, Btu/lbm

H_i specific enthalpy at entrance to stage or stage group, Btu/lbm

H_j specific enthalpy at exit of stage or stage group, Btu/lbm

The value of $H_{j,is}$ is calculated from $T_{j,is}$, which is the stage or stage group isentropic exit temperature; $T_{j,is}$ is based on the equation

$$\left(\frac{P_j}{P_i}\right)^{(\gamma_u - 1)/\gamma_u} = \frac{T_{j,is}}{T_i}$$

where γ_u is an effective γ.

The temperature coefficient for a fan or compressor stage or stage group TC(ψ_T) is given by

$$TC = \frac{C_p \Delta T}{U^2} = \frac{\Delta h}{U^2}$$

where

C_p specific heat at constant pressure; $C_p = (\gamma_u/\gamma_u - 1)R$, where R is the gas constant and γ_u the effective γ

ΔT total temperature rise across stage or stage group

U tip velocity of trailing edge of last rotor blade in stage group

24

The pressure coefficient for a fan or compressor stage or stage group $PC(\psi_p)$ is calculated from

$$PC = ETA \times TC$$

The flow coefficient for a fan or compressor stage or stage group $FC(\varphi)$ is given by

$$FC = \frac{V_Z}{U}$$

where

V_Z axial velocity at entrance to stage or stage group

U tip velocity of leading edge of first rotor blade in stage group

The Reynolds number index RNI is the ratio of Reynolds number at a specific test condition to the Reynolds number at sea-level conditions; RNI is calculated from the equation

$$RNI = \frac{\delta(T + S)}{\theta^2(T_{SLS} + S)}$$

where

δ ratio of total pressure to sea-level standard pressure

T total temperature

S Sutherland constant, 110. 4 K (198. 72° R)

θ ratio of total temperature to sea-level standard temperature

T_{SLS} sea-level static standard temperature

The equations and method of analysis employed to determine the rotor inlet relative flow angle, relative velocity, and relative Mach number of each CADDE (steady-state) data point presented in figure 8 are as follows: The governing radial equilibrium equations were taken from reference 7; they are included here for completeness:

$$\left(\frac{V_Z}{V_{Z,i}}\right)_{2.05} = \left(\frac{\sin \alpha}{\sin \alpha_i}\right)_{2.05} \exp\left[-\int_{r_i}^{r}\left(\frac{\cos^2\alpha}{r}\right)_{2.05} dr\right]$$

$$\dot{W}_A = 2\pi\rho_{T,2} \int_{r_h+\delta_h^*}^{r_t-\delta_t^*} \frac{\rho_{S,2.05}}{\rho_{T2}} V_{Z,2.05} \, r dr$$

$$\frac{\rho_{S,2.05}}{\rho_{T,2}} = \left[1 - \frac{\gamma-1}{2} \left(\frac{V_{2.05}}{a_{T,2}} \right)^2 \right]^{1/(\gamma-1)}$$

$$V_{Z,2.05} = V_{2.05} \sin \alpha$$

where

V_Z axial velocity

α absolute air angle relative to plane of rotor

r radius

$\dot{W}_A$ mass flow rate at station 1

ρ density

V velocity

a speed of sound

γ ratio of specific heats

Subscripts:

2.05   station 2.05 (first-stage rotor inlet)

i   reference condition taken at blade midspan

T   stagnation condition

2   station 2 (engine inlet)

S   static

The values for $\alpha(r)$ were determined from the data supplied by the manufacturer and the CIVV position. The other quantities were known, since it was assumed that there was no total-pressure loss across the inlet guide vanes. The equations just given were then solved along the blade span, by iterating on $V_{Z,i}$ until the expression on the right side of the equation for $\dot{W}_A$ was equal to the measured flow rate at station 1 within a.i acceptable tolerance limit.

A calculation procedure was required to correct for a leakage problem encountered in the station 2 pressure instrumentation preceding CADDE data point 216. The total

26

pressure at station 2 was calculated from the flow rate at station 1 rather than from the measured value at station 2 by using the following equations:

$$P_{T,2} = \frac{P_{S,2}}{\left[1 - \frac{\gamma - 1}{2}\left(\frac{V_2}{a_{T,2}}\right)^2\right]^{\gamma/(\gamma-1)}}$$

$$\frac{V_2}{a_{T,2}} = \frac{-P_{S,2}}{RT_{T,2}}\frac{a_{T,2}}{\gamma-1}\frac{A_2'}{\dot{W}_A} \pm \sqrt{\left(\frac{P_{S,2}}{RT_{T,2}}\frac{a_{T,2}}{\gamma-1}\frac{A_2'}{\dot{W}_A}\right)^2 + \frac{2}{\gamma-1}}$$

where the effective flow area A_2' is the product of the geometric flow area and the discharge coefficient. The latter was obtained on the basis of the calculated displacement thickness from the boundary-layer measurements at the tip wall δ_t^* and an estimated displacement thickness at the hub wall δ_h^*. The δ_h^* was estimated by using turbulent boundary-layer theory.

When this procedure was used, good agreement was obtained between the measured and calculated pressures at station 2 for all high-inlet-temperature data points preceding CADDE point 216. For CADDE point 216, the calculation resulted in a 1.3-percent reduction in the corrected mass flow at station 2.

REFERENCES

1. Fung, Yüan-Chên: An Introduction to the Theory of Aeroelasticity. Dover Publ. Inc., 1969.

2. Mikolajczak, A. A.; et al.: Advances in Fan and Compressor Blade Flutter Analysis and Predictions. J. Aircraft, vol. 12, no. 4, Apr. 1975, pp. 325-332.

3. Jeffers, James D., II; and Meece, Carl E., Jr.: F100 Fan Stall Flutter Problem Review and Solution. J. Aircraft, vol. 12, no. 4, Apr. 1975, pp. 350-357.

4. Kurosaka, M.: On the Unsteady Supersonic Cascade with a Subsonic Leading Edge - An Exact First-Order Theory - Part 2. J. Eng. Power, vol. 96, no. 1, Jan. 1974, pp. 23-31.

5. Jones, William H.; Bishop, Walter A.; Kirchgessner, Thomas A.; and Dicus, John H.: Experimental Apparatus for Investigation of Fan Aeroelastic Instabilities in Turbomachinery. NASA TM X-3508, 1977.

6. Lane, Frank: System Mode Shapes in the Flutter of Compressor Blade Rows. J. Aeron. Sci., vol. 23, no. 1, Jan. 1956, pp. 54-66.

7. Johnsen, Irving A.; and Bullock, Robert O., eds.: Aerodynamic Design of Axial-Flow Compressors. NASA SP-36, 1965, p. 300.

Station	Identification (a)	Radius (except where other-wise noted) cm	in.	Angular location (b)
0	PTO-0°-1	58.42	23.00	PTO and TO probes located on cross rake at bellmouth entrance
	PTO-0°-2	35.56	14.00	
	PTO-90°-1	48.26	19.00	
	PTO-90°-2	21.59	8.50	
	PTO-180°-1	58.42	23.00	
	PTO-180°-2	35.56	14.00	
	PTO-270°-1	48.26	19.00	
	PTO-270°-2	21.59	8.50	
	TO-0°-1	66.04	26.00	
	TO-0°-2	49.53	19.50	
	TO-0°-3	21.59	8.50	
	TO-90°-1	73.03	28.75	
	TO-90°-2	58.42	23.00	
	TO-90°-3	38.10	15.00	
	TO-180°-1	66.04	26.00	
	TO-180°-2	49.53	19.50	
	TO-180°-3	21.59	8.50	
	TO-270°-1	73.03	28.75	
	TO-270°-2	58.42	23.00	
	TO-270°-3	38.10	15.00	
1	Outer wall	41.66	16.40	Outer wall statics at 35°, 125°, 215°, and 305°
	PT1-1	41.478	16.330	
	PT1-2	41.128	16.192	
	PT1-3	40.777	16.054	Rakes containing PT1-1 to PT1-7 at 30°, 120°, 210°, and 300°
	PT1-4	40.427	15.916	
	PT1-5	40.076	15.778	
	PT1-6	39.726	15.640	
	PT1-7	38.456	15.140	
	PT1-8	35.94	14.150	Rakes containing PT1-8 and PT1-9 at 82° and 262°
	PT1-9	32.766	12.900	
	T1-1	35.306	13.900	T1 rakes at 75°, 165°, 225°, and 345°
	T1-2	28.956	11.400	
1.A	Outer wall	45.720	18.000	Outer wall statics at 60° and 240°
	Inner wall	14.27	5.620	-------------------------------------
1.B	Outer wall	46.558	18.330	Outer wall statics at 60° and 240°
	Inner wall	14.27	5.620	-------------------------------------
1.C	Outer wall	46.335	18.250	Outer wall statics at 60° and 240°
	Inner wall	14.27	5.620	-------------------------------------
1.D	Outer wall	44.450	17.500	Outer wall statics at 60° and 240°
	Inner wall	14.27	5.620	-------------------------------------
2	Outer wall	44.171	17.390	Outer wall statics at 5°, 50°, 95°, 140°, 185°, 230°, 275°, and 320°
	Inner wall	14.262	5.615	Inner wall statics at 5°, 95°, 185°, and 275°
	PT2-1	42.144	16.592	PT2 rakes at 90° and 270°
	PT2-2	37.767	14.869	
	PT2-3	32.812	12.918	
	PT2-4	26.962	10.615	
	PT2-5	19.426	7.648	
	PTBL2-θ-1	^{c}0.178	^{c}0.070	
	PTBL2-θ-2	^{c}.356	^{c}.140	
	PTBL2-θ-3	^{c}.889	^{c}.350	PTBL (boundary layer) rakes on outer wall at 60° and 240°
	PTBL2-θ-4	^{c}1.372	^{c}.540	
	PTBL2-θ-5	^{c}2.032	^{c}.800	
	PTBL2-θ-6	^{c}2.921	^{c}1.150	
	PTBL2-θ-7	^{c}4.445	^{c}1.750	

TABLE I. - Continued.

Station	Identification (a)	Radius (except where otherwise noted)		Angular location (b)
		cm	in.	
2.1 (First stage stator inlet)	Outer wall	42.59	16.767	Outer wall statics at 66° and 246°
	Inner wall	19.36	7.621	--------------------------------------
	PT2.1-1	40.846	16.081	⎫
	PT2.1-2	37.153	14.627	⎪
	PT2.1-3	33.048	13.011	⎬ PT2.1 rake at 63° in vane
	PT2.1-4	28.354	11.163	⎪
	PT2.1-5	22.713	8.942	⎭
	T2.1-1	40.846	16.081	⎫
	T2.1-2	37.153	14.627	⎪
	T2.1-3	33.048	13.011	⎬ T2.1 rake at 70° in vane
	T2.1-4	28.354	11.163	⎪
	T2.1-5	22.713	8.942	⎭
2.2 (Second stage stator inlet)	Outer wall	41.227	15.649	Outer wall statics at 64° and 244°
	Inner wall	22.07	8.688	--------------------------------------
	PT2.2-1	39.748	15.649	⎫
	PT2.2-2	36.563	14.395	⎪
	PT2.2-3	33.070	13.020	⎬ PT2.2 rake at 70° in vane
	PT2.2-4	29.205	11.498	⎪
	PT2.2-5	24.646	9.703	⎭
	T2.2-1	39.748	15.649	⎫
	T2.2-2	36.563	14.395	⎪
	T2.2-3	33.070	13.020	⎬ T2.2 rake at 67° in vane
	T2.2-4	29.205	11.498	⎪
	T2.2-5	24.646	9.703	⎭
2.3 (Third stage stator inlet)	Outer wall	39.65	15.609	⎫ Outer and inner wall statics at 78° and
	Inner wall	23.11	9.100	⎭ 258°
2.5 (Compressor inlet)	Outer wall	31.448	12.381	⎫ Outer and inner wall statics at 37°, 98°,
	Inner wall	22.301	8.780	⎭ and 278°
	PT2.5-1	29.621	11.662	⎫
	PT2.5-2	26.868	10.578	⎬ PT2.5 rakes at 23°, 113°, and 293°
	PT2.5-3	24.117	9.495	⎭
	T2.5-1	30.538	12.023	⎫
	T2.5-2	28.705	11.301	⎪
	T2.5-3	26.868	10.578	⎬ T2.5 rakes at 68°, 248°, and 338°
	T2.5-4	25.034	9.856	⎪
	T2.5-5	23.200	9.134	⎭
	PTBL2.5-θ-1	c0.203	c0.080	⎫
	PTBL2.5-θ-2	c.559	c.220	⎪
	PTBL2.5-θ-3	c.914	c.360	⎪
	PTBL2.5-θ-4	c1.270	c.500	⎪
	PTBL2.5-θ-5	c1.626	c.640	⎬ PTBL (boundary layer) rakes on outer and
	PTBL2.5-i-1	c.178	c.070	⎪ inner wall at 55° and 235°
	PTBL2.5-i-2	c.534	c.210	⎪
	PTBL2.5-i-3	c.889	c.350	⎪
	PTBL2.5-i-4	c1.245	c.490	⎪
	PTBL2.5-i-5	c1.600	c.630	⎭
2.5 (Fan exit and bypass duct inlet)	Outer wall	39.675	15.620	⎫ Outer and inner wall statics at 84°, 264°,
	Inner wall	34.366	13.530	⎭ and 321°
	PT2.5F-1	38.532	15.170	⎫
	PT2.5F-2	36.878	14.519	⎬ PT2.5F rakes at 68°, 248°, and 338°
	PT2.5F-3	35.227	13.869	⎭
	T2.5F-1	39.182	15.426	⎫
	T2.5F-2	38.064	14.986	⎪
	T2.5F-3	36.944	14.545	⎬ T2.5F rakes at 23°, 113°, and 293°
	T2.5F-4	35.824	14.104	⎪
	T2.5F-5	34.704	13.663	⎭
	PTBL2.5F-i-1	c0.179	c0.070	⎫
	PTBL2.5F-i-2	c.534	c.210	⎪
	PTBL2.5F-i-3	c.889	c.350	⎬ PTBL (boundary layer) rakes on inner
	PTBL2.5F-i-4	c1.245	c.490	⎪ wall at 55° and 235°
	PTBL2.5F-i-5	c1.600	c.630	⎭

TABLE I. - Concluded.

Station	Identification (a)	Radius (except where otherwise noted) cm	in.	Angular location (b)
3 (Compressor exit and combustor inlet)	Outer wall	24.338	9.582	Outer and inner wall statics at 50°, 143°, and 323°
	Inner wall	21.039	8.283	
	PT3-1	23.348	9.192	PT3 rakes at 67°, 157°, and 292°
	PT3-2	22.273	8.769	
	T3-1	23.614	9.297	
	T3-2	22.807	8.979	T2 rakes at 22°, 202°, and 292°
	T3-3	21.999	8.661	
Combustor exit	Outer wall	30.701	12.087	Outer and inner wall statics at 90° and 270°
	Inner wall	25.730	10.130	
4.5 (Fan turbine inlet)	Outer wall	31.780	12.512	Outer wall statics at 43° and 229°
	Inner wall	24.188	9.523	-----------------------------------
	PT4.5-1	29.733	11.706	PT4.5 rake located at 43° and 229° in vane
	PT4.5-2	26.616	10.479	
	T4.5-1	31.176	12.274	
	T4.5-2	28.219	11.110	T4.5 rake located at 31° and 217° in vane
	T4.5-3	24.912	9.808	
6 (Core turbine exit)	Outer wall	38.837	15.290	-----------------------------------
	Inner wall	19.358	7.632	
	PT6-1	37.681	14.835	
	PT6-2	31.039	12.220	PT6 rakes at 30°, 210°, and 345°
	PT6-3	22.466	8.845	
	T6-1	36.681	14.835	
	T6-2	31.039	12.220	T6 rakes at 75° and 300°
	T6-3	22.466	8.845	
6F (Bypass duct exit)	Outer wall	48.235	18.990	-----------------------------------
	Inner wall	38.862	15.300	
	PT6F-1	45.707	17.995	PT6F rakes at 30°, 210°, and 345°
	PT6F-2	42.113	16.580	
	T6F-1	45.707	17.995	T6F rakes at 75° and 300°
	T6F-2	42.113	16.580	
6.5 (Downstream of flameholder)	Outer wall (afterburner liner)	46.713	18.391	Statics flush with inside of afterburner liner at 37°, 167°, and 282°
6.8 (Liner exit)	Outer wall (afterburner liner)	46.713	18.391	Statics flush with inside of afterburner liner at 37°, 167°, and 282°

[a]Type of instrumentation (i.e., steady-state or high-response) can be obtained from fig. 2.
[b]All angles measured clockwise from top center, looking upstream.
[c]Distance from wall.

TABLE II. - SUMMARY OF INLET AND ENGINE OPERATING CONDITIONS DURING FAN FLUTTER MAPPING

Inlet temperature		Inlet pressure		Approximate fan speed, $N/\sqrt{\theta}$, rpm	Angle of inlet guide vanes, (CIVV), deg	Nozzle throat area, A_8		Type of test	Result
°C	°F	N/cm²	psia			m²	ft²		
4.4	40	17.24	25	8000 to 7000	5	0.265	2.85	Deceleration	--------
				7000 to 6000	0	.265	2.85	Deceleration	--------
				7750	-15 to 4	.237	2.56	CIVV excursion	Rotating stall at CIVV = 3°
				7750 to 6100	-5	.237	2.56	Deceleration	--------
				6600	0 to 1.4	.237	2.56	CIVV excursion	Rotating stall at CIVV = 1.4°
37.8	100	5.17	7.5	7000	-25 to -5	0.281	3.03	CIVV excursion	--------
				8000	-25 to -5	.281	3.03	CIVV excursion	--------
				9000	-25 to -5	.281	3.03	CIVV excursion	--------
		6.89	10	7000	-25 to 5	0.281	3.03	CIVV excursion	--------
				8000	-25 to 5	.281	3.03	CIVV excursion	--------
				9000	-25 to 5	.281	3.03	CIVV excursion	--------
		10.34	15	7000	-25 to 0	0.281	3.03	CIVV excursion	--------
				8000	-25 to 5	.281	3.03	CIVV excursion	--------
				9000	-25 to 5	.281	3.03	CIVV excursion	--------
		13.79	20	7000	-20 to 0	0.265	2.85	CIVV excursion	--------
93.3	200	10.34	15	6000	-20 to 0	0.265	2.85	CIVV excursion	--------
				7000	-20 to 5	.265	2.85	CIVV excursion	--------
		13.79	20	6000	-20 to 0	0.265	2.85	CIVV excursion	--------
				7000	-20 to 5	.265	2.85	CIVV excursion	--------
				9000 to 7000	5	.314	3.38	Deceleration	--------
				7000 to 6000	0	.314	3.38	Deceleration	--------
135	275	17.24	25	7400	-15	0.319 to 0.252	[a]3.43 to 2.71	Area closure	--------
171.1	340	10.34	15	6500	-15 to -7.5	0.284	[a]3.06	CIVV excursion	Flutter at CIVV = -7.5°
		13.79	20	6200	-15 to -7.5	0.237	[a]2.55	CIVV excursion	Flutter at CIVV = -7.5°
				6800	-15	0.311 to 0.289	[a]3.35 to 3.11	Area closure	Flutter at A_8 = 0.289 m² (3.11 ft²)
				7000	-15	0.289 to 0.281	[a]3.11 to 3.02	Area closure	Flutter at A_8 = 0.281 m² (3.02 ft²)
		17.24	25	7100	-15	0.311 to 0.284	[a]3.35 to 3.06	Area closure	Flutter at A_8 = 0.284 m² (3.06 ft²)

[a] Exhaust-nozzle plug installed.

32

TABLE III. – DATA READINGS FOR FAN FLUTTER MAPPING

Inlet pressure, $P_{T,2}$ N/cm²	psia	Inlet temperature, T_2 °C	°F	Fan speed, N_F, rpm	Core speed, N_C, rpm	Fan turbine inlet temperature, FTIT °C	°F	Angle of inlet guide vane, (CIVV), deg	Nozzle throat area, A_8 m²	ft²	Total corrected flow, $\frac{W_2\sqrt{\theta_2}}{\delta_2}$ kg/sec	lb/sec	Pressure ratio, $\frac{P_{T,2.5}}{P_{T,2}}$	Corrected fan speed, $\frac{N_F}{\sqrt{\theta_2}}$, rpm	Corrected core compressor speed, $\frac{N_C}{\sqrt{\theta_{2.5}}}$, rpm	CADDE reading	Analog reading
5.17	7.5	21.1	70	5156	8 476	335	635	-25	0.282	3.04	44.2	97.4	1.225	5094	8035	134	-----
				7056	9 822	540	1004	-25	.282	3.04	59.8	131.8	1.616	6962	8930	135	-----
				6717	9 556	502	936	-25	.281	3.03	56.5	124.5	1.535	6627	8758	136	-----
				8061	10 538	667	1232	-25	.282	3.04	a70.7	a155.8	1.934	7952	9291	137	-----
		23.9	75	7498	10 073	599	1110	-25	0.280	3.01	-----	------	-----	7379	9042	138	-----
				8975	10 854	742	1368	-25	.295	3.17	-----	------	-----	8828	9364	139	-----
		15.6	60	4863	8 260	305	581	-25	0.342	3.68	41.7	92.0	1.326	4854	7943	140	-----
				7822	10 288	614	1138		.284	3.06	67.9	149.8	1.856	7772	9210	141	-----
				5521	8 679	366	690		.284	3.06	47.1	103.9	1.284	5482	8913	142	-----
				6050	8 998	429	804		.284	3.06	51.3	113.1	1.391	6008	8413	143	-----
				6550	9 383	483	902		.281	3.03	55.7	122.8	1.503	6506	8678	144	-----
				7041	9 771	537	999		.281	3.03	60.4	133.1	1.629	6992	8930	145	-----
				7514	10 102	584	1084		.281	3.03	64.9	143.1	1.758	7459	9115	146	-----
				8030	-----	643	1189		.343	3.69	70.2	154.8	1.989	8620	----	147	-----
				8551	10 705	703	1297		.281	3.03	76.3	168.3	2.109	8478	9371	148	-----
				9013	10 966	755	1391		.281	3.03	81.5	179.6	2.272	8929	9475	149	-----
				9854	11 585	900	1652	-7.5	.281	3.03	97.7	215.5	2.792	9749	9639	150	-----
		37.8	100	7296	-----	597	1106	-25	0.283	3.05	60.2	132.8	1.647	6986	----	151	-----
				7296 to 7005	~10 120	---	----	-25 to -5	.283	3.05	-----	------	-----	----	----	----	30
				8323	10 767	709	1309	-25	.281	3.03	70.7	155.9	1.939	7980	9236	152	-----
				8323 to 7978	~10 767	---	----	-25 to -5	.281	3.03	-----	------	-----	----	----	----	31
				9372	11 330	833	1532	-25	.281	3.03	82.1	181.1	2.278	8980	9447	153	-----
				9372 to 8885	~11 330	---	----	-25 to -5	.281	3.03	-----	------	-----	----	----	----	32
6.89	10	37.8	100	7291	10 163	589	1092	-25	0.283	3.05	61.2	135.0	1.621	6969	8950	154	-----
				7290	~10 165	---	----	-25 to 5	.283	3.05	-----	------	-----	----	----	----	33
				8340	10 858	710	1310	-25	.281	3.03	72.1	158.9	1.960	7972	9293	155	-----
				8340 to 11 220	10 860	---	----	-25 to 5			-----	------	-----	----	----	----	34
				8415	-----	787	1448	5			76.9	169.5	2.108	8051	----	156	-----
				9310	11 379	818	1504	-25			82.6	182.0	2.288	8909	9494	157	-----
				9310 to 11 750	11 380	---	----	-25 to 5			-----	------	-----	----	----	----	35
				9328	-----	903	1657	5			91.5	201.8	2.564	----	----	158	-----
10.34	15	37.8	100	7287	10 038	569	1056	-25	0.281	3.03	60.6	133.7	1.620	6998	8866	159	-----
				7290 to 10 360	10 040	---	-----	-25 to 0			-----	------	-----	----	----	----	36
				8180	10 729	669	1236	-25			70.6	155.6	1.871	7846	9263	160	-----
				8180 to 11 075	10 729	---	----	-25 to 5			-----	------	-----	----	----	----	37
				8195	11 076	738	1360	5			75.0	165.4	2.163	7854	----	161	-----
				9206	11 303	797	1467	-25			82.6	182.1	2.217	8811	9472	162	-----
				9206 to 11 727	11 303	---	----	-25 to 5			-----	------	-----	----	----	----	38
				9245	11 727	889	1633	5			88.3	194.6	2.454	8831	9622	163	-----

aCorrected for $P_{s,1}$ measurement error.

TABLE III. - Continued.

Inlet pressure, $P_{T,2}$		Inlet temperature, T_2		Fan speed, N_F, rpm	Core speed, N_C, rpm	Fan turbine inlet temperature, FTIT		Angle of inlet guide vane, (CIVV), deg	Nozzle throat area, A_8		Total corrected flow, $\dfrac{W_2\sqrt{\theta_2}}{\delta_2}$		Pressure ratio, $\dfrac{P_{T,2.5}}{P_{T,2}}$	Corrected fan speed $\dfrac{N_F}{\sqrt{\theta_2}}$, rpm	Corrected core compressor speed, $\dfrac{N_C}{\sqrt{\theta_{2.5}}}$ rpm	CADDE reading	Analog reading
N/cm^2	psia	°C	°F			°C	°F		m^2	ft^2	kg/sec	lb/sec					
6.89	10	37.8	100	7038	10 049	582	1079	-25	0.265	2.85	58.3	128.8	1.587	6753	8921	164	-----
				8008	10 733	684	1263	-25	.265	2.85	67.5	148.9	1.876	7688	9277	165	-----
				9128	11 353	817	1503	-25	.265	2.85	80.7	177.9	2.252	8760	9512	166	-----
				9650	11 727	903	1657	-15	.265	2.85	88.9	196.1	2.514	9252	9626	167	-----
13.79	20	37.8	100	----	-------	---	----	-20	-----	----	-----	------	-----	----	----	168	-----
				7280	10 200 to 10 480	---	----	-20 to 0	0.265	2.85	-----	------	-----	----	----	----	39, 40
10.34	15	93.3	200	7951	11 046	750	1382	-20	0.266	2.86	60.6	133.6	1.662	7011	8947	169	-----
				7938	11 032	747	1377	-20	.265	2.85	60.4	133.2	1.668	7006	8947	170	-----
				7930	11 032 to 11 342	---	----	-20 to 5			-----	------	-----	----	----	----	41
				7869	11 342	796	1465	5			77.1	169.9	2.132	6932	9110	171	-----
				6775	10 175	614	1138	-20			50.8	112.0	1.400	5972	8453	172	-----
				6800	10 175 to 10 448	---	----	-20 to 0			-----	------	-----	----	----	----	42
				6834	10 448	654	1210	0			52.7	116.2	1.437	6028	8632	173	-----
13.79	20	93.3	200	6792	10 201	609	1129	-20	0.265	2.85	51.8	114.2	1.415	5988	8465	174	-----
				6800	10 201 to 10 471	---	----	-20 to 0	.265	2.85	-----	------	-----	----	----	----	43
				6862	10 471	651	1204	0	.265	2.85	52.9	116.6	1.443	6050	8639	175	-----
				7942	11 172	754	1389	-20	.274	2.95	60.3	132.9	1.660	7005	9049	176	-----
				7900	11 172 to 11 486	---	----	-20 to 5	.274	2.95	-----	------	-----	----	----	----	44
				7980	11 486	812	1493	5	.265	2.85	63.0	138.9	1.737	7037	9211	177	-----
9.38	13.6	37.8	100	6367	9 453	486	906	-25	0.285	3.07	52.3	115.3	1.415	6109	8536	179	-----
				9735	11 759	911	1672	-13.7	.285	3.07	90.7	200.0	2.574	9327	9625	180	-----
13.79	20	93.3	200	9784	11 981	915	1679	-20	0.319	3.43	81.4	179.5	2.100	8637	9329	181	-----
				9780	~11 981	---	----	-20 to -10			-----	------		----	----	----	45
				9405	11 972	914	1677	-5			80.3	177.1	2.070	8301	9341	182	-----
				9400 to 7900	-------	---	----	5			-----	------	-----	----	----	----	46
				7900 to 6100	-------	---	----	0			-----	------	-----	----	----	----	46
				6100 to 9400	-------	---	----	-20			-----	------	-----	----	----	----	-----
		4.4	40	7928	10 467	652	1205	-15	0.268	2.88	73.9	163.0	2.050	8037	9427	191	-----
17.24	25	4.4	40	7886	10 462	654	1210	-15	0.268	2.88	74.0	163.1	2.020	7990	9427	192	-----
				7700 to 7120	-------	---	----	5	.268	2.88	-----	------	-----	----	----	----	48
				7120 to 5800	-------	---	----	0	.268	2.88	-----	------	-----	----	----		
				7617	10 434	653	1208	-15	.244	2.63	69.0	152.1	1.970	7716	9442	193	-----
				7500	~10 430	---	----	-15 to 3			-----	------	-----	----	----	----	[b]49
				7879	10 533	671	1240	-15			70.8	156.0	2.038	7973	9476	194	-----
				7879 to 7747	~10 533	---	----	-15 to 4			-----	------	-----	----	----	----	[c]50
				7747	10 562	667	1232	-5			66.5	146.5	1.936	7841	9511	[d]195	-----
				7664	10 524	671	1240	-5	.243	2.62	69.4	153.0	2.017	7757	9475	197	-----
				7664 to 5770	10 524 to 9 050	---	----	-5			-----	------	-----	----	----	----	51
				7739	10 582	685	1265	0			69.9	154.0	2.035	7838	9504	198	-----
				7739 to 6527	-------	---	----	0			-----	------	-----	----	----	----	[e]52
				6527	9 740	---	----	0 to 1.4			-----	------	-----	----	----	----	[e]52

[b]Rotating stall at CIVV = +3°.
[c]Rotating stall at CIVV = +4°.
[d]Rotating stall.
[e]Stall.

TABLE III. - Concluded.

Inlet pressure, $P_{T,2}$		Inlet temperature, T_2		Fan speed, N_F, rpm	Core speed, N_C, rpm	Fan turbine inlet temperature, FTIT		Angle of inlet guide vane (CIVV), deg	Nozzle throat area, A_8		Total corrected flow, $\dfrac{W_2\sqrt{\theta_2}}{\delta_2}$		Pressure ratio, $\dfrac{P_{T,2.5}}{P_{T,2}}$	Corrected fan speed, $\dfrac{N_F}{\sqrt{\theta_2}}$, rpm	Corrected core compressor speed, $\dfrac{N_C}{\sqrt{\theta_{2.5}}}$, rpm	CADDE reading	Analog reading
N/cm²	psia	°C	°F			°C	°F		m²	ft²	kg/sec	lb/sec					
17.24	25	4.4	40	6527	9 738	531	987	1.4	0.242	2.61	57.8	127.5	1.610	6615	9096	e199	-----
10.34	15	37.8	100	7997	10 789	696	1285	-15	0.268	2.89	69.0	152.1	1.883	7665	9296	201	-----
				8031	10 969	744	1371	-15	.237	2.55	66.9	147.5	1.988	7696	9384	202	-----
				8012	10 862	721	1329	-15	.252	2.71	68.1	150.1	1.934	7668	9319	203	-----
		21.1	70	4435	8 215	336	636	-25	0.252	2.71	38.6	85.2	1.009	4386	7895	204	-----
				9480	11 540	897	1646	-18	.252	2.71	87.0	191.9	2.676	9334	9671	205	-----
13.79	20	171.1	340	8932	11 963	903	1658	-15	0.319	3.43	65.0	143.4	1.664	7174	8807	206	-----
17.24	25	171.1	340	8926	12 002	908	1666	-15	0.311	3.35	65.8	145.1	1.664	7186	8854	207	-----
				8925	12 000	---	----	-15	.311 to .284	3.35 to 3.06	-----	------	-----	----	----	----	f53
				8813	12 018	916	1681	-15	.291	3.13	65.0	143.3	1.648	7079	8864	208	-----
13.79	20	171.1	340	8707	11 974	921	1689	-15	0.289	3.11	62.4	137.5	1.641	6979	8834	209	-----
				8700	11 975	---	----	-15	.289 to .283	3.11 to 3.05	-----	------	-----	----	----	----	g54
10.34	15	171.1	340	8330	11 682	896	1644	-15	0.284	3.06	59.1	130.2	1.574	6701	8708	210	-----
				8325	11 680	---	----	-15	.252	2.71	-----	------	-----	----	----	----	55
				8055	11 476	859	1579	-15	.284	3.06	56.7	125.1	1.522	6470	8588	211	-----
				8100	11 600	---	----	-15 to -7.5	.284	3.06	-----	------	-----	----	----	----	h56
				8152	11 665	893	1640	-7.5	.284	3.06	58.2	128.2	1.548	6534	8679	i212	-----
13.79	20	171.1	340	8398	11 691	872	1602	-15	0.289	3.11	60.3	133.0	1.591	6779	8728	i213	-----
				7745	11 663	908	1666	-15	.237	2.55	52.9	116.6	1.534	6213	8734	214	-----
				7706	11 731	914	1678	-7.5	.237	2.55	53.2	117.3	1.536	6183	8782	i215	-----
17.24	25	135.0	275	8831	11 766	847	1557	-15	0.319	3.43	j70.9	j156.4	1.728	7441	9011	216	-----

[f]Flutter at $A_8 = 0.284$ m² (3.06 ft²).
[g]Flutter at $A_8 = 0.283$ m² (3.05 ft²).
[h]Flutter at CIVV = -7.5°.
[i]Flutter.
[j]Corrected for $P_{T,2}$ error (appendix C).

TABLE IV. - FAN FIRST-STAGE BLADE VIBRATORY STRESSES AND FREQUENCIES

Strain gage	Blade slot	Blade torsional natural frequency (blade alone)	Ratio of bench test local to maximum stress, σ/σ_{max} (a)	Analog reading 53				Analog reading 54			
				Stress		Frequency, Hz	σ/σ_{max}	Stress		Frequency, Hz	σ/σ_{max}
				kN/cm^2	ksi			kN/cm^2	ksi		
103 (TIP)	16	1061	0.80	3.78	5.48	1066	0.608	2.79	4.07	1080.5	0.575
109 (ASMT)	16	1061	.18	2.24	3.25	1066.5	.361	1.27	1.84	1080	.260
116 (ASTE)	16	1061	1.00	6.21	9.01	1068	1.00	4.87	7.07	1080.5	1.00
104 (TIP)	20	1067	----	11.31	16.40	1067	-----	7.56	10.96	1080.5	-----
113 (ASMT)	30	1135	----	2.24	3.25	1067.5	-----	.44	.64	1080.5	-----
117 (ASTE)	19	1091	----	13.40	19.44	1067	-----	9.99	14.49	1080	-----
122 (SHRD-CX)	11	1157	----	.92	1.34	1067.5	-----	.46	.67	1082	-----

aObtained by engine manufacturer by bench tests on blade alone for above-shroud torsional mode.

TABLE V. - INTERBLADE PHASE ANGLES FOR FIRST-STAGE ROTOR

Gage	Analog reading		
	53	54	56
	Flutter frequency, Hz		
	1062.5	1072.5	1087.5
	Phase angle between gages, deg		
103 compared with 104 (TIP) 116 compared with 117 (ASTE)	[a]-77 -58, -59.3	-63.5 -48	146 128.5, 133.8
	Phase angle between blades, deg		
TIP ASTE	-19.25 -19.3, -19.9	-15.9 -16	36.5 42.8, 44.6

[a]Negative values indicate trailing relation between gages and blades in direction of rotor rotation.

37

TABLE VI. - SAMPLE COMPUTER PRINTOUT FOR STEADY-STATE (CADDE) DATA

(a) Option 1

AVD

	1	2	3	4	5	6	7	8	9	10
0	8.8510	8.8510	14.047	14.040	149.21	299.12	149.20	299.20	8.8510H	248.81H
10	8.8823H	248.98	8.8667H	242.12H	8.8510H	37.183H	8.8197H	233.41	8.8354H	248.31
20	65.072H	245.46H	65.087H	233.58	64.978H	233.29	65.025H	250.03	65.103	244.67
30	61.534	232.78	56.557	233.08	65.322	224.41	63.225	224.62	57.183	228.43
40	149.18	227.43	8.8667H	36.597H	8.8197H	36.471	8.8354H	134.27	8.8510H	160.39
50	8.8667H	41.242	8.8510H	299.16	8.8510H	224.58	8.8354H	8.8929H	8.8510H	8.8929H
60	8.8667	8.8510	9272.8	11417.	2.8755	71.699	-0.0030003H	2961.3	14.907	0.00000H
70	-21.561	-24.242H	0.00000H	0.00000H	0.00000H	-2.8437	-2.3678	2.1968H	-3.0374	-12.057H
80	16.113	352.46H	-398.03H	14.060H	14.112H	6307.8	6342.6	6342.7	13.780	226.12
90	5.0436	1.5297	2.1791	0.23769	1.8938	1.4333	1.5198	-0.0044324	0.014405	-0.00055406
100	565.05	521.52	609.80	722.34H	609.76H	795.07H	652.46	562.63	609.71H	609.63H
110	542.55	542.91	543.04	544.10	544.06	543.93	540.16	539.58	540.43	540.60
120	543.93	543.93	543.26	541.76	541.84	542.07	539.85	539.80	538.16	538.25
130	999.43H	1009.7H	1018.4H	1023.8H	1030.8H	257.70H	1042.3H	1032.7H	1024.9H	1021.2H
140	1014.9H	839.72H	1004.4H	991.35H	609.67H	609.67H	609.58H	609.58H	609.67H	609.67H
150	531.44H	600.07	593.76	593.54	385.01H	628.19	602.29	594.59	563.73H	605.46
160	695.00	673.97	681.72	804.93H	677.45	703.07	674.92	716.26H	665.44	578.93H
170	609.50H	558.94H	682.86H	639.50H	687.92H	768.16H	794.66H	709.66H	690.63H	552.86H
180	721.81	713.97	713.97	723.32	722.96	718.28	742.90	720.14	5.6700H	728.09
190	747.97H	724.02	714.14	717.58	722.96	741.30	722.70	717.05	721.28	721.02
200	720.31	715.82	713.35	720.40	1107.3H	723.49	721.37	729.68	739.17	752.34
210	609.50H	609.50H	609.58H	609.58H	609.41H	609.58H	609.41H	609.58H	609.50H	609.50H
220	609.50H	609.58H	609.50H	609.50H	609.58H	1388.0	1395.4	1399.0	1148.1	609.67H
230	1522.3H	1367.7	1396.6	1371.9	1375.1	1405.7	1376.8	1370.0	1395.6	609.67H
240	1381.6H	2124.5	1836.4	1398.3H	578.76H	1866.6	609.67H	609.67H	609.67H	609.67H
250	2033.3	2005.5	2046.6	1967.4	2031.7	2035.3	2054.9	2022.6	609.67H	609.67H
260	5.6700H	1738.8	1685.4	609.67H	609.67H	609.67H	1787.8H	1744.8	1673.2	609.67H
270	796.64	809.49	668.88H	668.66H	759.61H	787.41	0.00000H	0.00000H	0.00000H	0.00000H
280	10.495	13.763	13.498	32.989	27.312	222.71	193.26	579.33	466.64	496.69
290	199.98	166.32	9.2079	7.5734	4.2463	682.29	618.82	661.75	238.55	14.156
300	26.380H	32.240	34.442	27.684	-0.13975H	32.277	32.541H	26.305H		

	1	2	3	4	5	6	7	8	9	10

DAMPR

	1	2	3	4	5	6	7	8	9	10
0	1.0053	1.0015	1.0053	1.0053	1.0053	35.716	35.713	35.705	35.705	35.709
10	14.226	14.230	14.226	14.230	14.226	0.96893	0.97809	0.96893	0.95978	0.95978
20	87.734	87.760	87.734	87.760	87.734	14.216	14.216	14.197	14.206	14.206
30	0.92814	0.93736	0.92814	0.92814	0.93736	87.818	87.809	87.800	87.809	87.809
40	14.166	14.166	14.156	14.156	14.156	14.237	18.028	11.607	0.037421H	0.037421H
50	13.736	13.740	13.752	13.740	13.752	13.763	13.752	13.760	13.736	9.5610H
60	8.8510	8.8317	8.8549	13.732	13.752	13.775	13.756	13.752	13.721	9.5880H
70	12.324	13.313	13.511	13.585	13.565	13.647	13.662	13.725	12.708	12.684
80	12.331	13.193	13.414H	13.523	13.565	13.585	13.592	13.611	12.723	12.700
90	12.312	13.336	13.492	13.592	13.627	13.655	13.651	13.690	12.293	12.281
100	12.316	13.200	13.363	13.476	13.530H	13.565	13.612	13.659	11.967	11.936
110	9.4529H	9.4490H	9.4104H	9.4220H	9.4760H	9.4027H	9.3873H	9.5147H	9.4027H	9.6382H
120	13.317	13.387	13.437	13.460	13.453	10.337H	9.8390H	9.3564H	9.9201H	9.3950H
130	10.156H	9.5726H	8.8970H	9.4606H	9.6614H	9.4220H	9.5301H	9.3718H	9.4606H	9.3950H
140	13.278	13.387	13.460	13.402	13.495	9.4799H	9.4413H	9.4374H	9.5417H	9.5378H
150	11.924	11.905	11.967	11.967	11.959	11.940	11.982	11.936	0.037421H	12.021
160	0.037421H	12.033	10.577H	12.704	12.867	13.134	13.204	13.294	13.379	13.429
170	9.5494H	9.5687H	9.5494H	12.665	12.820	13.142	13.212	13.247	13.294	13.332
180	20.248H	19.105H	18.407H	18.350H	19.710H	17.996	18.702	17.291	17.300	18.702
190	15.229	14.090H	-0.91489H	15.072	15.195	14.881	13.845	12.725	11.162	-0.91489H
200	8.9350H	8.9444H	8.9444H	8.9068H	8.9162H	8.8973H	8.9068H	8.8973H	8.9068H	-0.91489H
210	25.983	25.246	25.199	25.492	26.994	25.955	25.086	25.133	25.275	27.004
220	8.8916H	8.9010H	8.9104H	8.9010H	8.9104H	8.9010H	8.9010H	8.9104H	8.9104H	31.128H
230	21.372	21.183	20.361	18.700	15.964	-0.13975H	-0.13975H	-0.13975H	11.572H	21.127H
240	-0.13975H	-0.13975H	-0.13975H	-0.13975H	-0.13975H	-0.13975H	-0.13975H	-0.13975H	29.657	28.109H
250	-0.13975H	-0.13975H	-0.13975H	-0.13975H	-0.13975H	-0.13975H	-0.13975H	-0.13975H	14.166H	28.033
260	-0.13975H	-0.13975H	-0.13975H	-0.13975H	-0.13975H	-0.13975H	-0.13975H	26.862	77.193	27.051
270	-0.13975H	-0.13975H	-0.13975H	-0.13975H	-0.13975H	-0.13975H	9.6778H	28.307	28.316	28.420
280	-0.13975H	-0.13975H	-0.13975H	-0.13975H	-0.13975H	-0.13975H	-0.13975H	1.9066	49.598	13.498
290	-0.13975H	-0.13975H	-0.13975H	-0.13975H	-0.13975H	-0.13975H	-0.13975H	8.8916	8.9010	14.156
300	26.380H	32.240	34.442	27.684	-0.13975H	32.277	32.541H	26.305H	28.005	27.023H
310	31.486	32.371	9.2940H	78.392	-0.13975H	32.390	32.833	32.089	28.260	-0.13975H
320	31.599	32.494	33.953	28.128	27.797	32.918H	32.532	29.496H	28.288	27.674
330	27.731H	30.392	31.279	30.128	30.251	21.882H	30.317	30.392	31.062	-0.13975H
340	30.666	29.723	29.845	29.411H	30.496	29.666	-0.13975H	-0.13975H	-0.13975H	-0.13975H
350	8.8691H	8.8973H	8.8973H	8.8973H	8.8973H	8.8973H	8.8879H	8.8879H	8.8879H	8.8973H
360	8.8879H	8.9068H	8.8973H	8.8879H	8.8973H	8.8785H	8.8879H	8.8785H	8.8879H	8.9785H
370	8.8785H	8.8879H	8.8879H	8.8879H	8.8973H	8.8879H	8.8879H	8.8879H	8.8879H	8.8879H
380	8.8879H	8.8973H	8.8973H	8.8785H	8.8691H	8.9256H	8.8973H	8.9162H	8.8879H	8.8879H
390	8.8879H	8.8973H	8.8879H	8.9068H	8.8879H	-0.91489H	-0.91489H	-0.91489H		

TABLE VI. - Continued.

(b) Option 3

TO	PT2	C2WA2	WA2	C2.5W2.5	WA2.5
543.11	13.408	183.47	163.93	51.207	96.144

PCN1	PCN2	PC2WA2	PC2.5W2.5
0.93906	0.95891	0.84732	0.94062

FPR	ETR	BPR	C2N1	C2.5N2	N1	N2
2.2561	2.4618	0.70503	9061.9	9656.2	9272.8	11417.

T4.5	C2T4.5	C2T4	FTIT.R	C2FTIT.R	PT2	T3
2045.2	1953.3	2557.7	2024.9	1933.9	246.80	1367.4

			FTIT.F	C2FTIT.F
			1565.3	1474.2

RCVV-1	RCVV-2	RCVV-3	RCVV-4	RCVV-5
-2.8437	-2.3678	2.1968H	-3.0374	-12.057H

CIVV-1	CIVV-2
-21.561	-24.242H

PLA	A8	WFE	C2WFE
71.699	2.8755	6307.9	7074.8

PT2.5M/PT2	PT3/PT2.5
2.4254	7.5647

TTC-5 928.30	TTC-11 935.70	TTC-22 939.29	TTC-90 668.38
TC05 927.78	TC11 935.76	TC22 937.76	TC90 702.78
TOL +75.	TOL +90.	TOL +90.	CONST. LIMIT OF 1000°F.
PSTC-5 36.471	PSTC-11 134.27	PSTC-22 160.39	PSTC-90 41.242
PC05 40.474	PC11 137.31	PC22 161.24	
TOL +5.0	TOL +,-20.	TOL -0.0	

PB 222.71	PSBB 226.22

(c) Option 4

	P. & W.	ENERGY BALANCE. (NASA)
T4	2678.1	2759.3
WA2.5	96.144	89.831
DELPP	0.042955	
WG4	84.787	79.301
WA4	83.034	77.549
FAE	0.021102	0.022594

(d) Option 5

	PT	PS	T		PT	PS	T
0	13.758		543.11	2.1L	17.998	14.090H	607.63
1	13.758	12.321	539.60	2.2R	25.783	11.572H	682.04
2	13.408	11.963	543.11	2.2L	25.691	21.127H	681.14
2.1	17.998	15.229	604.43	2.3R	8.9020H	29.657	630.66H
2.2	25.737	16.349H	679.62	2.3L	12.395H	28.033	714.65H
2.3	10.649H	28.845	672.66H	2.5F	32.031	28.392	725.03
2.5	32.625	28.000	725.14	2.5L	32.608	27.962	728.90
2.5F	32.367	28.057	734.46	2.5FR	32.277	28.005	731.17
2.5M	32.518	28.023	729.00	2.5FL	32.436	28.260	738.17
3	246.80	233.23	1387.4	2.5MR	32.133		727.57
6F	30.005		797.57	2.5ML	32.537		732.73
2R	13.411	11.994	875.77H	3R	248.98	233.41	1383.2
2L	13.405	12.008	609.63H	3L	247.24	232.93	1390.2
2.1R	19.164H	15.229	595.79	4.5	63.805	56.870	2045.2
6	30.572		1722.0	6M	30.250		1337.1

39

TABLE VI. - Concluded.

(e) Option 6

	GAMMA	H	M	DELTA	THETA	RNI
0	1.3984	0.86508	0.00000	0.93719	1.0471	0.58290
1	1.3965	0.89378	0.40042	0.93619	1.0403	0.89020
2	1.3984	0.86508	0.40702	0.91233	1.0471	0.86040
2.1	1.3974	9.1031	0.49484	1.2247	1.1653	1.0095
2.2	1.3952	19.235	0.83312	1.7513	1.3103	1.2485
2.3	1.3955	18.295	0.00000	0.72460	1.2968	0.52315
2.5	1.3935	25.391	0.47349	2.2200	1.3980	1.4621
2.5F	1.3932	26.654	0.45757	2.2025	1.4160	1.4282
2.5M	1.3934	25.913	0.46698	2.2127	1.4055	1.4480
3	1.3553	116.27	0.28993	16.793	2.6749	5.1842
5F	1.3904	35.229	0.00000	2.0417	1.5377	1.1986
2P	1.3864	45.319	0.40446	0.91254	1.6884	0.47915
2L	1.3972	9.2037	0.40002	0.91212	1.6884	0.74384
2.1P	1.3976	7.9420	0.58298	1.3040	1.1436	1.0944
2.1L	1.3973	9.5341	0.60239	1.2247	1.1715	1.0029
2.2P	1.3951	19.562	1.1355	1.7544	1.3149	1.2453
2.2L	1.3952	19.441	0.53693	1.7481	1.3132	1.2478
2.3P	1.3967	12.636	0.00000	0.60575	1.2159	0.47358
2.3L	1.3940	23.971	0.00000	0.84345	1.3778	0.56546
2.5R	1.3936	25.376	0.41957	2.1795	1.3978	1.4358
2.5L	1.3934	25.900	0.47481	2.2138	1.4053	1.4522
2.5FR	1.3933	26.208	0.45607	2.1963	1.4096	1.4321
2.5FL	1.3930	27.156	0.44920	2.2071	1.4231	1.4226
2.5MR	1.3935	25.720	0.44747	2.1865	1.4027	1.4342
2.5ML	1.3932	26.419	0.46790	2.2140	1.4127	1.4398
3R	1.3556	117.65	0.30996	16.942	2.6667	5.2481
3L	1.3552	118.66	0.29775	16.823	2.6801	5.1820
4.5	1.3262	13.104	0.41950			
6	1.3380	168.04	0.00000			
6M	1.3583	110.94	0.00000			

	F/A
	0.021102
	0.021102
	0.016688

(f) Option 7

I	J	PT(J)/PT(I)	T(J)/T(I)	FTA(I-J)	PC(I-J)	FC(I-J)	
2	2.1	1.3424	1.1129	0.77506	0.19758	0.15313	0.36407
2.1	2.2	1.4200	1.1244	0.86028	0.25891	0.22274	0.37413
2.2	2.3	0.41375	0.98975	0.00000	0.00000	0.00000	0.00000
2.2	2.5M	1.2635	1.0727	0.94268	0.18403	0.17348	0.35226
2	2.5M	2.4254	1.3422	0.83831	0.68880	0.57743	0.36407
2.5	3	7.5647	1.9133	0.83869	4.4526	3.7344	0.50110
2P	2.1P	1.4290	0.68031	0.00000	0.00000	0.00000	0.00000
2.1P	2.2P	1.3454	1.1418	0.00000	0.00000	0.00000	0.00000
2.2P	2.3P	0.34527	0.92468	0.00000	0.00000	0.00000	0.00000
2.2P	2.5MR	1.2463	1.0668	0.96369	0.16972	0.16356	0.35288
2P	2.5MR	2.3960	0.83078	0.00000	0.00000	0.00000	0.00000
2.5	3R	7.6316	1.9075	0.84932	4.4240	3.7574	0.50110
2L	2.1L	1.3427	0.99571	0.00000	0.00000	0.00000	0.00000
2.1L	2.2L	1.4274	1.1210	0.87963	0.25316	0.22274	0.37633
2.2L	2.4L	0.48749	1.0492	0.00000	0.00000	0.00000	0.00000
2.2L	2.5ML	1.2665	1.0757	0.91363	0.19228	0.17568	0.35384
2	2.5ML	2.4267	1.3491	0.82230	0.70264	0.57778	0.36407
2.5	3L	7.5782	1.9171	0.83614	4.4708	3.7382	0.50110

TABLE VII. – HEADING IDENTIFICATION FOR OPTION 1 OF CADDE PRINTOUT

(a) Automatic voltage digitizer (AVD) identification

	AVD word number from table VI									
	1	2	3	4	5	6	7	8	9	10
0	1 L.R.	2 L.R.	1 ATM	2 ATM	1 H.R.	2 H.R.	1 H.R.	2 H.R.	PSM-45°	PT3-67°-1
10	PSM-45°	PT3-67°-1	PSM-225°	PT3-67°-2	PSVD-1	PS3-50°-θ	PSVD-2	PS3-50°-i	PSVD-3	PT3-157°-1
20	PSVD-4	PT3-157°-2	PSVD-5	PS3-143°-θ	PSVD-6	PS3-143°-i	PT4.5-43°-1	PT3-292°-1	PT4.5-43°-1	PT3-292°-2
30	PT4.5-43°-2	PS3-323°-θ	PS4.5-43°-θ	PS3-323°-i	PT4.5-229°-1	PSBR-90°-θ	PT4.5-229°-2	PSBR-90°-i	PS4.5-229°-θ	PSBR-270°-θ
40	PREF-3A	PSBR-270°-1	------	PSTC-5	------	PSTC-5	------	PSTC-11	------	PSTC-22
50	------	PSTC-90	------	PREF-3B	------	PREF-3C	------	------	------	------
60	1 L.R.	2 L.R.	N1	N2	A8	PLA	BL-s.u.	CTSRO	CPSRi	------
70	CIVV-90°L-1	CIVV-90°L-2	------	------	------	RCVV-90°L-1	RCVV-90°L-2	RCVV-270°L-1	RCVV-270°L-2	RCVV-270°R-1
80	PS-A/B-1	PS-A/B-2	PS-A/B-3	PS-A/B-4	PS-A/B-5	WFE	WFTHI-1	WFTHI-2	WFTLO-1	WFTLO-2
90	VICV	VICH	VICA	V2.3B	VDCR	VGBV	VGBH	VADV	VSRV	------
100	TFE	TFT	------	TJ-1	TJ-2	TJ-3	TTANK-1	TTANK-2	TTANK-3	------
110	T0-0°-1	T0-0°-2	T0-0°-3	T0-90°-1	T0-90°-2	T0-90°-3	T1-15°-1	T1-15°-2	T1-105°-1	T1-105°-2
120	T0-180°-1	T0-180°-2	T0-180°-3	T0-270°-1	T0-270°-2	T0-270°-3	T1-195°-1	T1-195°-2	T1-285°-1	T1-285°-2
130	T2-30°-1	T2-30°-2	T2-30°-3	T2-30°-4	T2-30°-5	T2-120°-1	T2-120°-2	T2-120°-3	T2-120°-4	T2-120°-5
140	T2-210°-1	T2-210°-2	T2-210°-3	T2-210°-4	T2-210°-5	T2-300°-1	T2-300°-2	T2-300°-3	T2-300°-4	T2-300°-5
150	T2.1-70°-1	T2.1-70°-2	T2.1-70°-3	T2.1-70°-4	T2.1-70°-5	T2.1-250°-1	T2.1-250°-2	T2.1-250°-3	T2.1-250°-4	T2.1-250°-5
160	T2.2-67°-1	T2.2-67°-2	T2.2-67°-3	T2.2-67°-4	T2.2-67°-5	T2.2-247°-1	T2.2-247°-2	T2.2-247°-3	T2.2-247°-4	T2.2-247°-5
170	T2.3-68°-1	T2.3-68°-2	T2.3-68°-3	T2.3-68°-4	T2.3-68°-5	T2.3-248°-1	T2.3-248°-2	T2.3-248°-3	T2.3-248°-4	T2.3-248°-5
180	T2.5-68°-1	T2.5-68°-2	T2.5-68°-3	T2.5-68°-4	T2.5-68°-5	T2.5F-23°-1	T2.5F-23°-2	T2.5F-23°-3	T2.5F-23°-4	T2.5F-23°-5
190	T2.5-248°-1	T2.5-248°-2	T2.5-248°-3	T2.5-248°-4	T2.5-248°-5	T2.5F-113°-1	T2.5F-113°-2	T2.5F-113°-3	T2.5F-113°-4	T2.5F-113°-5
200	T2.5-338°-1	T2.5-338°-2	T2.5-338°-3	T2.5-338°-4	T2.5-338°-5	T2.5F-293°-1	T2.5F-293°-2	T2.5F-293°-3	T2.5F-293°-4	T2.5F-293°-5
210	------	------	------	------	------	------	------	------	------	------
220	------	------	------	------	------	TTC-5	TTC-11	TTC-22	TTC-90	------
230	T3-22°-1	T3-22°-2	T3-22°-3	T3-202°-1	T3-202°-2	T3-202°-3	T3-337°-1	T3-337°-2	T3-337°-3	------
240	T4.5-43°-1	T4.5-43°-2	T4.5-43°-3	T4.5-229°-1	T4.5-229°-2	T4.5-229°-3	------	------	------	------
250	T4.5-PW-5°	T4.5-PW-52°	T4.5-PW-110°	T4.5-PW-156°	T4.5-PW-203°	T4.5-PW-273°	T4.5-PW-319°	FTIT(PW)	------	------
260	T6-75°-1	T6-75°-2	T6-75°-3	T6-120°-1	T6-120°-2	T6-120°-3	T6-300°-1	T6-300°-2	T6-300°-3	------
270	T6F-75°-1	T6F-75°-2	TS05-1	TS05-2	T6F-300°-1	T6F-300°-2	------	------	------	------
280	PS-PLEN-2	ΔP(PSPLEN-PS1-55-θ)	PT2-285°	PT2.5F-68°-2	PT6-210°-2	PB	PF1	PF2	PF4	PF1A
290	PFCB	POBP	PS01	PS04	PS05	TS01	TS04	TDOT	PT3-67°-2	------

41

TABLE VII. - Concluded.

(b) Digital automatic multiple pressure recorder (DAMPR) identification (steady-state pressures, psia); words 1 to 45 are DAMPR system reference pressures

Inner wall designated by i; outer wall designated by θ.

	DAMPR word number from table VI									
	1	2	3	4	5	6	7	8	9	10
0	LOW, 5K, OR	LOW, 5K, OR	LOW, 5K, OR	LOW, 5K, OR	LOW, 5K, OR	HIGH, 5K, OR	HIGH, 5K, OR	HIGH, 5K, RED	HIGH, 5K, RED	HIGH, 5K, OR
10	ATM, 5K, OR	ATM, 5K, OR	ATM, 5K, OR	ATM, 5K, OR	ATM, 5K, OR	LOW, 5K, RED	LOW, 5K, RED	LOW, 5K, RED	LOW, 5K, RED	LOW, 5K, RED
20	HIGH, 5K, RED	HIGH, 5K, RED	HIGH, 5K, RED	HIGH, 5K, RED	HIGH, 5K, RED	ATM, 5K, RED	ATM, 5K, RED	ATM, 5K, RED	ATM, 5K, RED	ATM, 5K, RED
30	LOW, 12½K, BRN	LOW, 12½K, BRN	LOW, 12½K, BRN	LOW, 12½K, BRN	LOW, 12½K, BRN	HIGH, 12½K, BRN	HIGH, 12½K, BRN	HIGH, 12½K, BRN	HIGH, 12½K, BRN	HIGH, 12½K, BRN
40	ATM, 12½K, BRN	ATM, 12½K, BRN	ATM, 12½K, BRN	ATM, 12½K, BRN	ATM, 12½K, BRN	PREF-1A	PREF-1B	PREF-1C		
50	PSPLEN-1	PSPLEN-2	PSPLEN-3	PT0-0°-1	PT0-0°-2	PT0-90°-1	PT0-90°-2	PT1-82°-1	PT1-82°-2	
60	PSTANK-1	PSTANK-2	PSTANK-3	PT0-180°-1	PT0-180°-2	PT0-270°-1	PT0-270°-2	PT1-262°-1	PT1-262°-2	
70	PS1-55°-θ	PT1-60°-1	PT1-60°-2	PT1-60°-3	PT1-60°-4	PT1-60°-5	PT1-60°-6	PT1-60°-7	PS1.A-60°	PS1.A-240°
80	PS1-145°-θ	PT1-150°-1	PT1-150°-2	PT1-150°-3	PT1-150°-4	PT1-150°-5	PT1-150°-6	PT1-150°-7	PS1.B-60°	PS1.B-240°
90	PS1-235°-θ	PT1-240°-1	PT1-240°-2	PT1-240°-3	PT1-240°-4	PT1-240°-5	PT1-240°-6	PT1-240°-7	PS1.C-60°	PS1.C-240°
100	PS1-325°-θ	PT1-330°-1	PT1-330°-2	PT1-330°-3	PT1-330°-4	PT1-330°-5	PT1-330°-6	PT1-330°-7	PS1.D-60°	PS1.D-240°
110	PT2-0°-1	PT2-0°-2	PT2-0°-3	PT2-0°-4	PT2-0°-5	PT2-45°-1	PT2-45°-2	PT2-45°-3	PT2-45°-4	PT2-45°-5
120	PT2-90°-1	PT2-90°-2	PT2-90°-3	PT2-90°-4	PT2-90°-5	PT2-135°-1	PT2-135°-2	PT2-135°-3	PT2-135°-4	PT2-135°-5
130	PT2-180°-1	PT2-180°-2	PT2-180°-3	PT2-180°-4	PT2-180°-5	PT2-275°-1	PT2-275°-2	PT2-275°-3	PT2-275°-4	PT2-275°-5
140	PT2-270°-1	PT2-270°-2	PT2-270°-3	PT2-270°-4	PT2-270°-5	PT2-315°-1	PT2-315°-2	PT2-315°-3	PT2-315°-4	PT2-315°-5
150	PS2-θ-5°	PS2-θ-50°	PS2-θ-95°	PS2-θ-140°	PS2-θ-185°	PS2-θ-230°	PS2-θ-275°	PS2-θ-320°	PS2-i-5°	PS2-i-95°
160	PS2-i-185°	PS2-i-275°								
170	------	------	------	BL2-θ-60°-1	BL2-θ-60°-2	BL2-θ-60°-3	BL2-θ-60°-4	BL2-θ-60°-5	BL2-θ-60°-6	BL2-θ-60°-7
180	PT2.1-63°-1	PT2.1-63°-2	PT2.1-63°-3	PT2.1-63°-4	PT2.1-63°-5	PT2.1-243°-1	PT2.1-243°-2	PT2.1-243°-3	PT2.1-243°-4	PT2.1-243°-5
190	PS2.1-66°-θ	PS2.1-246°-θ	------	BT2.1-1	BT2.1-2	BT2.1-3	BT2.1-4	BT2.1-5	BT2.1-6	BT2.1-7
200	PS-EXH.-1 UPSTREAM	PS-EXH.-2 MIDDLE	PS-EXH.-3 DOWNSTREAM	PT-EXH.-1A UPSTREAM	PT-EXH.-2A DOWNSTREAM	PT-EXH.-1B UPSTREAM	PT-EXH.-2B DOWNSTREAM			
210	PT2.2-70°-1	PT2.2-70°-2	PT2.2-70°-3	PT2.2-70°-4	PT2.2-70°-5	PT2.2-250°-1	PT2.2-250°-2	PT2.2-250°-3	PT2.2-250°-4	PT2.2-250°-5
220	PT2.3-68°-1	PT2.3-68°-2	PT2.3-68°-3	PT2.3-68°-4	PT2.3-68°-5	PT2.3-248°-1	PT2.3-248°-2	PT2.3-248°-3	PT2.3-248°-4	PT2.3-248°-5
230	BT2.2-1	BT2.2-2	BT2.2-3	BT2.2-4	BT2.2-5	BT2.2-6	BT2.2-7			
240	BL2.5F-55°-i-1	BL2.5F-55°-i-2	BL2.5F-55°-i-3	BL2.5F-55°-i-4	BL2.5F-55°-i-5	------	------	------	------	------
250	BL2.5-55°-θ-1	BL2.5-55°-θ-2	BL2.5-55°-θ-3	BL2.5-55°-θ-4	BL2.5-55°-θ-5	------	PS86.5-37°-θ	PS6.5-37°-θ	PS6.5-167°-θ	------
260	BL2.5-55°-i-1	BL2.5-55°-i-2	BL2.5-55°-i-3	BL2.5-55°-i-4	BL2.5-55°-i-5	------	PS86.8-37°-θ	PS6.8-37°-θ	PS6.8-167°-θ	------
270	BL2.5F-235°-i-1	BL2.5F-235°-i-2	BL2.5F-235°-i-3	BL2.5F-235°-i-4	BL2.5F-235°-i-5	------	PREF-2A	PREF-2B	PREF-2C	------
280	BL2.5-235°-θ-1	BL2.5-235°-θ-2	BL2.5-235°-θ-3	BL2.5-235°-θ-4	BL2.5-235°-θ-5	------	PREF-3A	PREF-3B	PREF-3C	------
290	BL2.5-235°-i-1	BL2.5-235°-i-2	BL2.5-235°-i-3	BL2.5-235°-i-4	BL2.5-235°-i-5	------	------	------	------	------
300	PT2.5-23°-1	PT2.5-23°-2	PT2.5-23°-3	PS2.5-37°-θ	PS2.5-37°-i	PT2.5F-68°-1	PT2.5F-68°-2	PT2.5F-68°-3	PS2.2-64°-θ	PS2.2-244°-θ
310	PT2.5-113°-1	PT2.5-113°-2	PT2.5-113°-3	PS2.5-98°-θ	PS2.5-98°-i	PT2.5F-248°-1	PT2.5F-248°-2	PT2.5F-248°-3	PS2.3-78°-i	PS2.3-258°-θ
320	PT2.5-293°-1	PT2.5-293°-2	PT2.5-293°-3	PS2.5-278°-θ	PS2.5-278°-i	PT2.5F-338°-1	PT2.5F-338°-2	PT2.5F-338°-3	PS2.5F-84°-i	PS2.5F-264°-i
330	PT6-30°-1	PT6-30°-2	PT6-30°-3	PT6-210°-1	PT6-210°-2	PT6-210°-3	PT6-345°-1	PT6-345°-2	PT6-345°-3	
340	PT6F-30°-1	PT6F-30°-2	PT6F-210°-1	PT6F-210°-2	PT6F-345°-1	PT6F-345°-2	(a)	(a)	(a)	(a)
350	(a)	(a)	(a)	(a)	(a)	(a)	(a)	(a)	(a)	(a)
360	(a)	(a)	(a)	(a)	(a)	(a)	(a)	(a)	(a)	(a)
370	(a)	(a)	(a)	(a)	(a)	(a)	(a)	(a)	(a)	(a)
380	(a)	(a)	(a)	(a)	(a)	(a)	(a)	(a)	(a)	(a)
390	(a)	(a)	(a)	(a)	(a)	(a)	(a)	(a)	(a)	(a)

[a]Block of 45 set aside for CIVV exit angle probes (3 rakes, 3 probes/rake, 5 pressures/probe).

42

TABLE VIII. - SAMPLE COMPUTER PRINTOUT FOR DIGITAL TRANSIENT DATA SYSTEM

MO:DAY:HR:MN:SC:MSEC	44	45	46	47	48	49	50	51	52	53
10 19 22 58 54 711	5.180	5.207	5.168	5.904	10.32	6.471	16.64	17.39	18.43	16.87
10 19 22 58 54 753	5.274	5.184	5.227	6.018	10.39	6.628	16.42	17.10	17.05	16.63
10 19 22 58 54 794	5.217	5.190	5.155	5.849	10.22	6.534	16.62	17.28	18.26	16.80
10 19 22 58 54 836	5.217	5.125	5.140	5.876	10.32	6.628	16.58	17.35	17.95	16.72
10 19 22 58 54 878	5.134	5.153	5.140	5.994	10.44	6.534	16.76	17.00	18.26	16.81
10 19 22 58 54 919	5.274	5.157	5.199	6.019	10.44	6.744	16.32	17.22	18.02	16.69
10 19 22 58 54 961	5.196	5.125	5.195	5.987	10.44	6.587	16.65	17.17	17.00	16.98
10 19 22 58 55 2	5.132	5.066	5.100	6.093	10.27	6.524	16.20	17.21	18.07	16.55
10 19 22 58 55 44	5.134	5.098	5.096	6.056	10.27	6.576	16.64	16.99	18.07	17.09
10 19 22 58 55 86	5.078	5.098	5.140	6.207	10.43	6.471	16.26	17.10	18.19	16.48
10 19 22 58 55 127	5.079	5.125	5.113	6.069	10.43	6.419	16.69	17.27	17.95	16.92
10 19 22 58 55 169	5.130	5.066	5.092	6.065	10.50	6.639	16.65	17.44	17.66	16.72
10 19 22 58 55 210	5.074	5.094	5.027	6.120	10.30	6.492	16.81	17.33	18.38	16.93
10 19 22 58 55 252	5.110	5.129	5.063	6.211	10.41	6.524	16.53	17.05	17.71	16.29
10 19 22 58 55 294	5.191	5.172	5.133	6.133	10.39	6.692	16.70	17.17	18.50	16.96
10 19 22 58 55 335	5.192	5.020	5.054	5.845	10.27	6.576	16.26	17.21	17.95	16.48
10 19 22 58 55 377	5.191	5.145	5.160	6.117	10.32	6.602	16.72	17.02	17.59	16.55
10 19 22 58 55 418	5.161	5.084	5.140	6.042	10.47	6.482	16.54	17.11	17.90	16.47
10 19 22 58 55 460	5.192	5.094	5.163	6.038	10.22	6.482	16.48	17.11	18.38	16.33
10 19 22 58 55 502	5.130	4.956	5.027	5.762	10.27	6.314	16.15	17.05	17.82	16.19
10 19 22 58 55 543	5.130	5.129	5.109	5.936	10.05	6.209	16.47	16.75	18.19	16.36
10 19 22 58 55 585	5.213	5.011	5.092	5.872	10.16	6.209	16.20	17.16	17.95	16.59
10 19 22 58 55 626	5.079	5.070	5.113	5.987	10.11	5.947	16.42	16.94	17.35	16.09
10 19 22 58 55 668	5.130	5.066	5.054	6.065	10.16	6.104	15.93	16.89	18.07	16.28
10 19 22 58 55 710	5.165	5.129	5.145	5.742	10.06	6.115	16.54	17.00	18.02	16.25
10 19 22 58 55 751	5.133	5.011	5.000	5.845	10.17	6.272	16.32	17.11	18.02	16.33
10 19 22 58 55 793	5.050	5.070	5.113	5.601	10.25	6.010	16.32	16.95	17.66	15.84
10 19 22 58 55 834	4.995	5.190	5.004	5.766	10.06	5.958	15.94	16.73	17.90	15.48
10 19 22 58 55 876	5.074	5.011	4.972	5.707	10.01	5.748	16.32	17.06	18.02	15.98
10 19 22 58 55 918	5.019	5.011	5.054	5.679	9.944	5.738	15.76	16.83	17.59	15.76
10 19 22 58 55 959	5.199	4.998	4.999	5.766	9.836	5.685	16.04	16.89	18.19	16.00
10 19 22 58 56 1	5.134	4.999	4.977	5.976	9.895	5.685	16.09	16.72	18.19	15.61
10 19 22 58 56 42	5.023	4.999	5.059	5.656	10.06	5.853	16.21	17.00	18.02	16.35
10 19 22 58 56 84	5.113	5.074	5.026	5.799	9.741	5.738	15.82	16.72	17.71	16.36
10 19 22 58 56 126	4.966	5.047	5.000	6.046	9.944	5.528	16.06	16.94	17.59	15.76
10 19 22 58 56 167	5.010	5.011	4.945	5.762	9.727	5.423	15.71	16.56	17.95	15.83
10 19 22 58 56 209	5.079	4.960	4.945	5.902	9.702	5.381	15.94	16.57	18.02	15.16
10 19 22 58 56 250	4.909	4.974	4.945	5.707	9.944	5.318	15.32	16.34	17.35	14.69
10 19 22 58 56 292	4.967	4.906	4.977	5.845	9.845	4.910	15.55	15.69	17.66	14.99
10 19 22 58 56 334	4.967	4.906	4.945	5.656	9.627	4.726	14.95	15.91	17.42	14.75
10 19 22 58 56 375	4.930	4.960	4.922	5.704	9.736	4.700	15.33	15.80	17.30	14.70
10 19 22 58 56 417	4.967	4.878	4.895	5.711	9.786	4.407	14.92	15.50	16.67	14.45
10 19 22 58 56 458	4.914	4.910	4.900	5.743	9.510	4.532	15.43	16.12	17.23	14.35
10 19 22 58 56 500	4.930	4.822	4.813	5.735	9.573	4.753	15.00	15.58	17.06	14.63
10 19 22 58 56 542	4.797	4.792	4.781	5.624	9.682	4.491	14.95	15.69	17.24	14.29
10 19 22 58 56 583	4.943	4.882	4.804	5.660	9.510	4.699	14.61	15.19	16.51	14.86
10 19 22 58 56 625	4.852	4.792	4.863	5.762	9.541	4.721	15.25	15.50	16.67	14.36
10 19 22 58 56 666	4.829	4.769	4.840	5.573	9.627	4.505	14.81	15.31	16.34	14.17
10 19 22 58 56 708	4.898	4.882	4.872	5.853	9.682	4.543	15.22	15.64	16.94	14.44
10 19 22 58 56 750	4.956	4.864	4.796	5.573	9.456	4.490	14.67	15.35	17.23	14.49

43

TABLE IX. - CHANNEL IDENTIFICATION FOR DIGITAL TRANSIENT DATA SYSTEM

Channel	Identification	Channel	Identification	Channel	Identification	Channel	Identification
0	MARKER	51	PT2.5-23°-2	101	T2.1-250°-2	151	T2.5F-293°-2
1	PREF-1	52	PT2.5-23°-3	102	T2.1-250°-3	152	T2.5F-293°-3
2	PREF-2	53	PT2.5-113°-1	103	T2.1-250°-4	153	T2.5F-293°-4
3	PREF-3	54	PT2.5-113°-2	104	T2.1-250°-5	154	T2.5F-293°-5
4	N1	55	PT2.5-293°-1	105	T2.2-67°-1	155	T3-22°-1
5	N2	56	PT2.5-293°-2	106	T2.2-67°-2	156	T3-22°-2
6	A8	57	PT2.5-293°-3	107	T2.2-67°-3	157	T3-22°-3
7	PLA	58	PS2.5-98°-i	108	T2.2-67°-4	158	T3-202°-1
8	SPARE	59	PS2.5-278°-θ	109	T2.2-67°-5	159	T3-202°-2
9	CIVV	60	PS2.5-278°-i	110	T2.2-247°-1	160	T3-202°-3
10	RCVV	61	PT2.5F-68°-1	111	T2.2-247°-2	161	T3-337°-1
11	WFE	62	PT2.5F-68°-3	112	T2.2-247°-3	162	T3-337°-2
12	WFTHI-1	63	PT2.5F-248°-1	113	T2.2-247°-4	163	T3-337°-3
13	TFE	64	PT2.5F-248°-2	114	T2.2-247°-5	164	T4.5-43°-1
14	TFT	65	PT2.5F-248°-3	115	T2.3-68°-1	165	T4.5-43°-2
15	PT2-90°-3	66	PT2.5F-338°-1	116	T2.3-68°-2	166	T4.5-43°-3
16	PS2-95°-θ	67	PT2.5F-338°-2	117	T2.3-68°-3	167	T4.5-229°-1
17	PS2.1-66°-θ	68	PT2.5F-338°-3	118	T2.3-68°-4	168	T4.5-229°-2
18	PS2.2-64°-θ	69	PS2.5F-84°-i	119	T2.3-68°-5	169	T4.5-229°-3
19	PS2.3-78°-θ	70	PS2.5F-264°-θ	120	T2.3-248°-1	170	FTIT-5°
20	PT2.5-113°-2	71	PS2.5F-264°-i	121	T2.3-248°-2	171	FTIT-52°
21	PS2.5-98°-θ	72	PT3-67°-1	122	T2.3-248°-3	172	FTIT-110°
22	PT2.5F-68°-2	73	PT3-157°-1	123	T2.3-248°-4	173	FTIT-156°
23	PS2.5F-84°-θ	74	PT3-157°-2	124	T2.3-248°-5	174	FTIT-203°
24	PT3-67°-2	75	PS3-143°-θ	125	T2.5-68°-1	175	FTIT-273°
25	PS3-50°-θ	76	PT3-292°-1	126	T2.5-68°-2	176	FTIT-319°
26	PS6.5-37°-θ	77	PT3-292°-2	127	T2.5-68°-3	177	FTIT(AVG)
27	PS6.8-37°-θ	78	PS3-323°-θ	128	T2.5-68°-4	173	T6-75°-1
28	SPARE	79	PS6.5-167°-θ	129	T2.5-68°-5	179	T6-75°-2
29	SPARE	80	PS6.5-282°-θ	130	T2.5-248°-1	180	T6-75°-3
30	SPARE	81	PS6.8-167°-θ	131	T2.5-248°-2	181	T6-210°-1
31	PT2-90°-1	82	PS6.8-282°-θ	132	T2.5-248°-3	182	T6-210°-2
32	PT2-90°-2	83	PS1.A-60°-θ	133	T2.5-248°-4	183	T6-210°-3
33	PT2-90°-4	84	PS1.A-240°-θ	134	T2.5-248°-5	184	T6-300°-1
34	PT2-90°-5	85	PS1.B-60°-θ	135	T2.5-338°-1	185	T6-300°-2
35	PT2-270°-1	86	PS1.B-240°-θ	136	T2.5-338°-2	186	T6-300°-3
36	PT2-270°-2	87	PS1.C-60°-θ	137	T2.5-338°-3	187	T6F-75°-1
37	PT2-270°-3	88	PS1.C-240°-θ	138	T2.5-338°-4	188	T6F-75°-2
38	PT2-270°-4	89	PS1.D-60°-θ	139	T2.5-338°-5	189	TSO5-1
39	PT2-270°-5	90	PS1.D-240°-θ	140	T2.5F-23°-1	190	TSO5-2
40	PS2-5°-θ	91	T1-15°-2	141	T2.5F-23°-2	191	T6F-300°-1
41	PS2-50°-θ	92	T1-105°-2	142	T2.5F-23°-3	192	T6F-300°-2
42	PS2-140°-θ	93	T1-195°-2	143	T2.5F-23°-4	193	SPARE
43	PS2-185°-θ	94	T1-285°-2	144	T2.5F-23°-5	194	
44	PS2-230°-θ	95	T2.1-70°-1	145	T2.5F-113°-1	195	
45	PS2-275°-θ	96	T2.1-70°-2	146	T2.5F-113°-2	196	
46	PS2-320°-θ	97	T2.1-70°-3	147	T2.5F-113°-3	197	
47	PS2.1-246°-θ	98	T2.1-70°-4	148	T2.5F-113°-4	198	
48	PS2.2-244°-θ	99	T2.1-70°-5	149	T2.5F-113°-5	199	
49	PS2.3-258°-θ	100	T2.1-250°-1	150	T2.5F-293°-1	200	
50	PT2.5-23°-1						

TABLE X. - CENTER FREQUENCIES FOR INTERRANGE-INSTRUMENT-GROUP-

(IRIG-) BASED ANALOG MULTIPLEX SYSTEM

Channel	Center frequency, kHz	Full-scale deviation, kHz
1	128	±16
2	192	
3	256	
4	320	
5	384	
6	448	
7	512	
8	576	
9	640	
10	704	
11	768	
12	832	
13	896	
14	960	
15	1024	
Tape speed compensation	1408	±32

TABLE XI. - ANALOG TRANSIENT DATA SYSTEM INSTRUMENTATION

Channel	Multiplex unit											
	1	2	3	4	5	6	7	8	9	10	11	12
1	$PT2-90^{o}-1$	TIP101	$PS2.1-66^{o}-\theta$	ASMT107	$PT3-67^{o}-1$	ASTE115	CX121	ASTE212	Marker PT2 (Stathum)	TIP202	ODLE1	ASMT207
2	$PT2-90^{o}-2$	TIP102	$PS2.1-246^{o}-\theta$	ASMT108	$PT3-67^{o}-2$	ASTE116	CX122	ASTE213		TIP203	ODLE2	ASMT208
3	$PT2-90^{o}-3$	TIP103	$PS2.2-64^{o}-\theta$	ASMT109	$PT3-157^{o}-1$	ASTE117	CX123	CC219	TT2	TIP204	ODLE3	ASMT209
4	$PT2-90^{o}-4$	TIP104	$PS2.2-244^{o}-\theta$	ASMT110	$PT3-157^{o}-2$	ASTE118	CX124	CC220	A8	TIP205	ODLE4	ASMT210
5	$PT2-90^{o}-5$	TIP106	$PS2.3-78^{o}-\theta$	ASMT111	$PT3-292^{o}-1$	ASTE119	CC125	TIP302	CIVV	CX215	ODMT6	WEB226
6	$PT2-270^{o}-1$	WEB137	$PS2.3-258^{o}-\theta$	ASMT112	$PT3-292^{o}-2$	ASTE120	CC126	TIP303	RCVV	CX216	ODMT7	WEB227
7	$PT2-270^{o}-2$	WEB139	$PT2.5-23^{o}-1$	ASMT113	$PT2.5F-68^{o}-1$	FILLET133	CC127	TIP304	CX311	CX217	ODMT8	WEB228
8	$PT2-270^{o}-3$	WEB140	$PT2.5-23^{o}-2$	ASMT114	$PT2.5F-68^{o}-2$	FILLET134	CC128	TIP305	CX312	RMT222	MSMT9	WEB320
9	$PT2-270^{o}-4$	RMT129	$PT2.5-23^{o}-3$	RMT131	$PT2.5F-68^{o}-3$	FILLET135	1/REV N1A,AC	ASMT308	CC314	RMT223	MSMT10	WEB321
10	$PT2-270^{o}-5$	RMT130	$PT2.5-113^{o}-1$	RMT132	$PT2.5F-248^{o}-1$	FILLET136	40/REV N2,AC	ASMT309	CC315	RMT224	MSMT11	WEB322
11	$PS2-95^{o}-\theta$	$PS2.5-98^{o}-\theta$	$PT2.5-113^{o}-2$	$PS2.5-98^{o}-i$	$PT2.5F-248^{o}-2$	38/REV N1B,AC	N1, DC	TIP301	CX310	TIP201	ODMT13	WEB319
12	$PS2-275^{o}-\theta$	$PS2.5-278^{o}-\theta$	$PT2.5-113^{o}-3$	$PS2.5-278^{o}-i$	$PT2.5F-248^{o}-3$	--------	N2, DC	ASMT306	CC313	ASMT206	ODMT14	RMT221
13	$PS3-50^{o}-\theta$	$PS2.5F-84^{o}-\theta$	$PT2.5-293^{o}-1$	$PS2.5F-84^{o}-i$	$PT2.5F-338^{o}-1$	--------	MSMT-CX22	ASMT307	RMT316	ASTE211	ODMT16	WEB225
14	$PS3-143^{o}-\theta$	$PS2.5F-264^{o}-\theta$	$PT2.5-293^{o}-2$	$PS2.5F-264^{o}-i$	$PT2.5F-338^{o}-2$	--------	MSMT-CX23	--------	RMT317	CX214	ODTE18	--------
15	$PS3-323^{o}-\theta$	$PS6.5-37^{o}-\theta$	$PT2.5-293^{o}-3$	$PS6.8-37^{o}-\theta$	$PT2.5F-338^{o}-3$	--------	MSMT-CX24	--------	RMT318	CC218	--------	--------
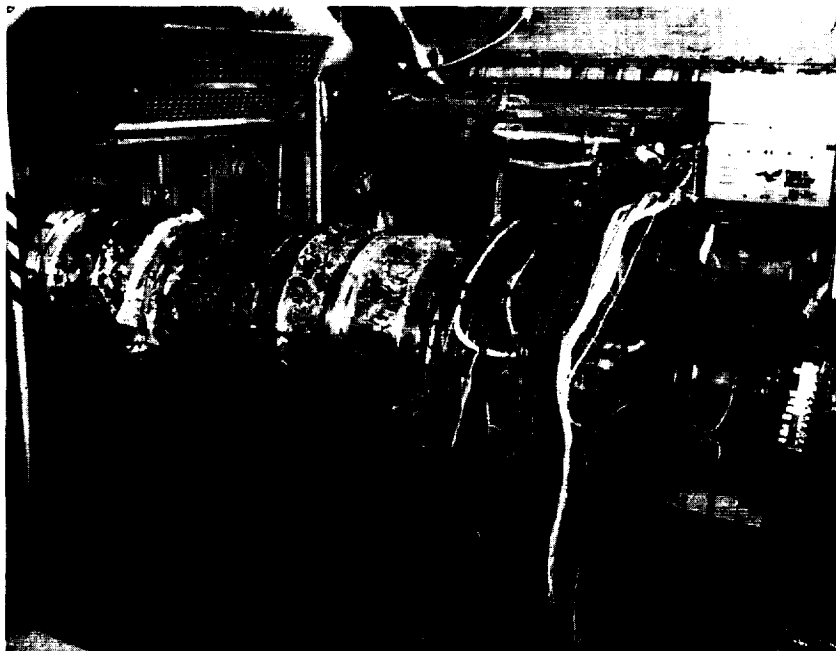
(a) Inlet duct and forward half of engine.
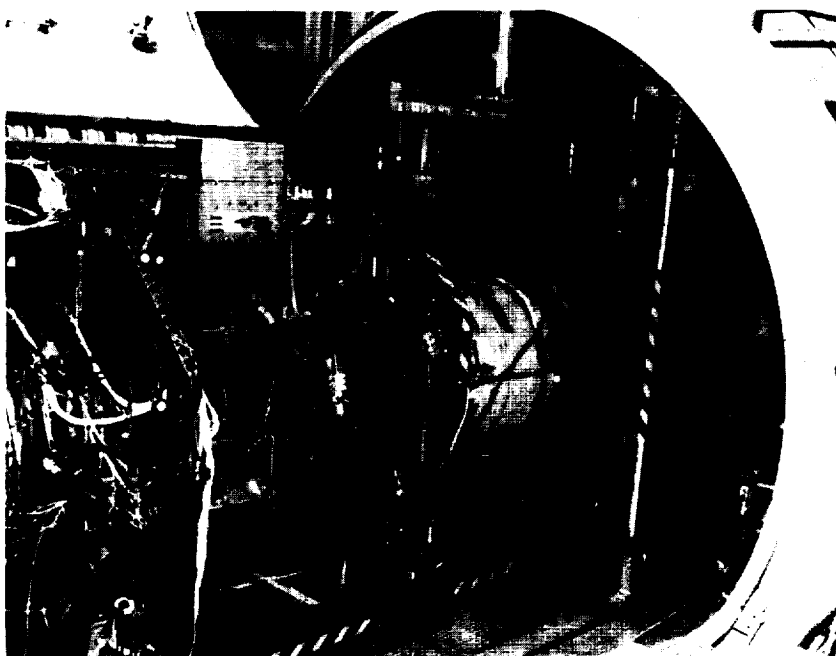
(b) Engine, nozzle plug support, and exhaust collector.

Figure 1. - Engine installation.

Location	Distance upstream from inlet flange	
	cm	in.
Station 0	389.9	153.5
Station 1	235.0	92.5
Support grid	61.0	24.0
Station 2	13.7	5.4

(a) Engine installation.

(b) Fan.
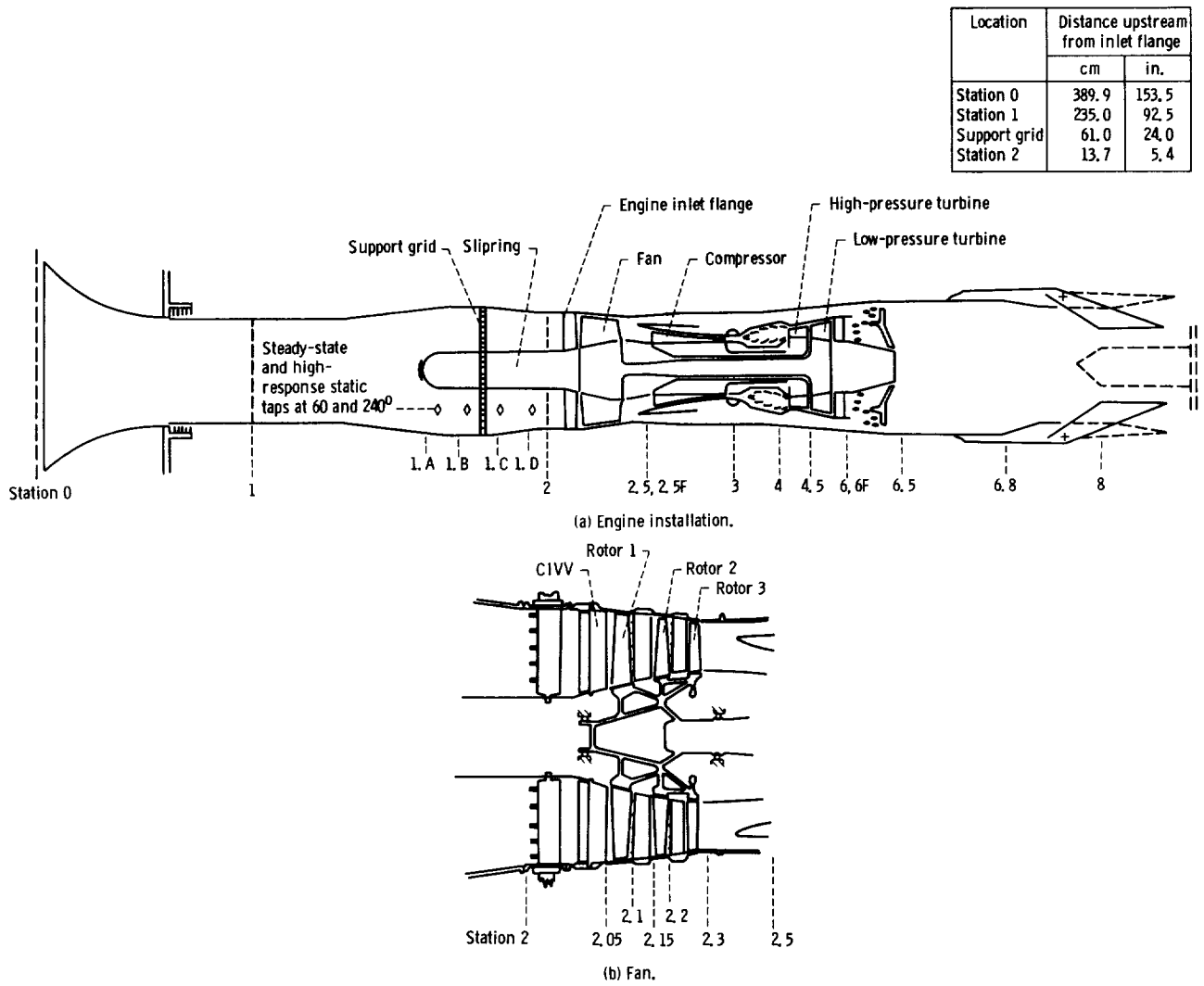
Figure 2. - Schematic of YF100 engine installation and aerodynamic measuring stations.

48

Station 0 (bellmouth inlet)

Station 1 (airflow meas-
uring station)

Station 2 (engine inlet
instrumentation)

Station 2. 1 (in stator
vanes)

Station 2. 2 (in stator
vanes)

Station 2. 3 (between
rotor and stator)

Station 2. 5 (fan exit
and high-pressure-
compressor inlet)

Station 3 (high-pressure-
compressor exit)

Station 4 (combustor exit)

Station 4. 5 (high-pressure-
turbine exit)

Station 6 (low-pressure-
turbine and fan
duct exit)

Station 6. 5 and 6. 8 (after-
burner liner wall)

×	Thermocouple (steady-state)
○	Total-pressure tap (steady-state and high-response)
●	Total-pressure tap (steady-state)
◇	Static-pressure wall tap (steady-state and high-response)
◆	Static-pressure wall tap (steady-state)

(c) Schematic of aerodynamic instrumentation locations at each measuring station (viewed looking upstream).

Figure 2. - Concluded.
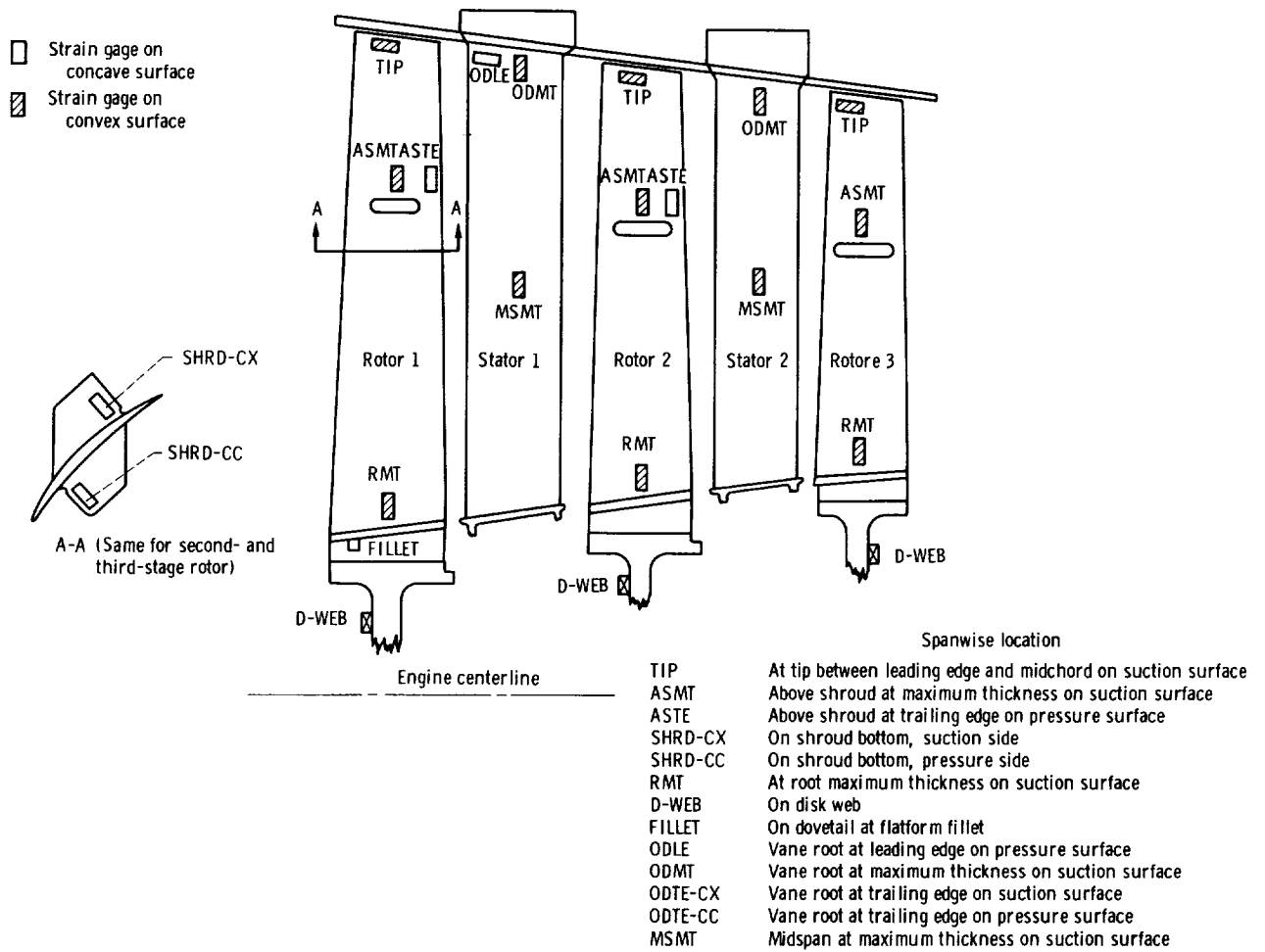
Figure 3. - Locations and designations of fan strain gages.

Strain gage on concave surface

Strain gage on convex surface

Spanwise location

TIP	At tip between leading edge and midchord on suction surface
ASMT	Above shroud at maximum thickness on suction surface
ASTE	Above shroud at trailing edge on pressure surface
SHRD-CX	On shroud bottom, suction side
SHRD-CC	On shroud bottom, pressure side
RMT	At root maximum thickness on suction surface
D-WEB	On disk web
FILLET	On dovetail at flatform fillet
ODLE	Vane root at leading edge on pressure surface
ODMT	Vane root at maximum thickness on suction surface
ODTE-CX	Vane root at trailing edge on suction surface
ODTE-CC	Vane root at trailing edge on pressure surface
MSMT	Midspan at maximum thickness on suction surface

(a) Radial-axial plane.

50

Strain gage		Spanwise location
101-106	TIP	At tip between leading edge and midchord on suction surface
107-114	ASMT	Above shroud at maximum thickness on suction surface
115-120	ASTE	Above shroud at trailing edge on pressure surface
121-124	SHRD-CX	On shroud bottom, suction surface
125-128	SHRD-CC	On shroud bottom, pressure surface
129-132	RMT	At root maximum thickness on suction surface
133-136	FILLET	On dovetail at platform fillet
137-140	D-WEB	On disk web

(b) First-stage rotor strain-gage circumferential locations (looking upstream).

Figure 3. – Continued.

Strain
gage
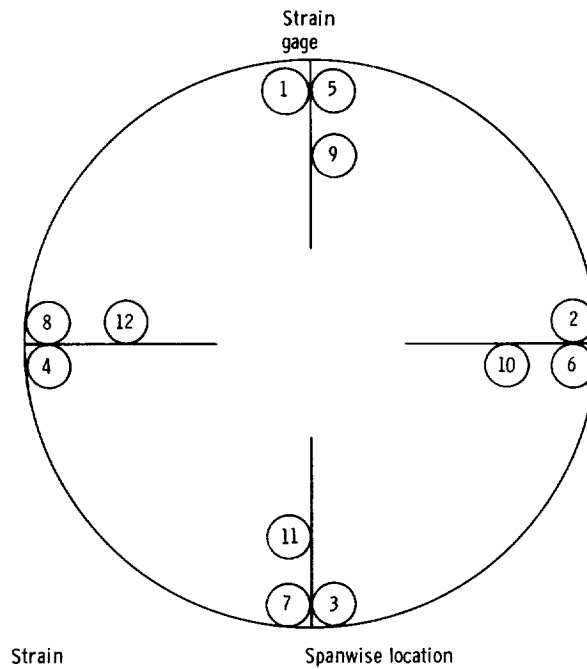
Strain gage		Spanwise location
1-4	ODLE	Vane root at leading edge on pressure surface
5-8	ODMT	Vane root at maximum thickness on suction surface
9-12	MSMT	Midspan at maximum thickness on suction surface

(c) First-stage stator strain-gage circumferential locations (looking upstream).

Figure 3. – Continued.

52
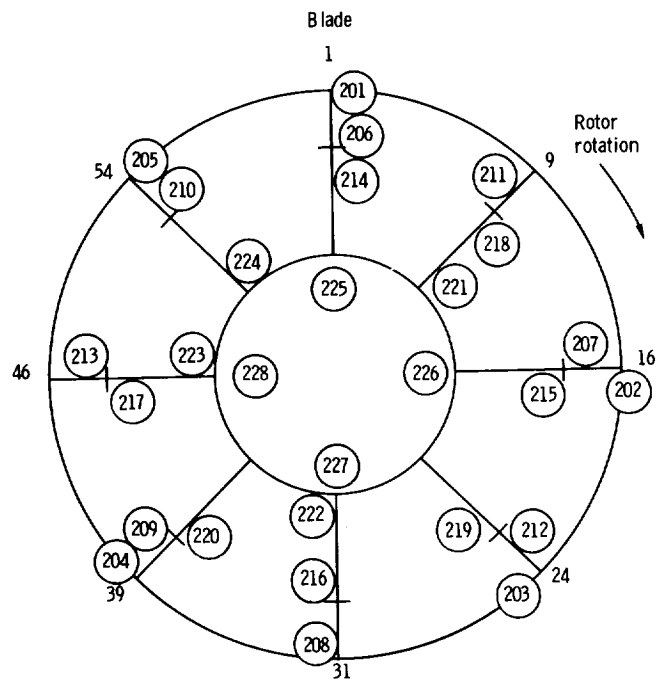
Strain gage		Spanwise location
201-205	TIP	At tip between leading edge and midchord on suction surface
206-210	ASMT	Above shroud at maximum thickness on suction surface
211-213	ASTE	Above shroud at trailing edge on pressure surface
214-217	SHRD-CX	On shroud bottom, suction side
218-220	SHRD-CC	On shroud bottom, pressure side
221-224	RMT	At root maximum thickness on suction surface
225-228	D-WEB	On disk web

(d) Second-stage rotor strain-gage circumferential locations (looking upstream).

Figure 3. - Continued.

53

Strain gage		Spanwise location
13-16	ODMT	Vane root at maximum thickness on suction surface
17-18	ODTE-CX	Vane root at trailing edge on suction surface
19-20	ODTE-CC	Vane root at trailing edge on pressure surface
21-24	MSMT	Midspan at maximum thickness on suction surface
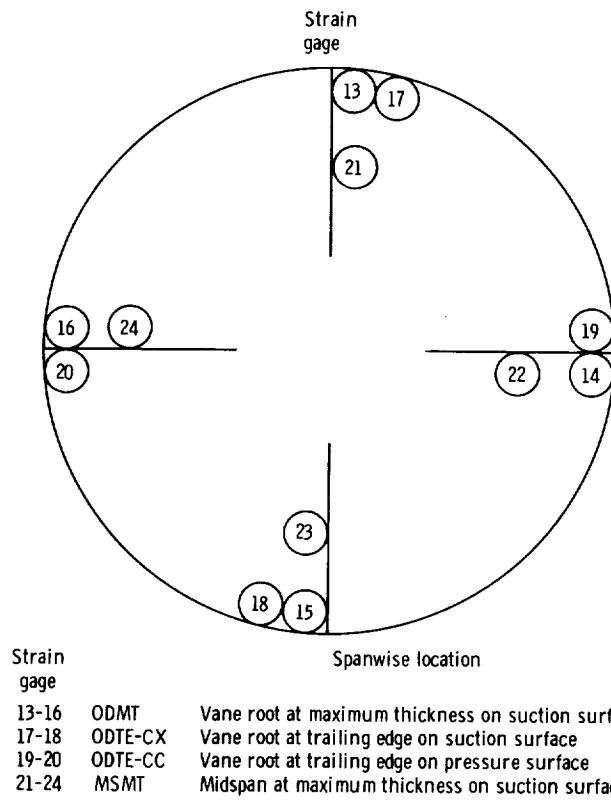
(e) Second-stage stator strain-gage circumferential locations (looking upstream).

Figure 3. – Continued.
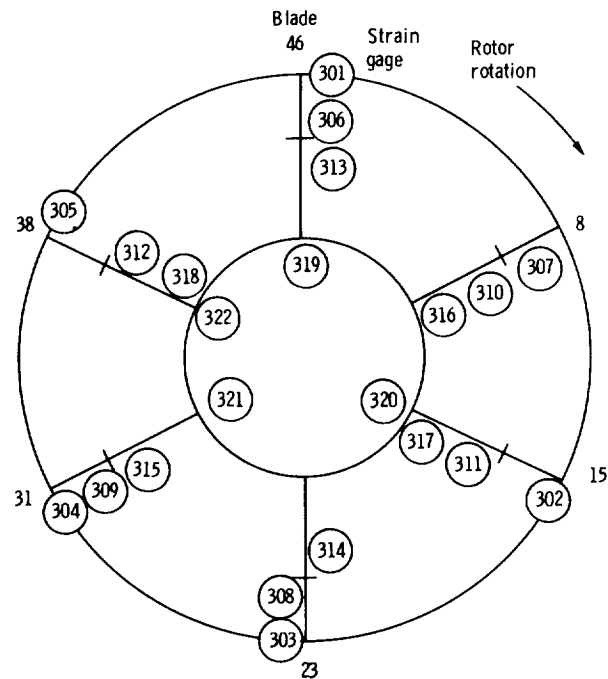
Strain gage		Spanwise location
301-305	TIP	At tip between leading edge and midchord on suction surface
306-309	ASMT	Above shroud at maximum thickness on suction surface
310-312	SHRD-CX	On shroud bottom, suction side
313-315	SHRD-CC	On shroud bottom, pressure side
316-318	RMT	At root maximum thickness on suction side
319-322	D-WEB	On disk web

(f) Third-stage rotor strain-gage circumferential locations (looking upstream).

Figure 3. – Concluded.
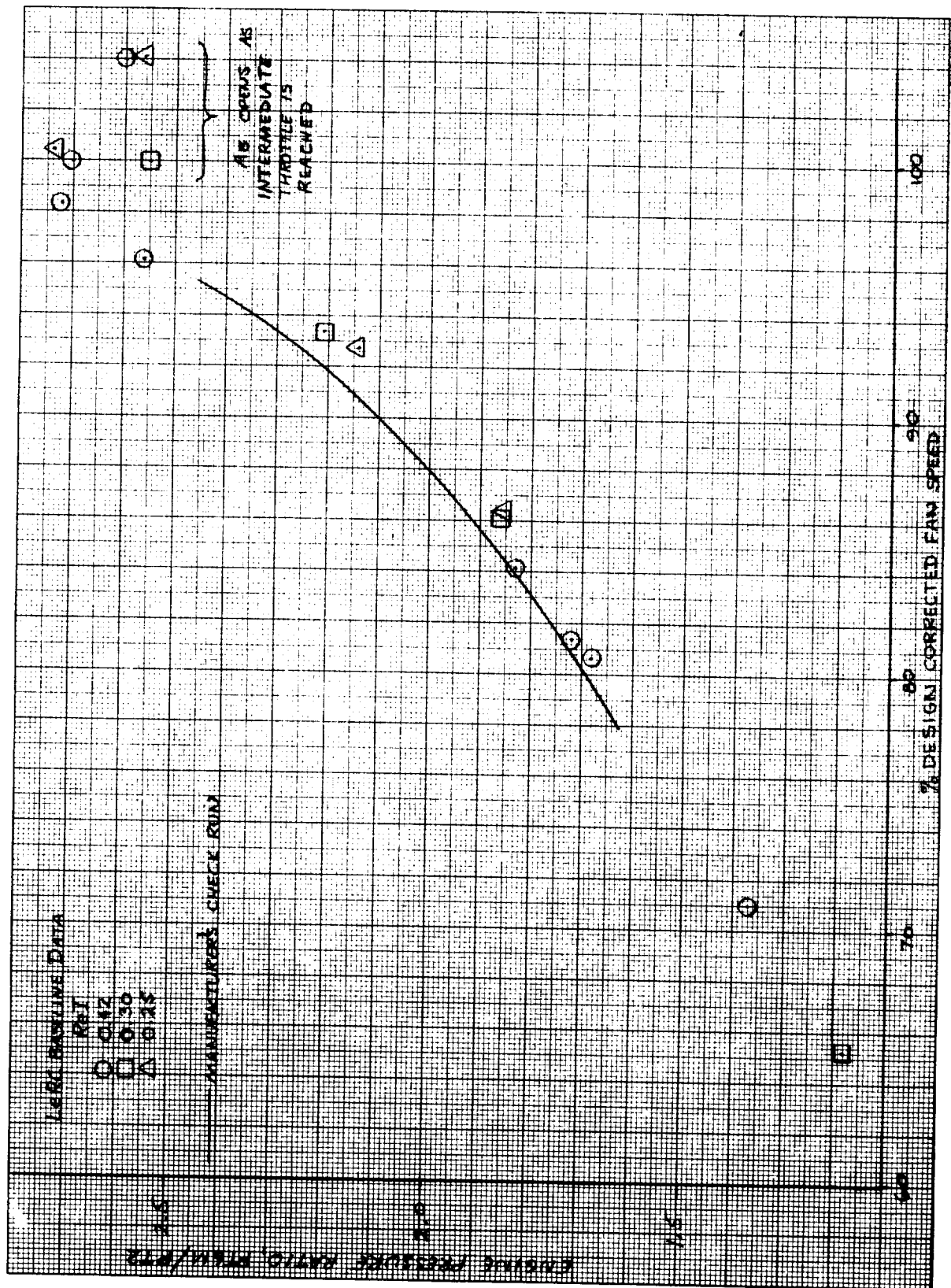
(a) Engine pressure ratio.

Figure 4. – Engine operating characteristics.

56

(b) Engine bypass ratio.

Figure 4. – Continued.

57
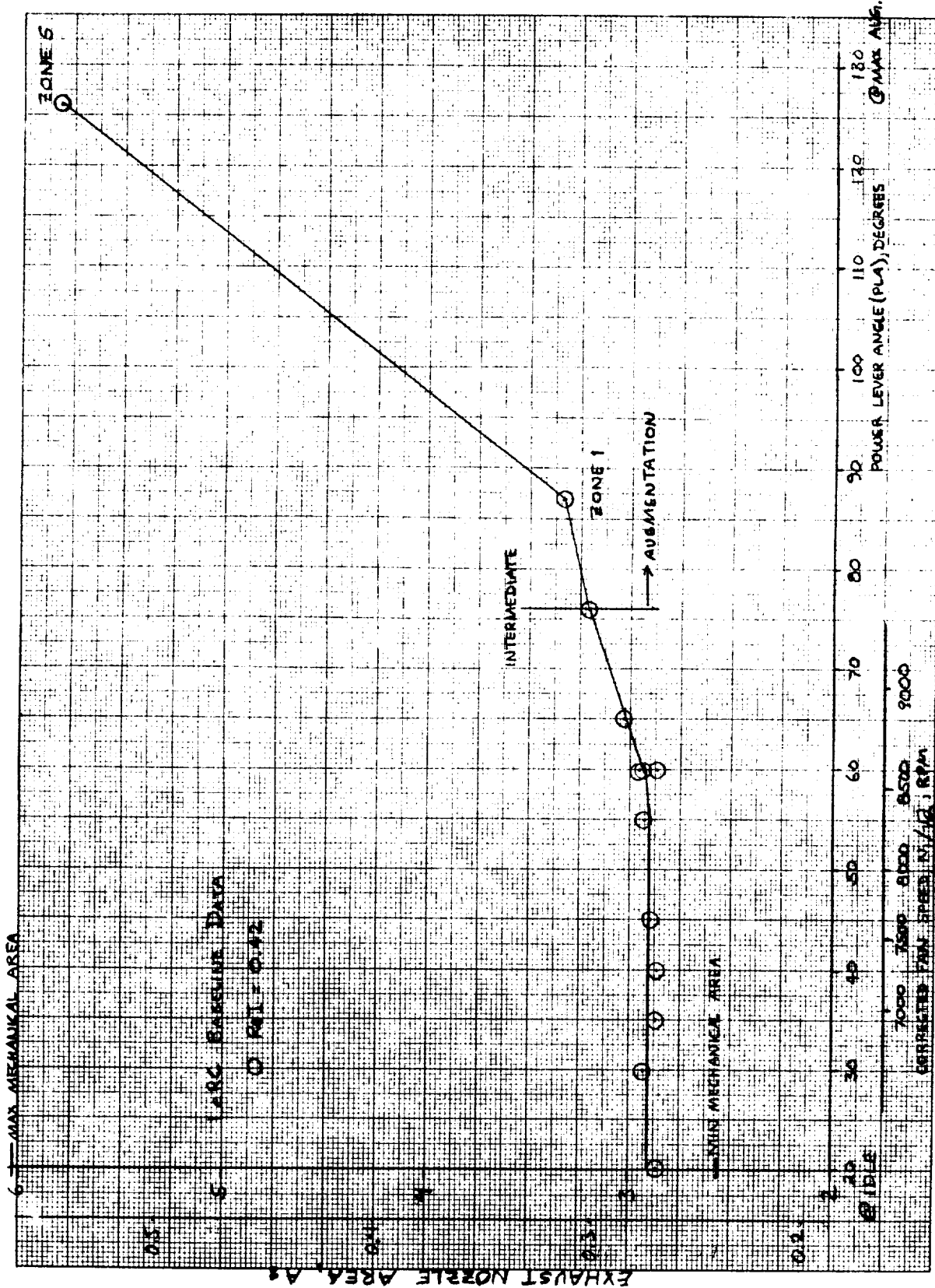
(c) Engine exhaust-nozzle throat area; idle area reset off.

Figure 4. – Concluded.
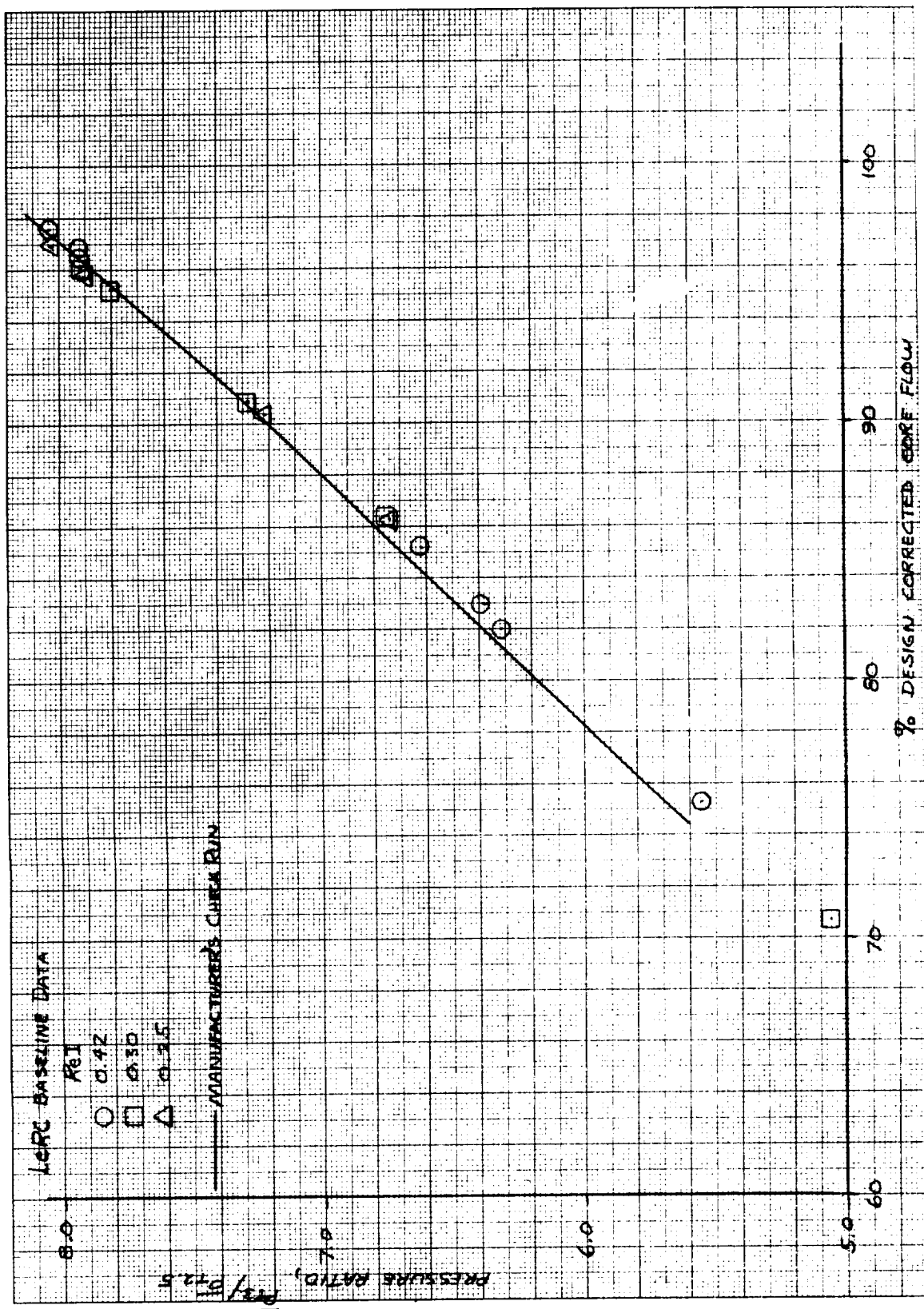
(a) Core compressor operating line.

Figure 5. – Compressor system operating characteristics.

59
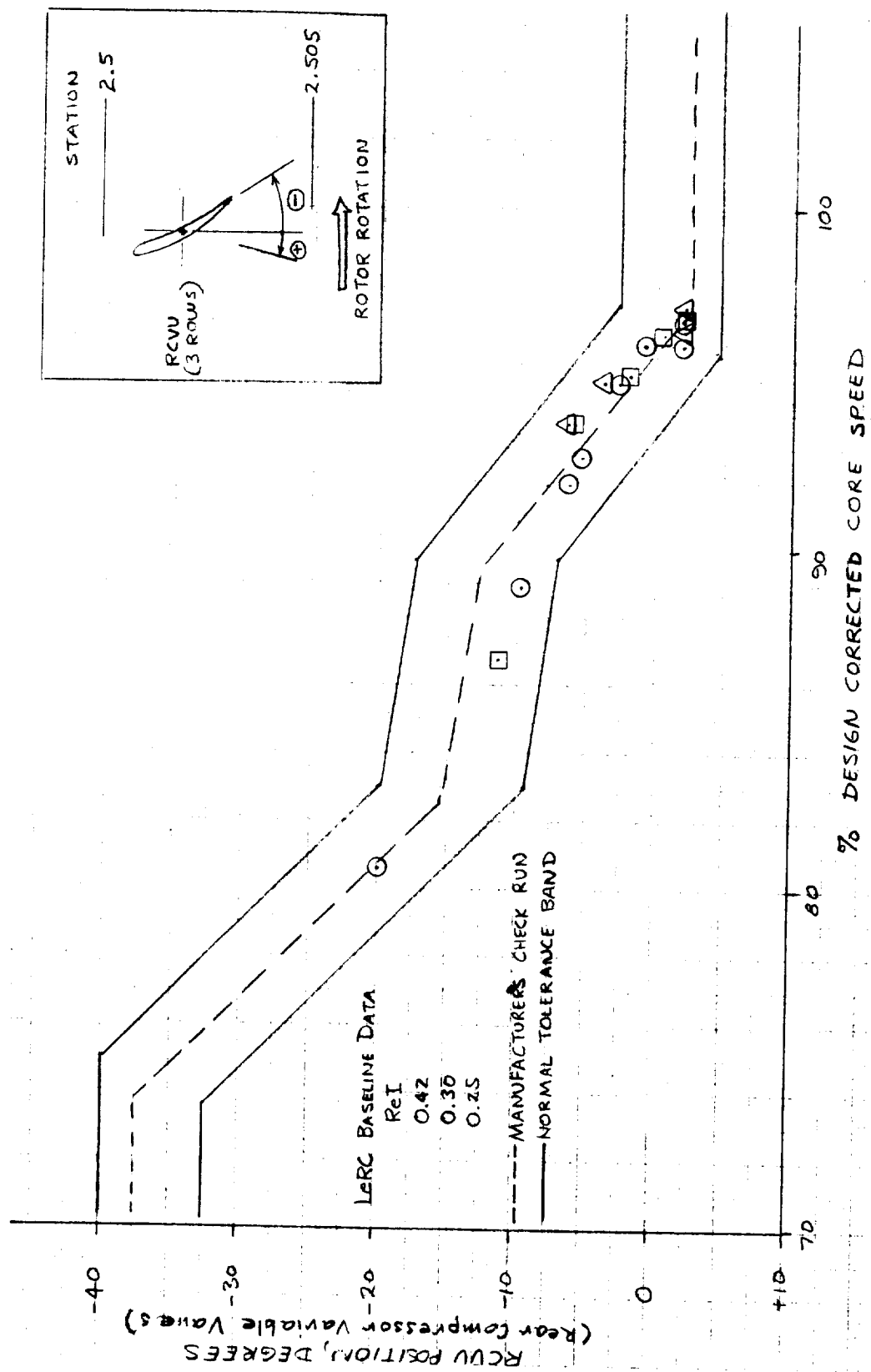
(b) Core compressor variable vane schedule.

Figure 5. – Continued.

60
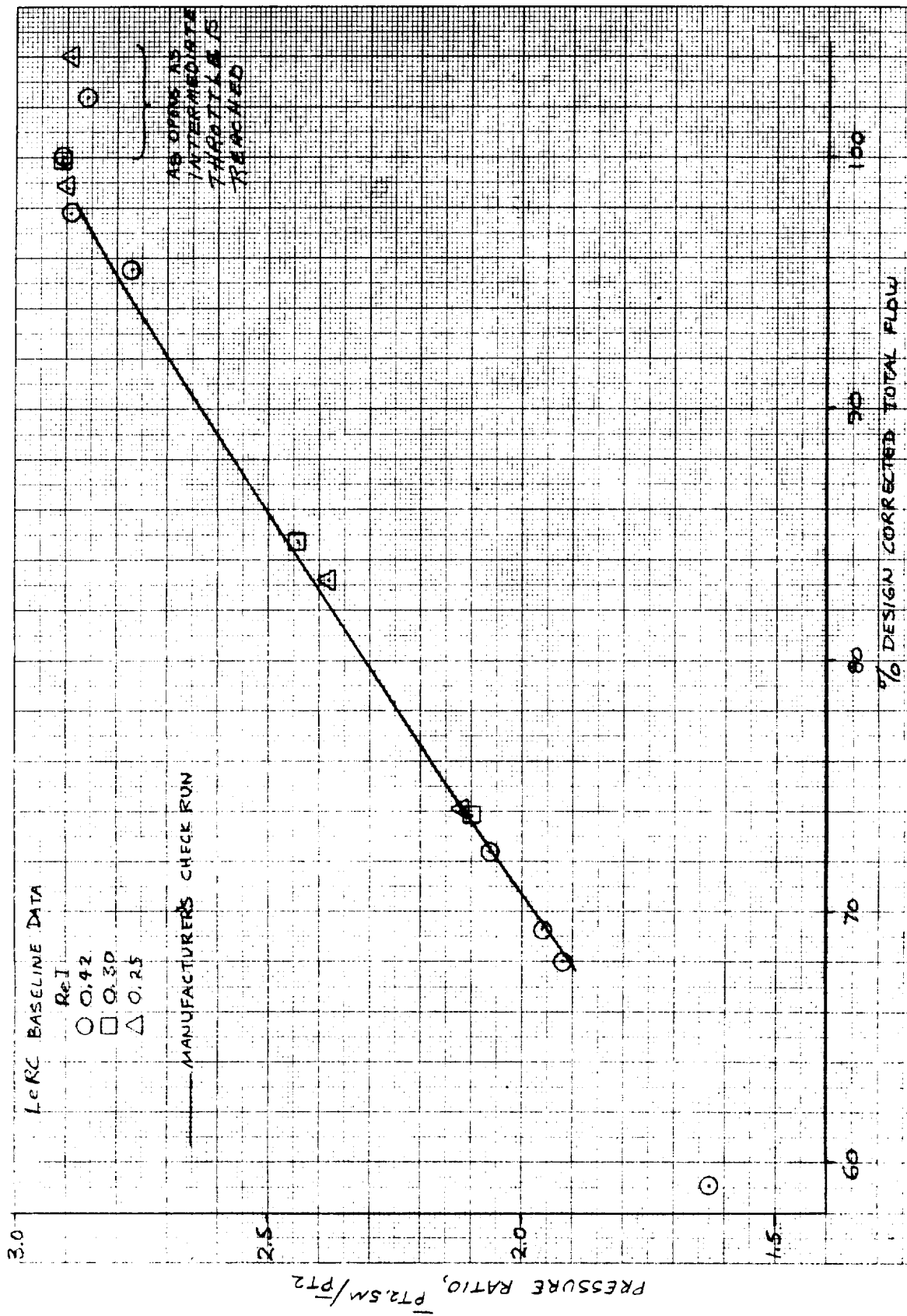
(c) Fan operating line.

Figure 5. – Continued.

61

(d) Fan inlet variable vane schedule.

Figure 5. – Concluded.

62
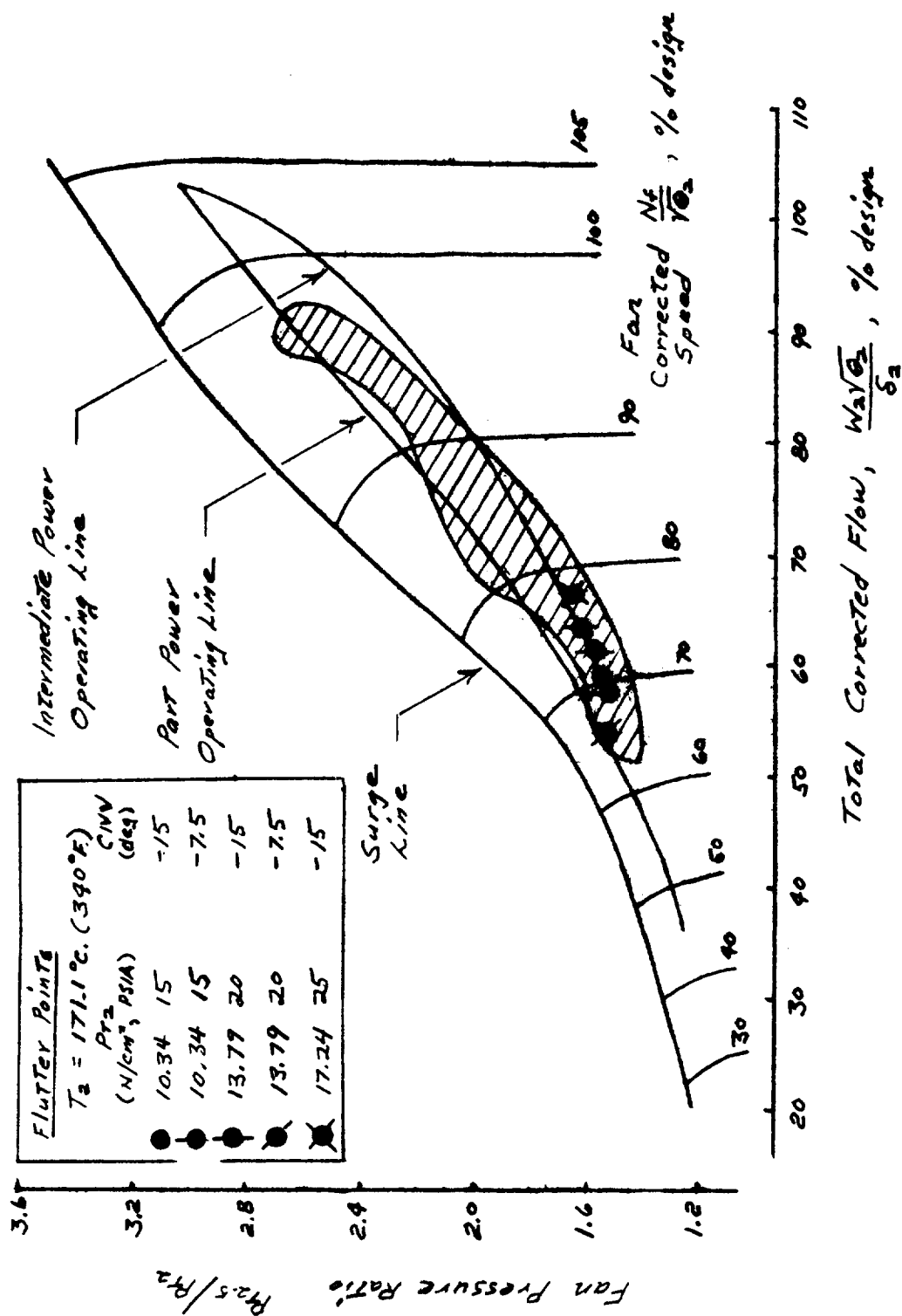
(a) Region covered on design performance map.

Figure 6. – Fan flutter mapping.

63
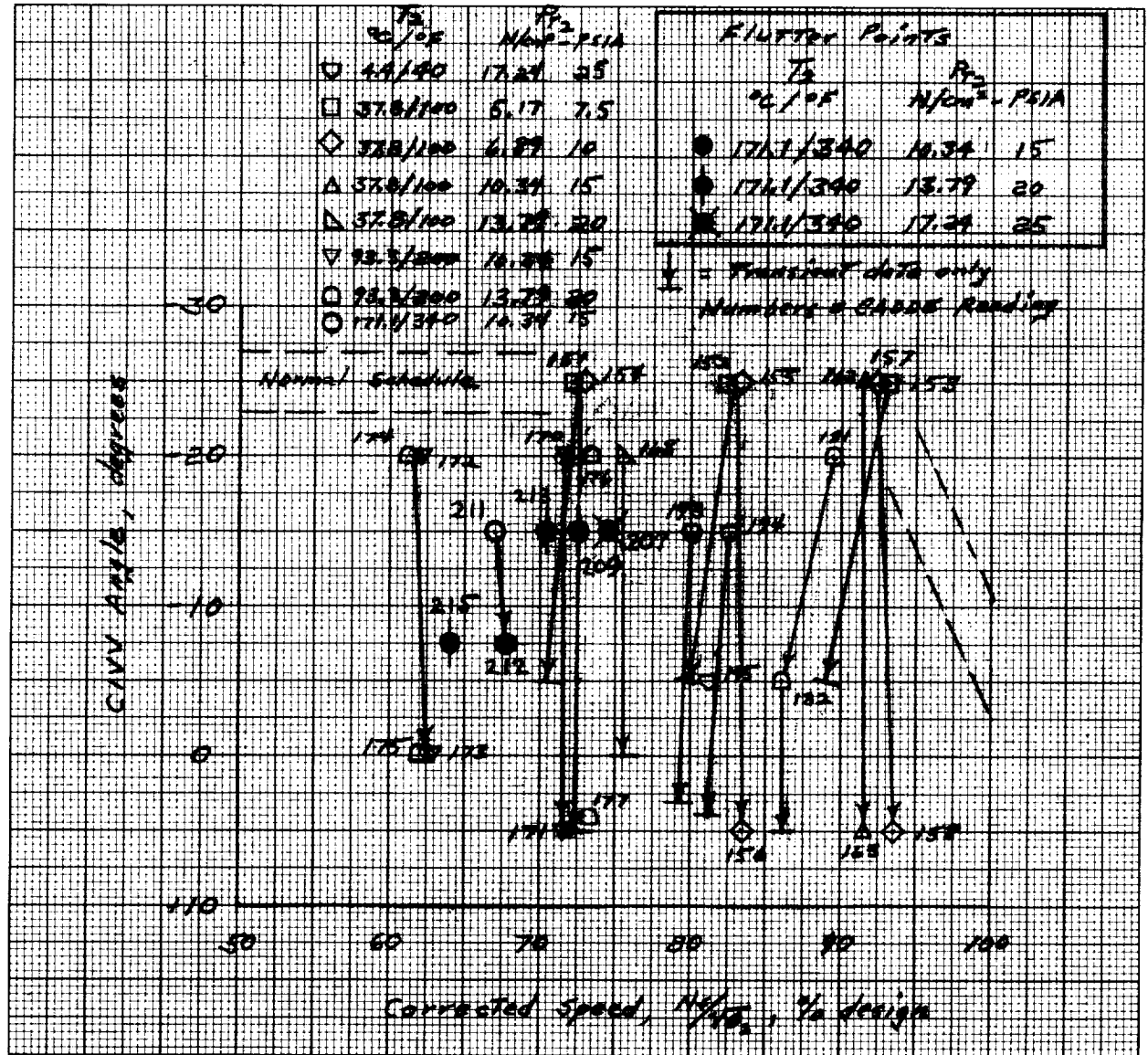
(b) Excursions in CIVV angle.

Figure 6. - Continued.

64
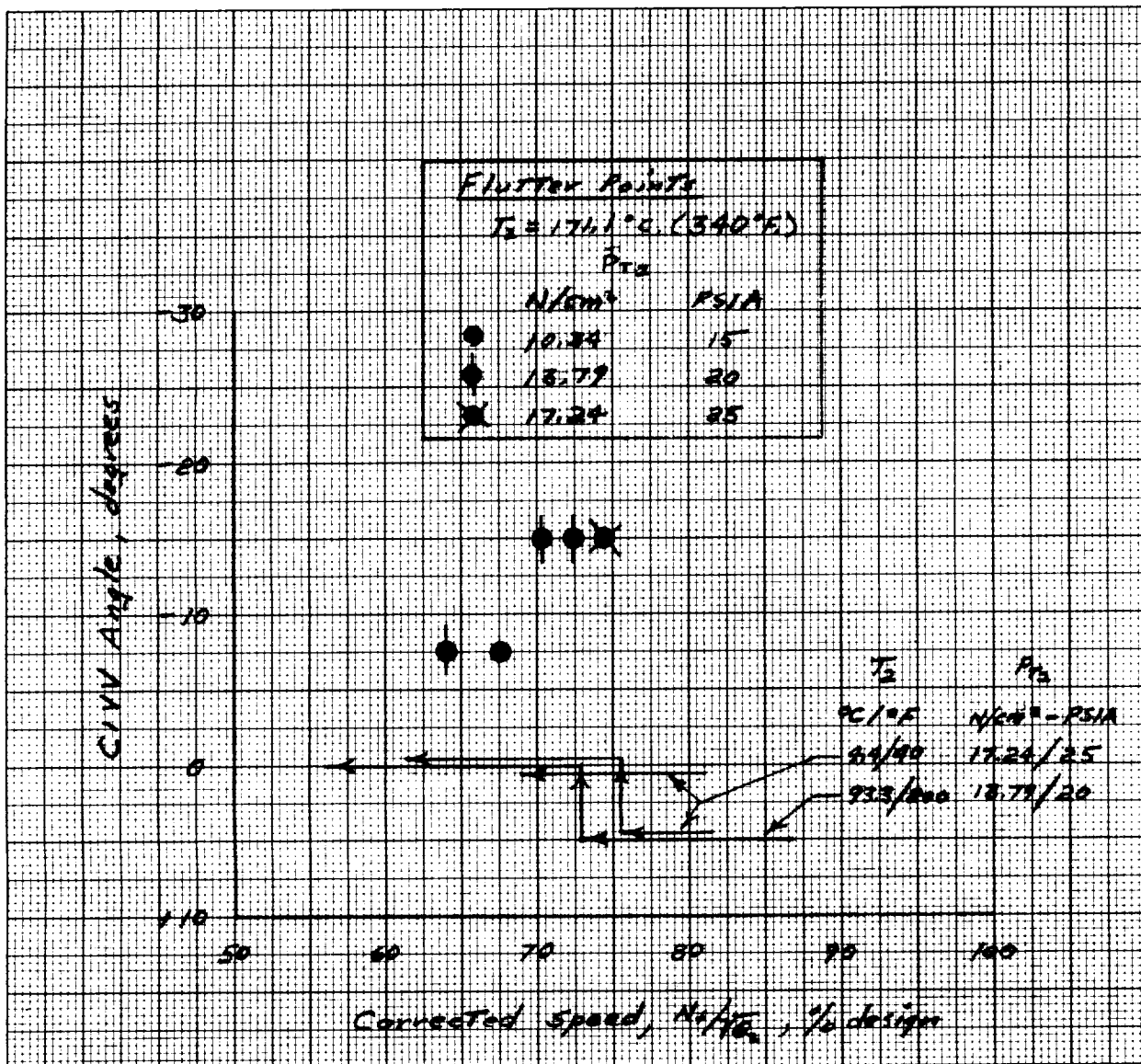
(c) Decelerations.

Figure 6. - Concluded.
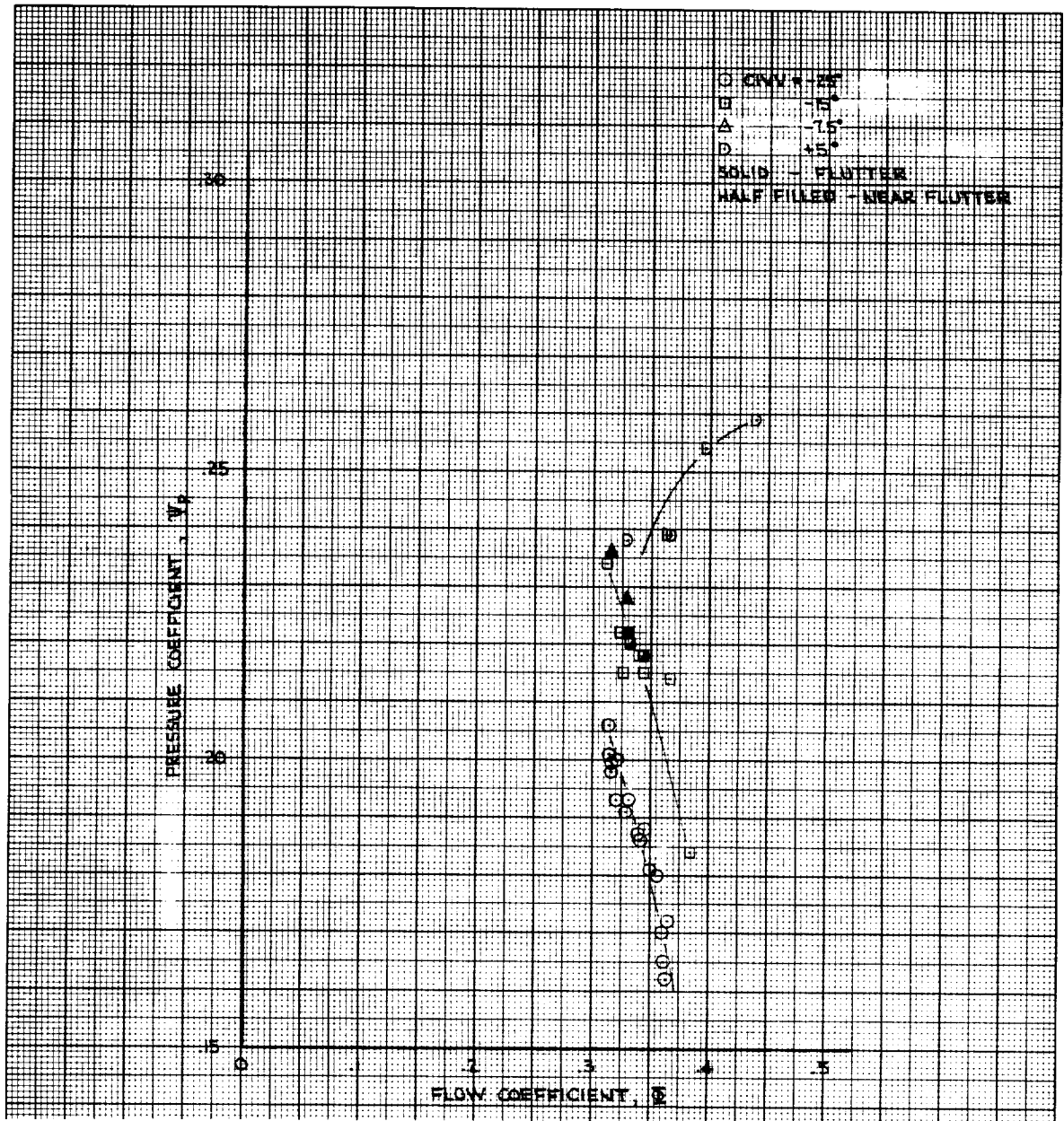
(a) Radially averaged pressure coefficient.

Figure 7. - Fan first-stage performance characteristics.
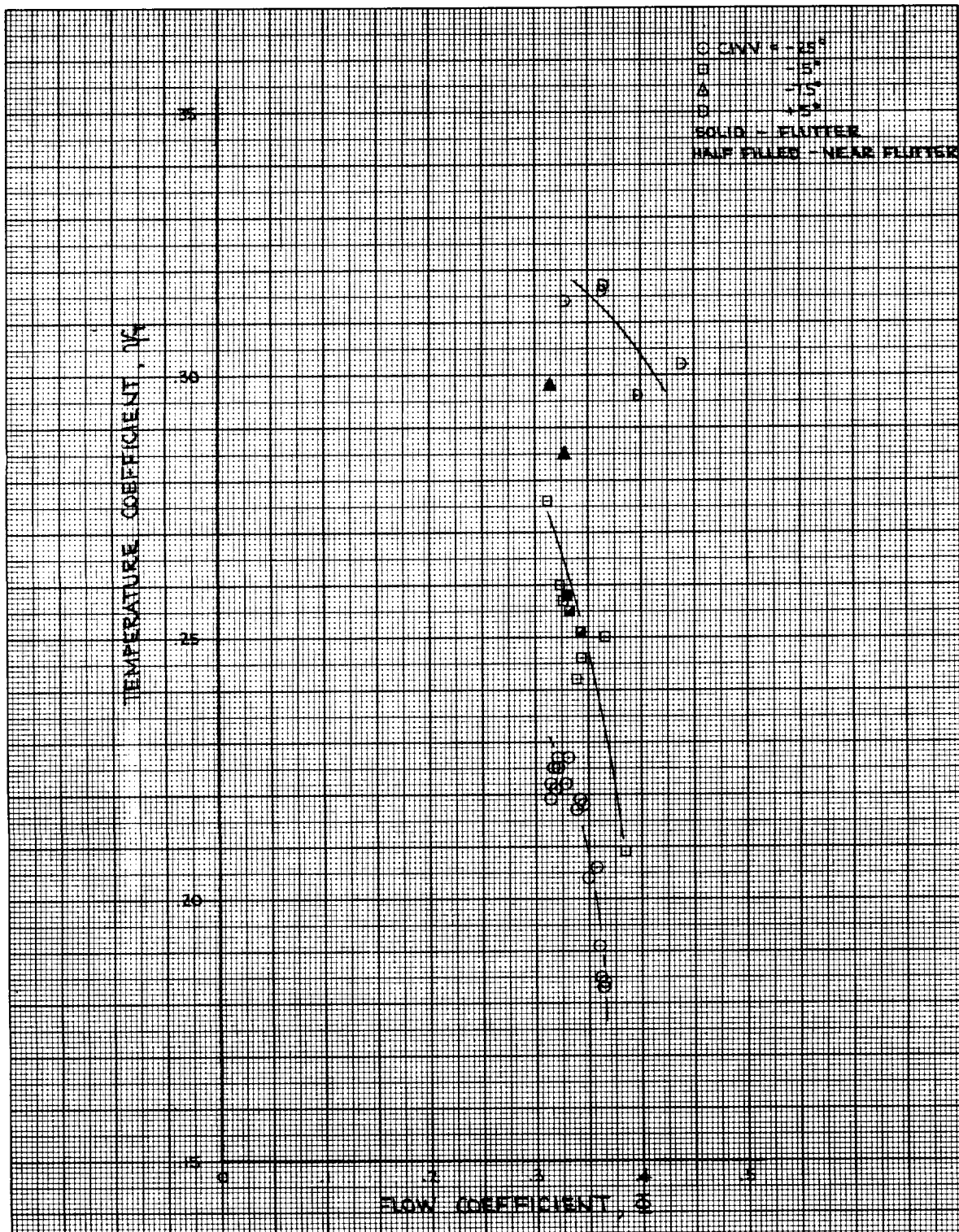
(b) Radially averaged temperature coefficient.

Figure 7. - Continued.
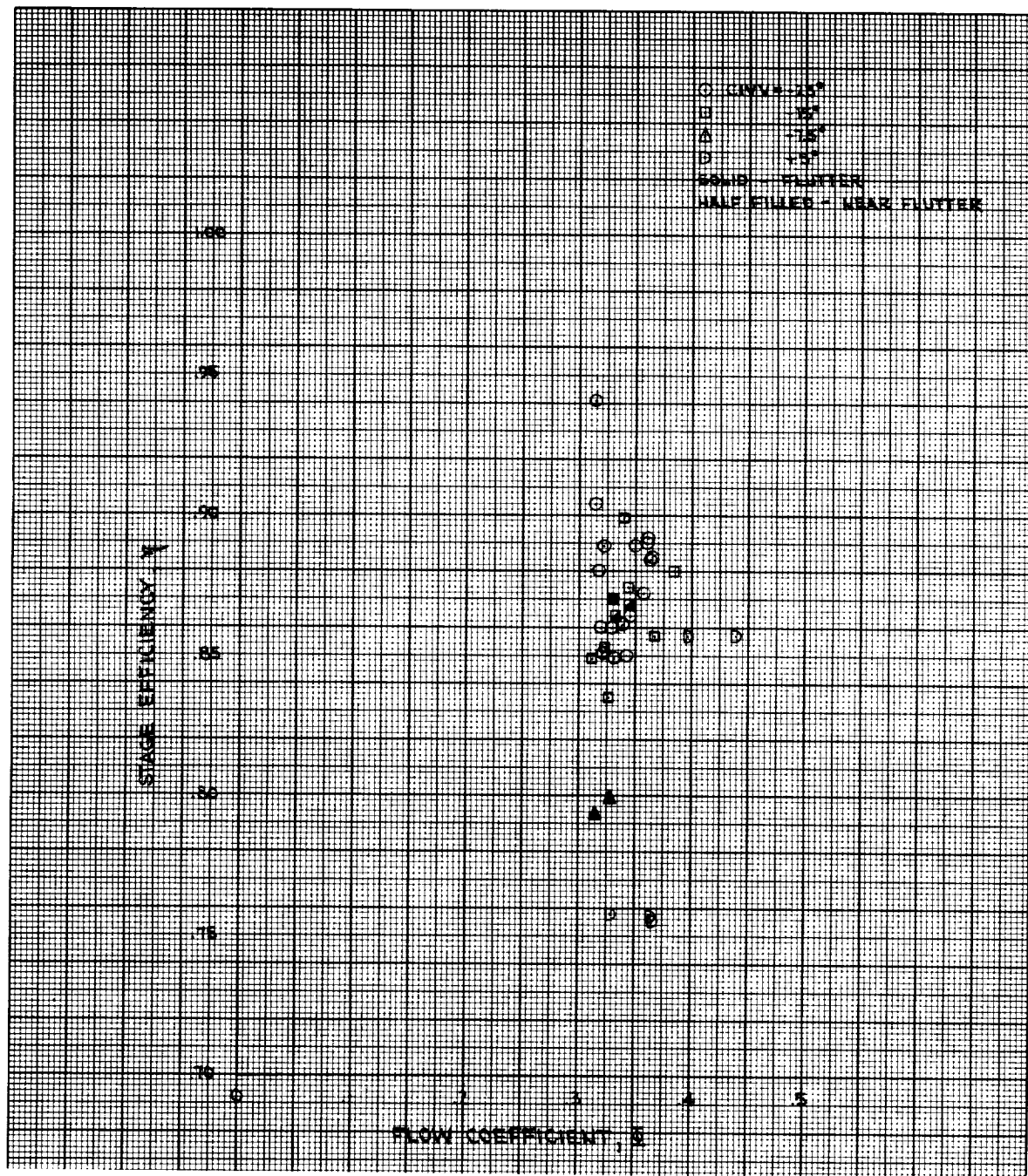
(c) Radially averaged efficiency.

Figure 7. - Continued.

68
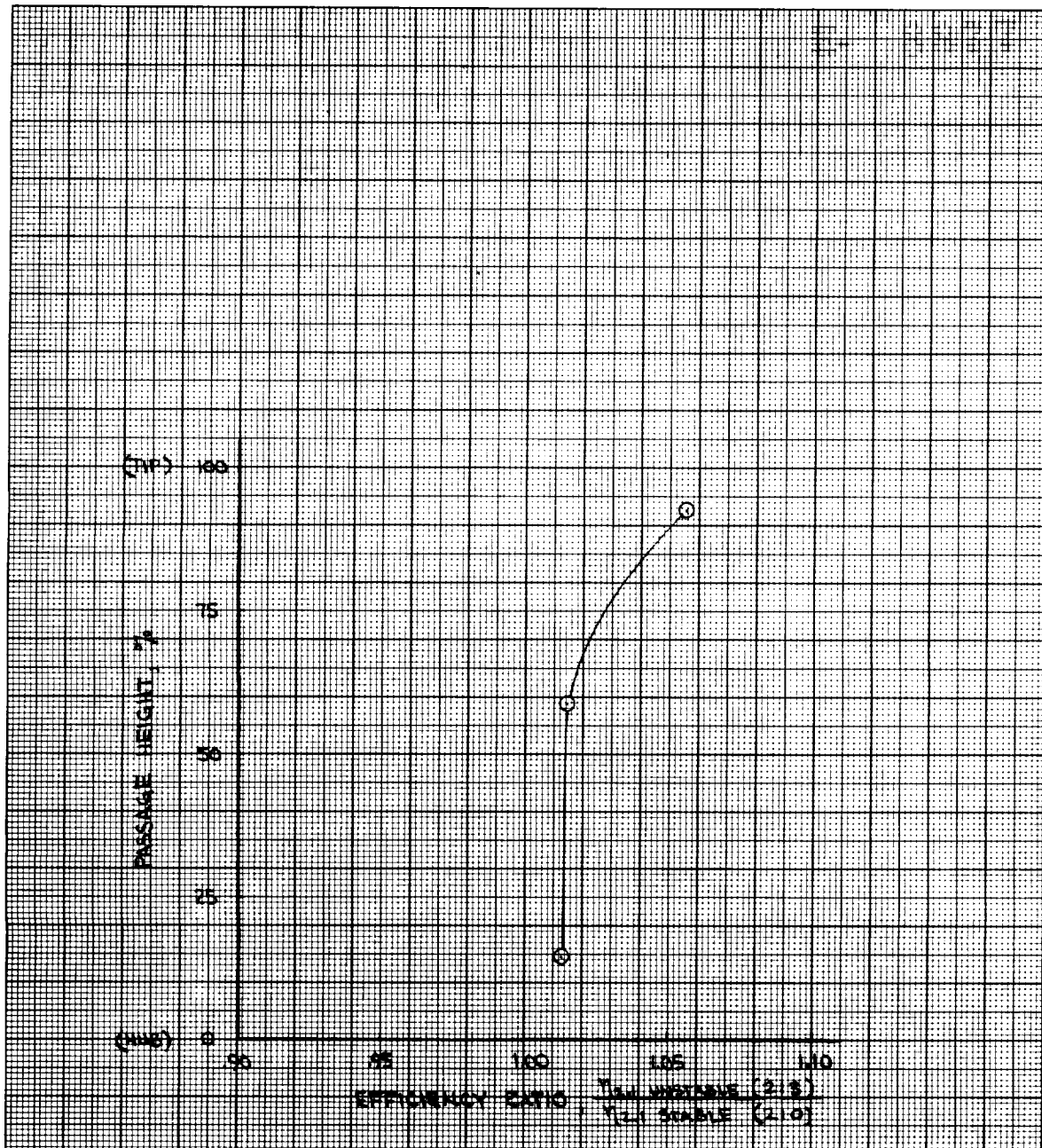
.(d) Radial variation of efficiency.

Figure 7. - Continued.
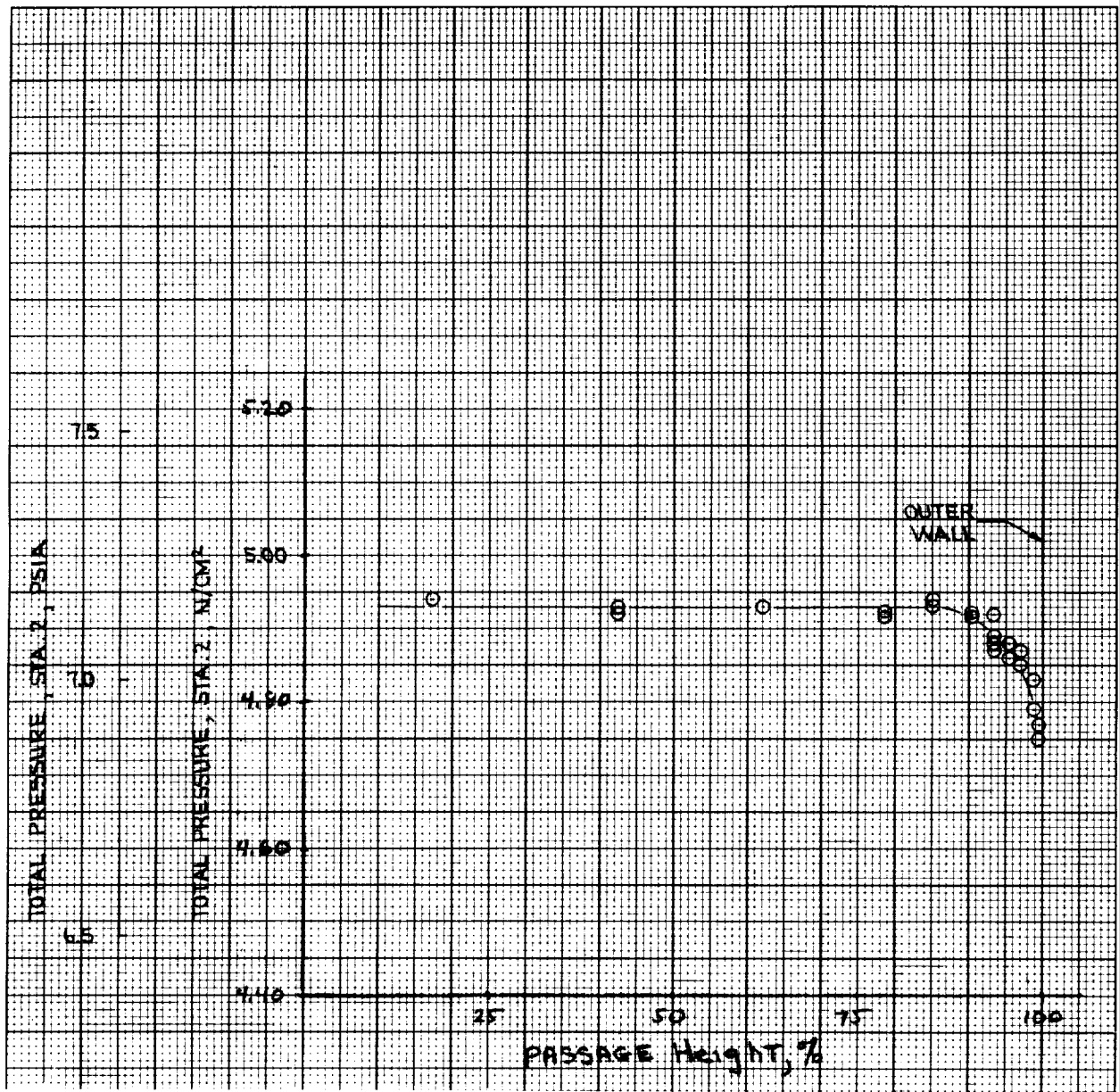
(e) Inlet radial pressure profile.

Figure 7. - Concluded.

(a) Fan map.
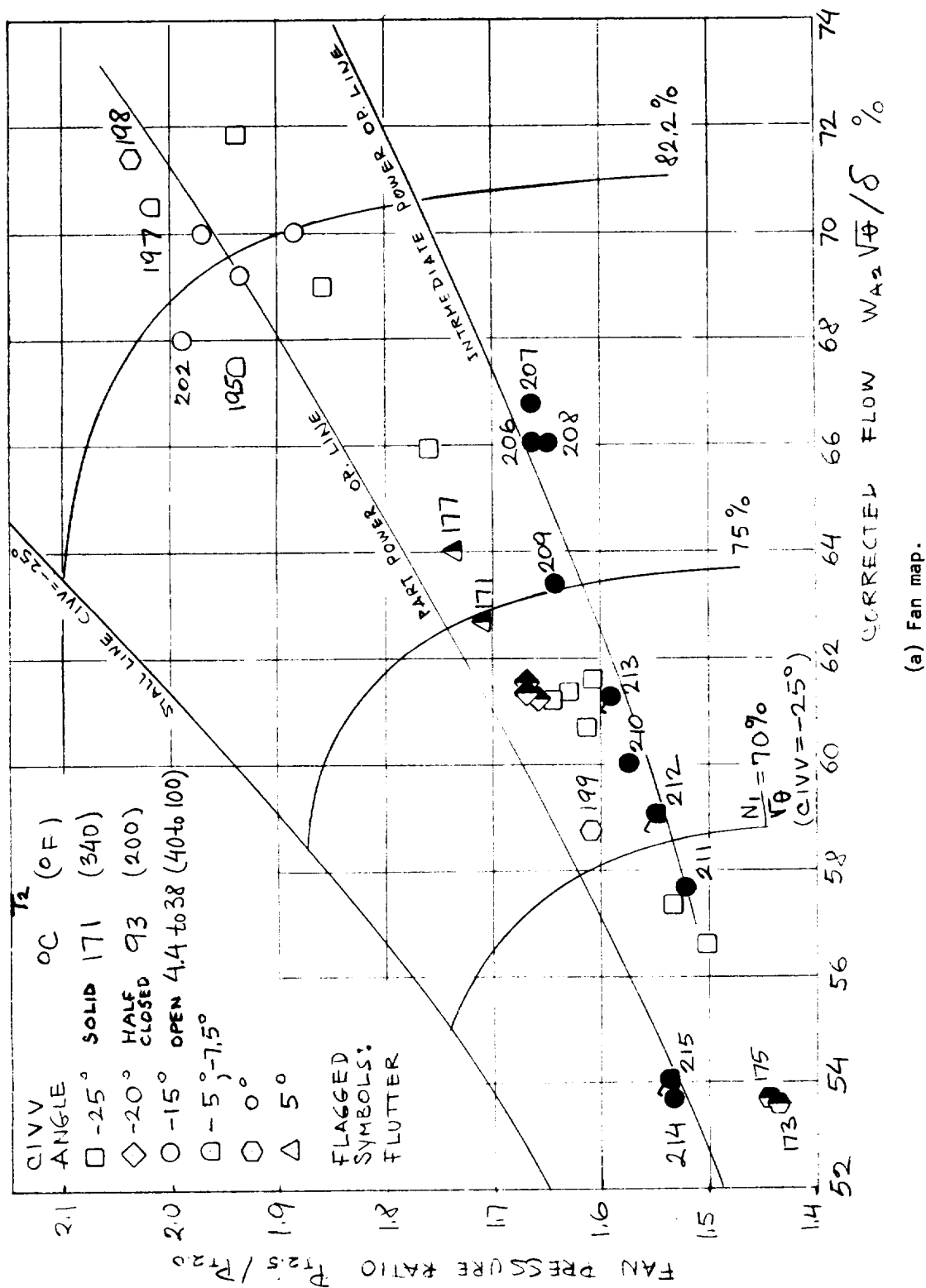
Figure 8. – Flutter boundary correlation. Numbers with data points denote CADDE readings.

P_{T_2}	$\frac{N}{cm^2}$ (PSIA)		T_2 °C (°F)
□	5 (7.5)	SOLID	171 (340)
◇	10 (15)	HALF CLOSED	93 (200)
○	14 (20)	OPEN	4.4 to 38 (40 to 100)
⌀	17 (25)	FLAGGED SYMBOL FLUTTER	
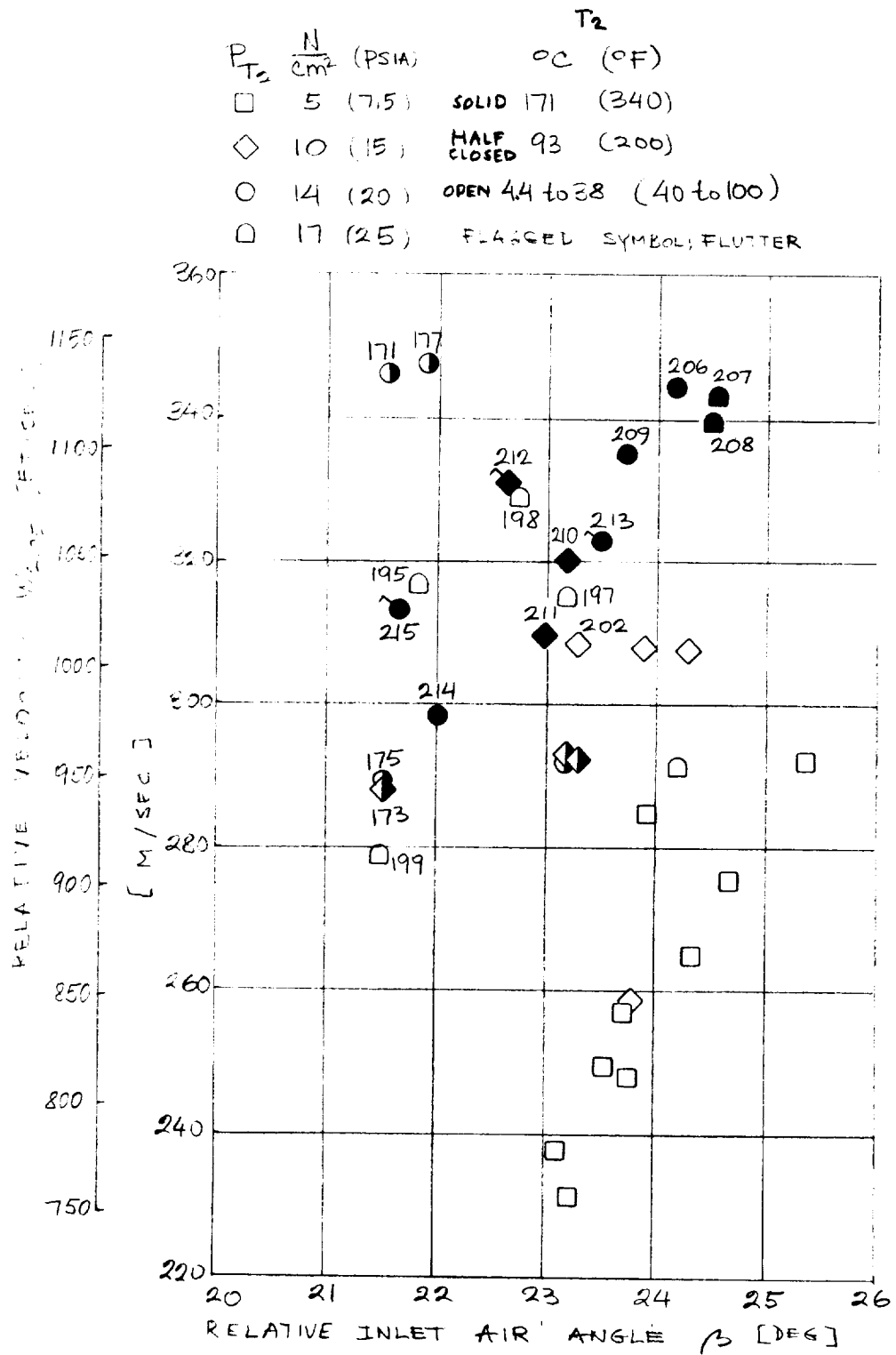
(b) Correlation of relative velocity and inlet air angle.

Figure 8. - Continued.

72

P_{T_2} $\frac{N}{cm^2}$ (PSIA) $\circ_C$ T_2 ($\circ$F)

☐   5 (7.5)   SOLID 171   (340)

◇   10 (15)   HALF CLOSED 93   (200)

○   14 (20)   OPEN 4.4 to 38 (40 to 100)

◔   17 (25)   FLAGGED SYMBOL: FLUTTER

RELATIVE MACH NUMBER $M_{2.05}$

○ 198

○ 195   ○ 197

177
171 ◐   ◑

202
◇   ◇   ◑

○ 199   ☐   ☐
                 206 207
                 ●   ◑
                 ●   ☐
                    208
             209
212   ●
◆   213
             ◑
210   ☐
175 ◑◇
173 ●
215
211   ◇
◆   ☐☐

● 214
             ☐

             ☐

.65   .70   .75   .80   .85   .90   .95   1.0

RELATIVE INLET AIR ANGLE β [DEG]

20   21   22   23   24   25   26
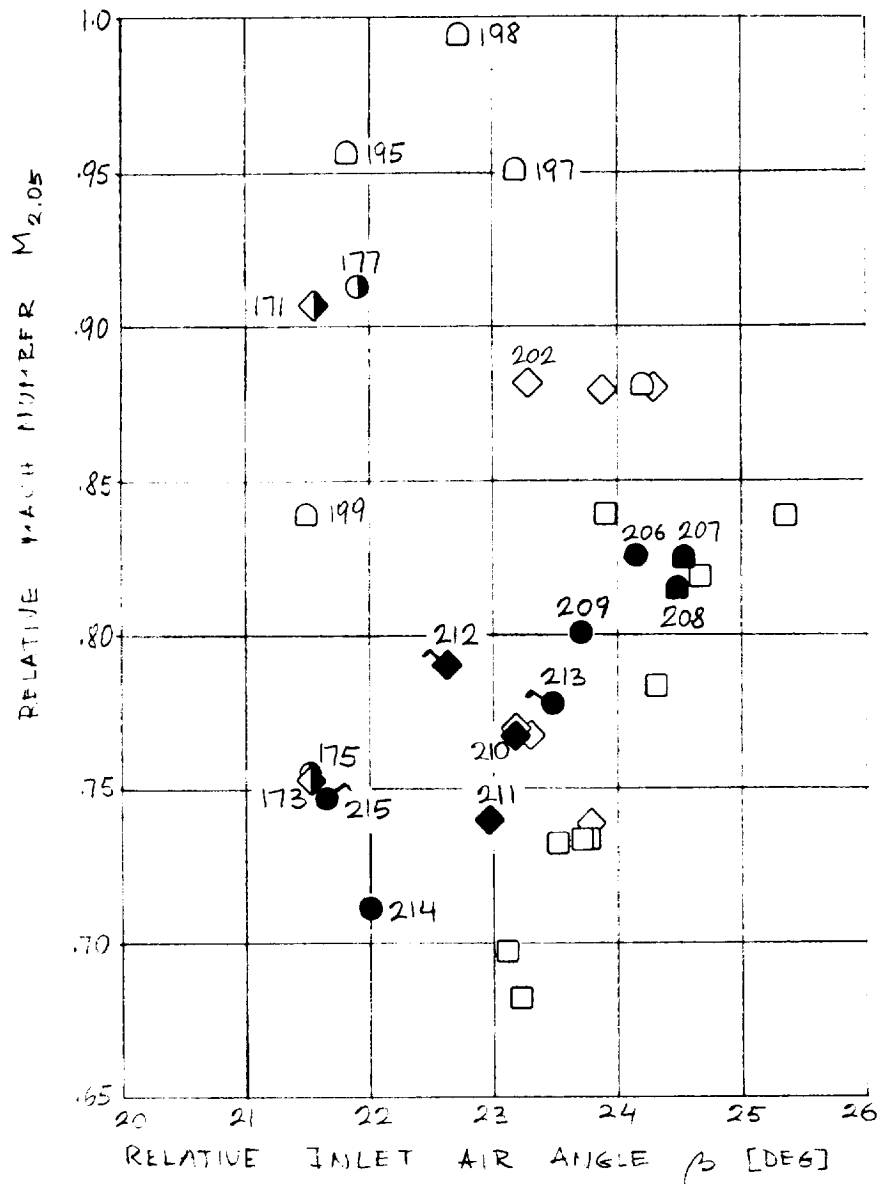
(c) Correlation of relative Mach number and inlet air angle.

Figure 8. - Concluded.
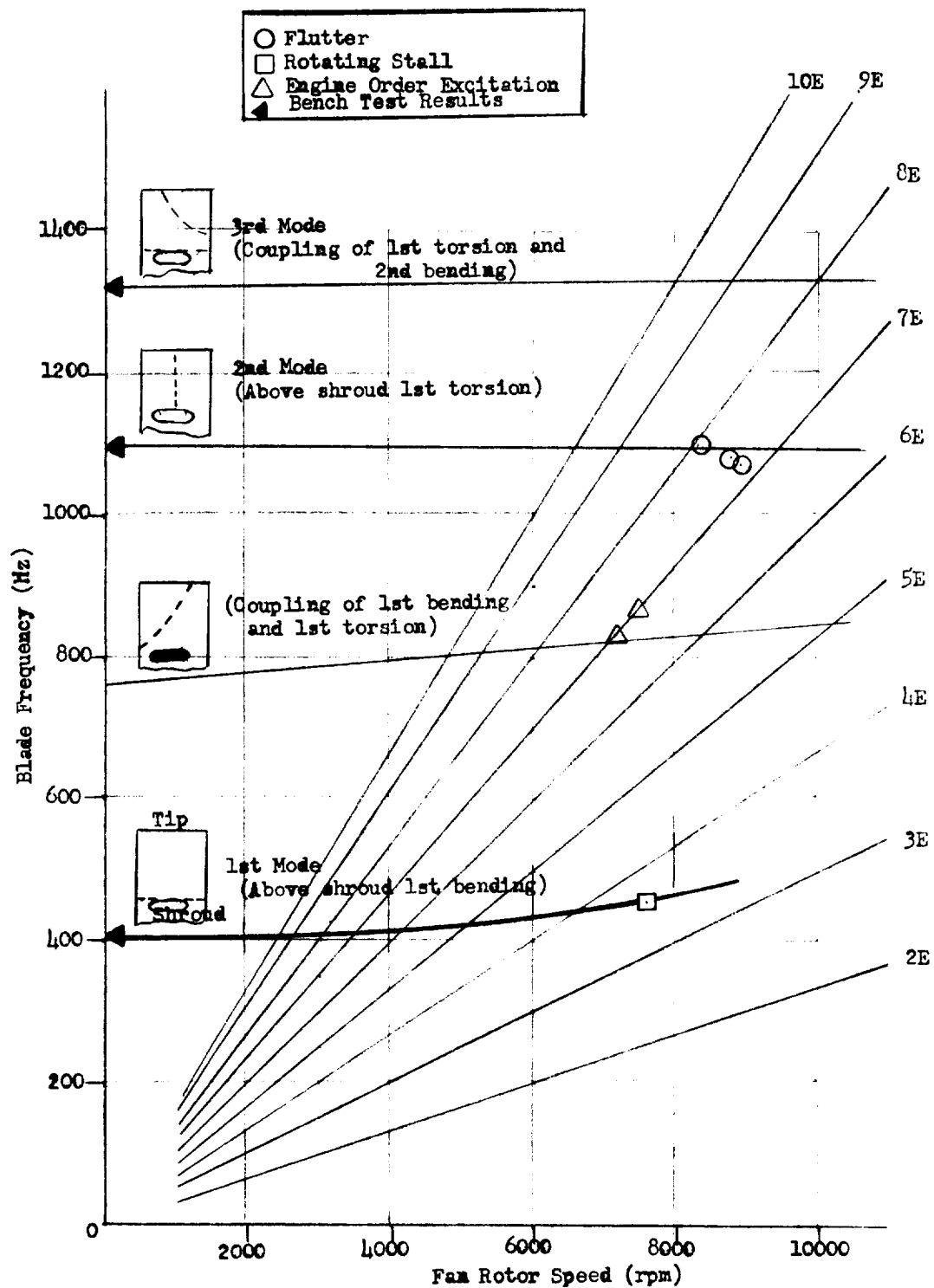
Figure 9. - Campbell diagram for fan first-stage rotor.
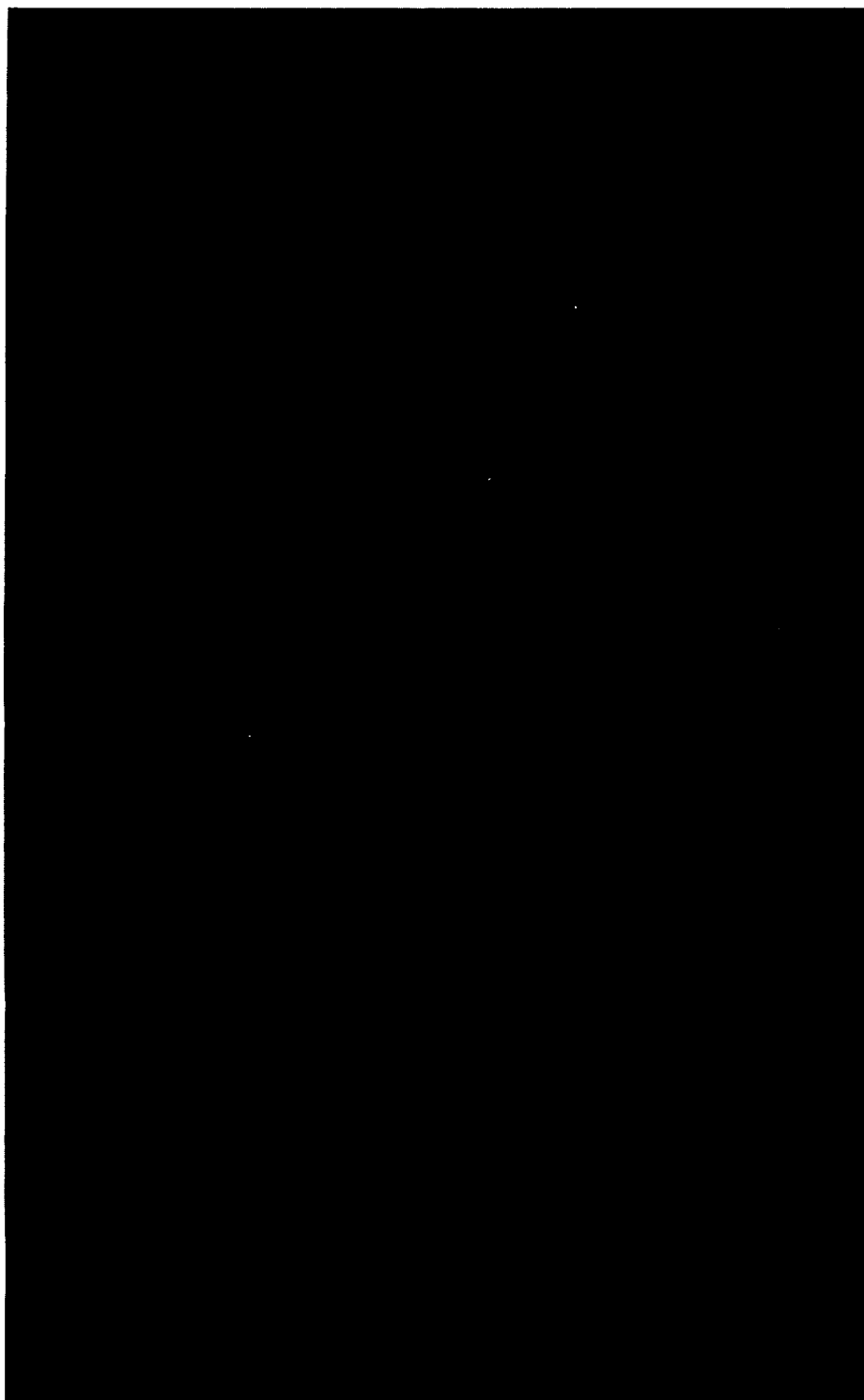
(a) Rotating stall; analog reading 49.

Figure 10. - Strain-gage response characteristics for first-stage fan rotor.
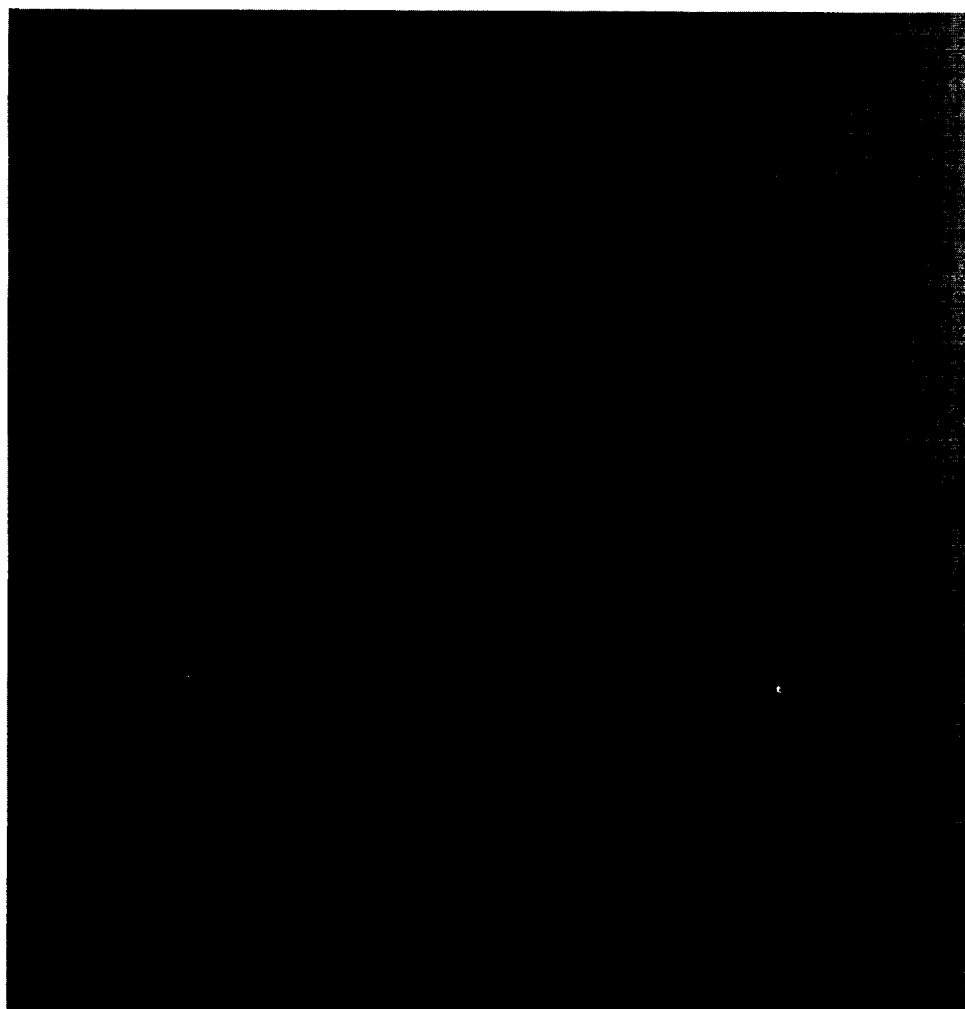
(b) Flutter; analog reading 53.

Figure 10. - Continued.

(c) Flutter; analog reading 54, $P_{T,2}$ = 13.79 N/cm^2 (20 psia); T_2 = 171° C (339° F).

Figure 10. – Continued.
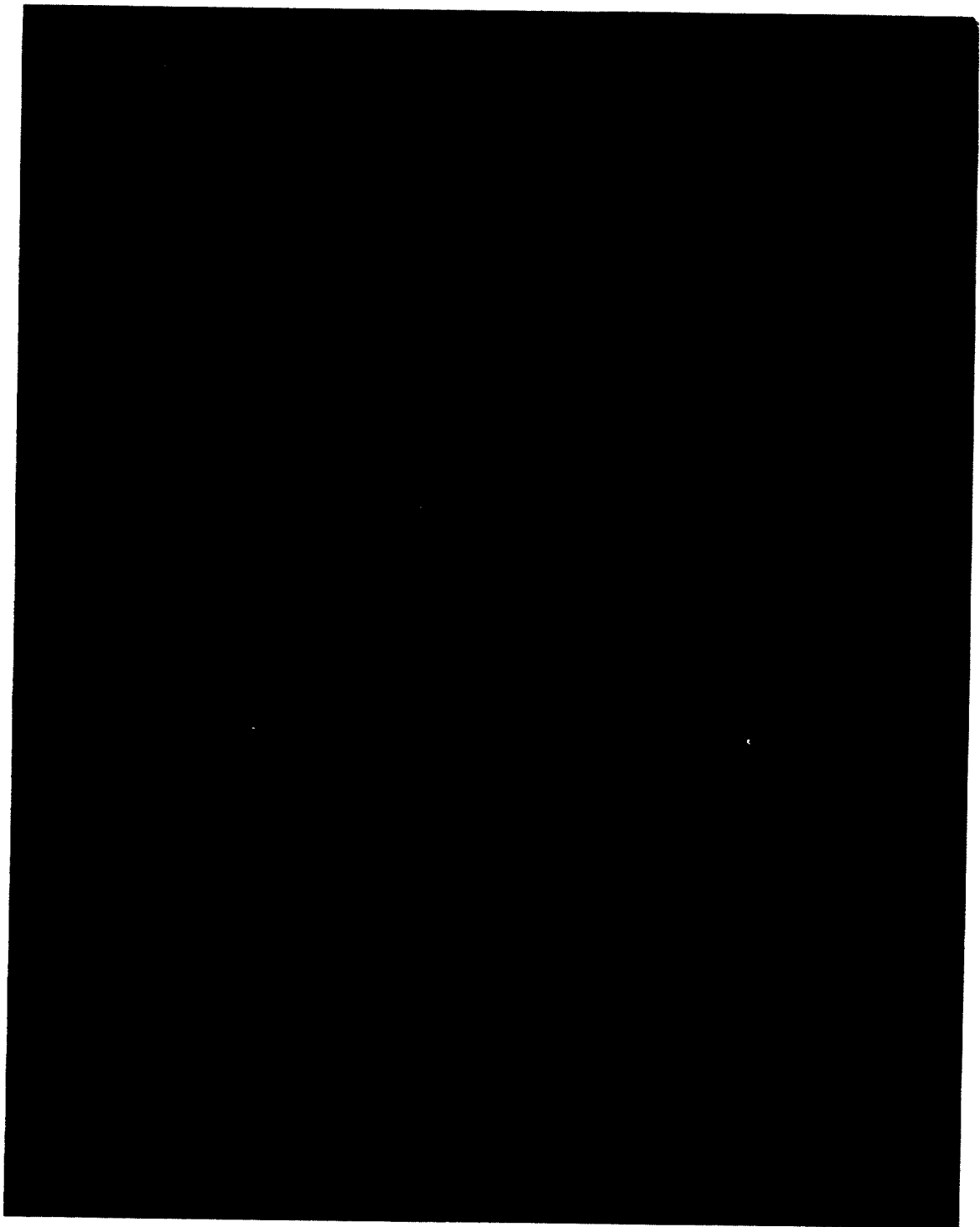
(d) Flutter; analog reading 56, $P_{T,2}$ = 10.34 N/cm^2 (15 psia); T_2 = 171° C (339° F).

Figure 10. – Concluded.
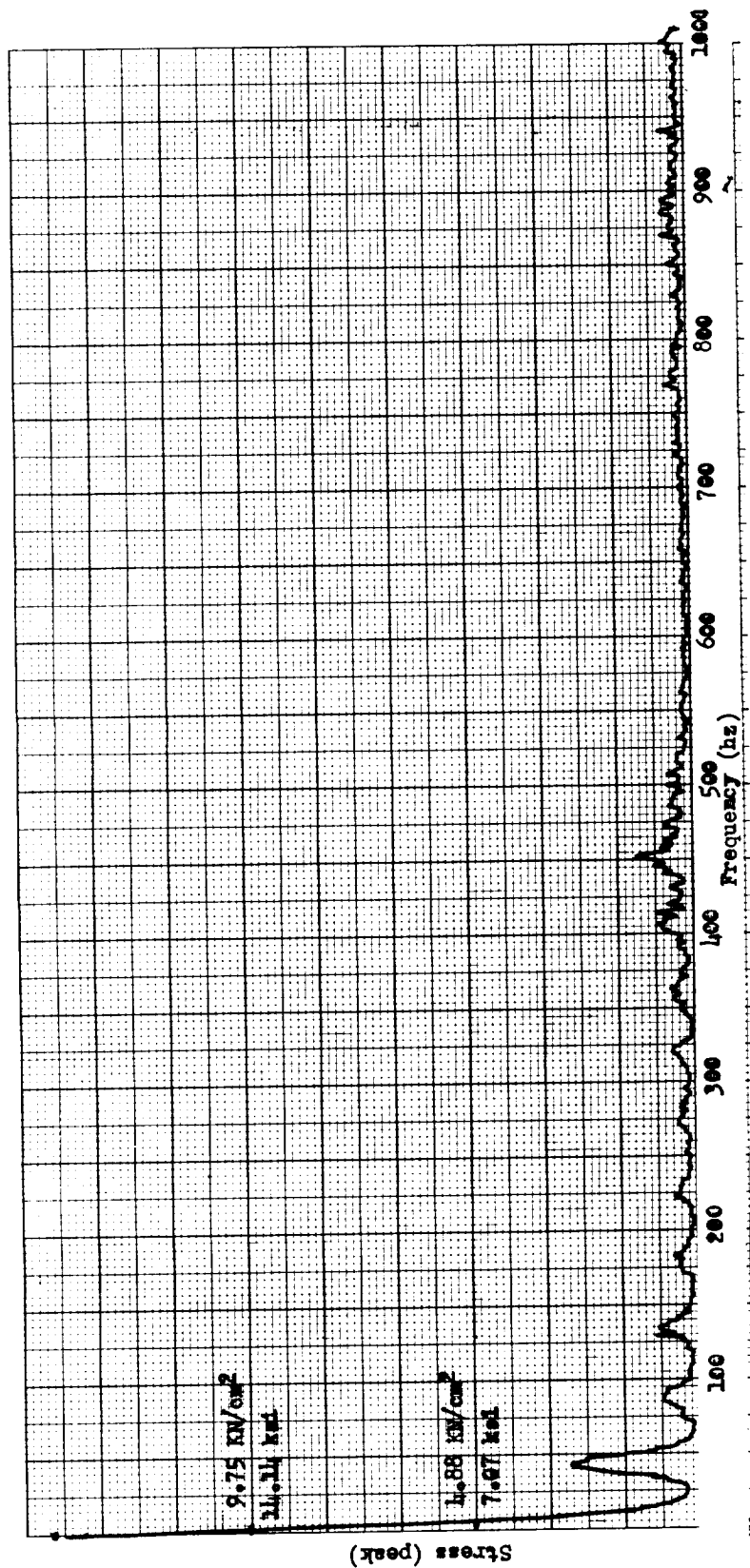
(a) Strain gage 117, ASTE; rotating stall; analog reading 49.

Figure 11. - Spectral content from strain gages on fan first-stage rotor.

79
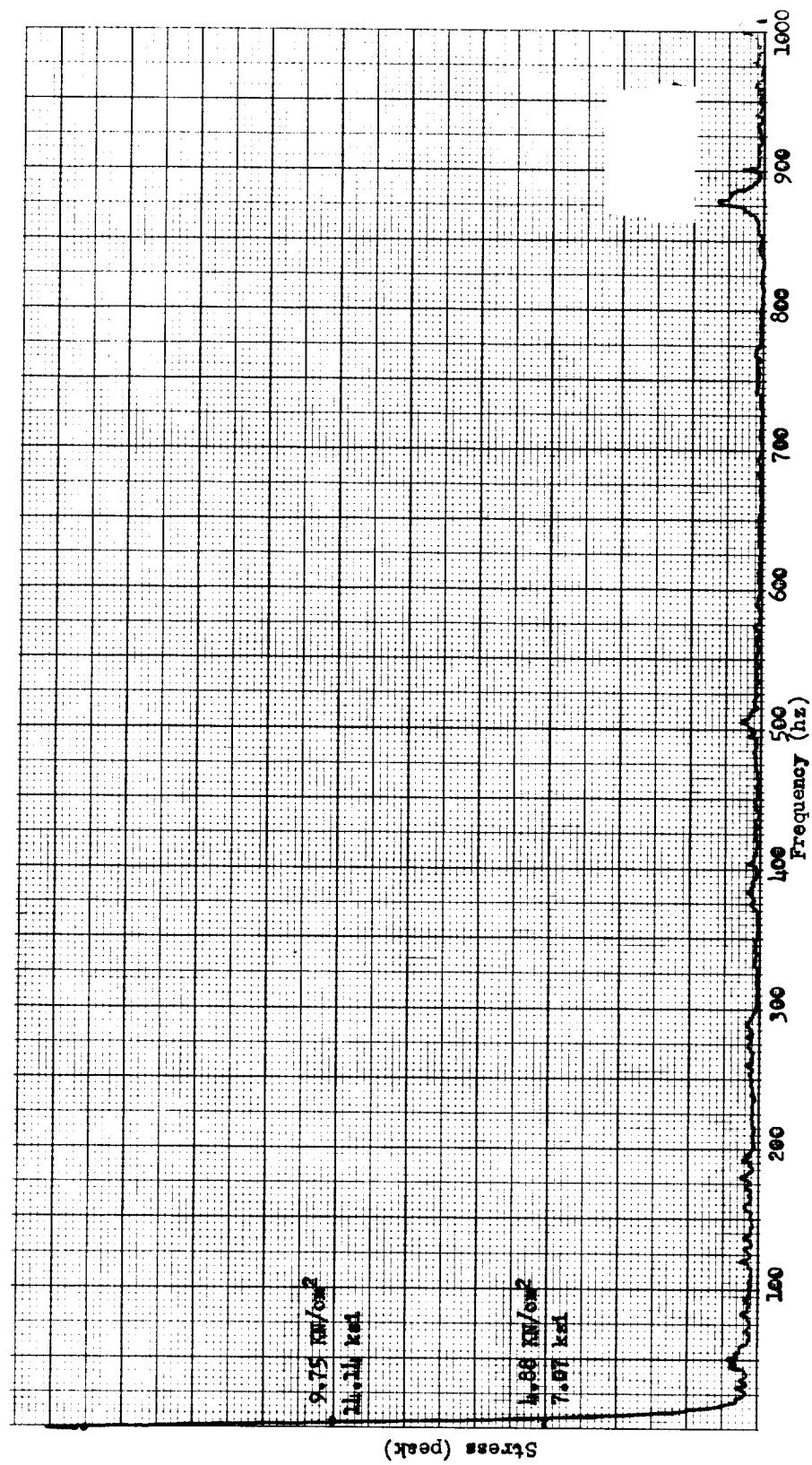
(b) Strain gage 103, TIP; prior to rotating stall; analog reading 50.

Figure 11. – Continued.

80
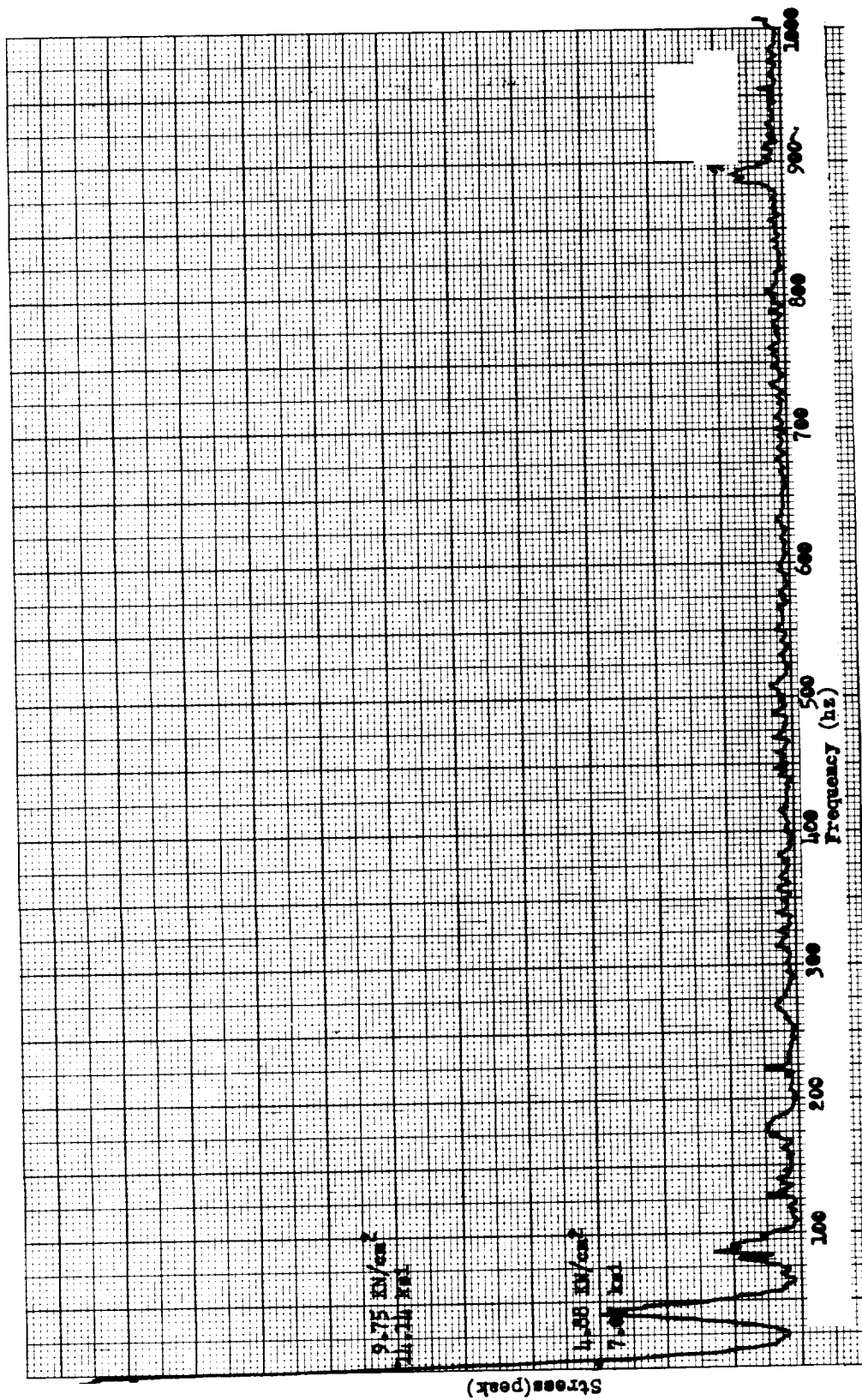
(c) Strain gage 103, TIP; rotating stall; analog reading 50.

Figure 11. – Continued.

81
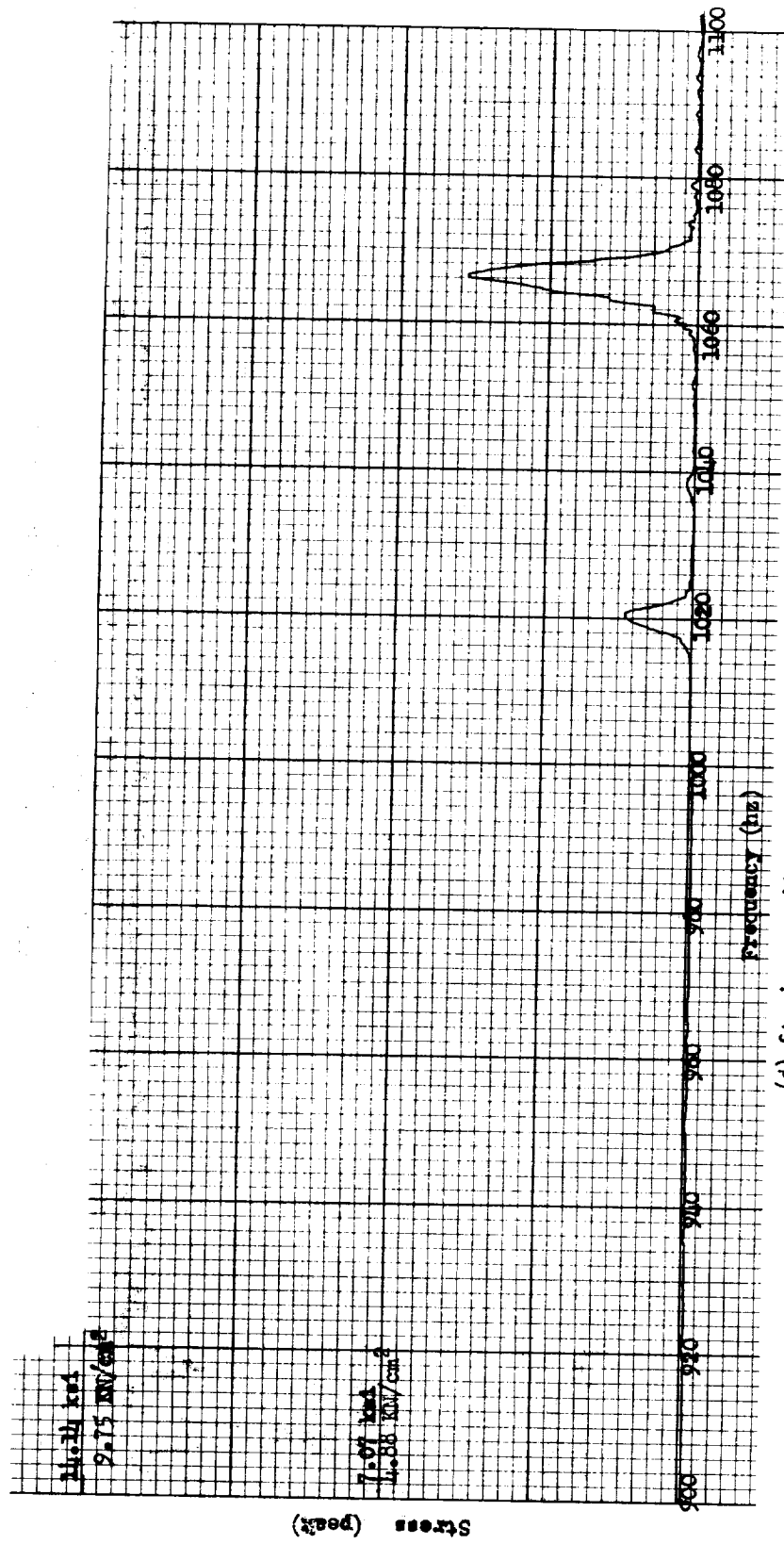
(d) Strain gage 103, TIP; flutter; analog reading 53.

Figure 11. - Continued.

82
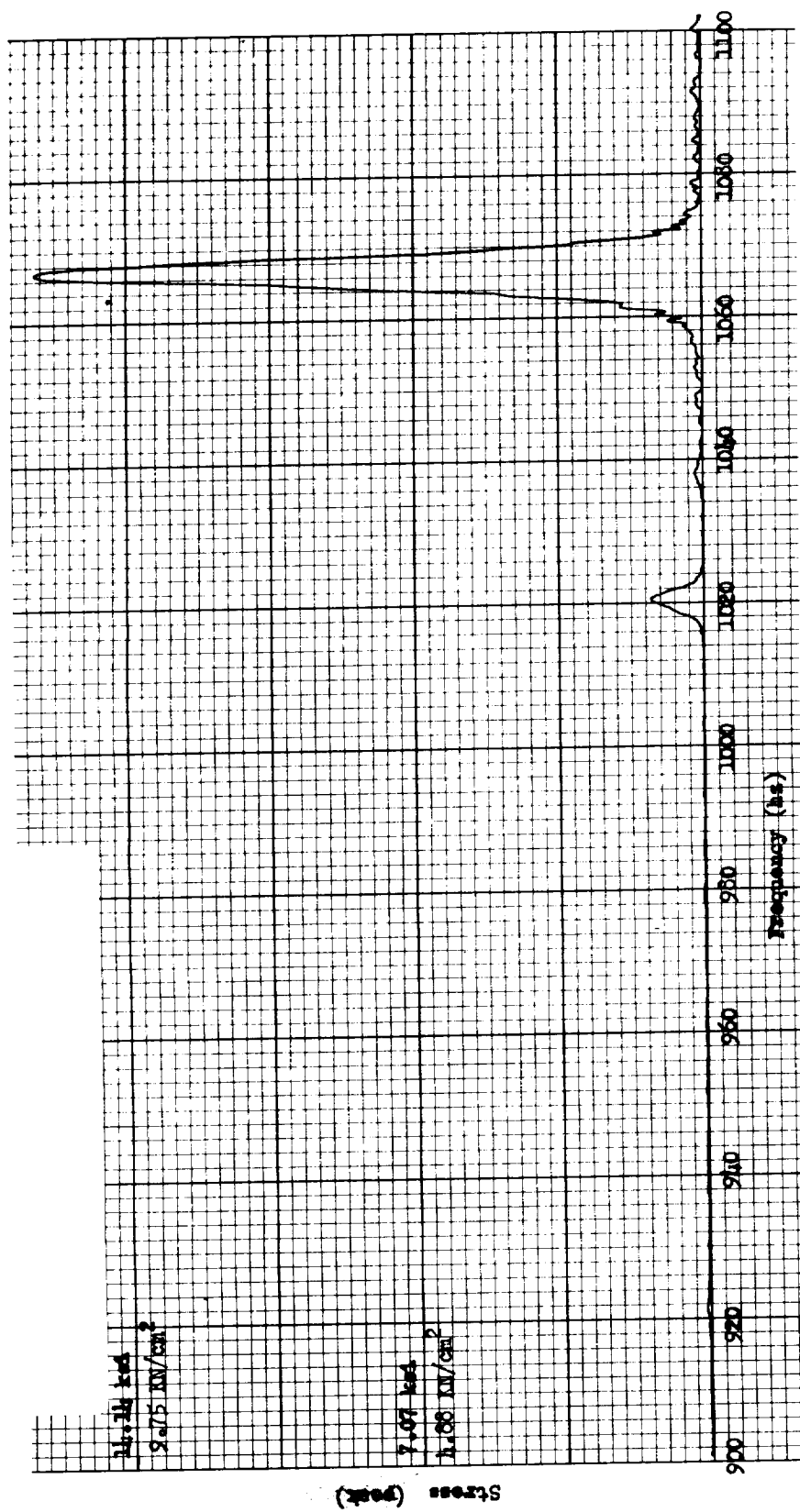
(e) Strain gage 104, TIP; flutter; analog reading 53.
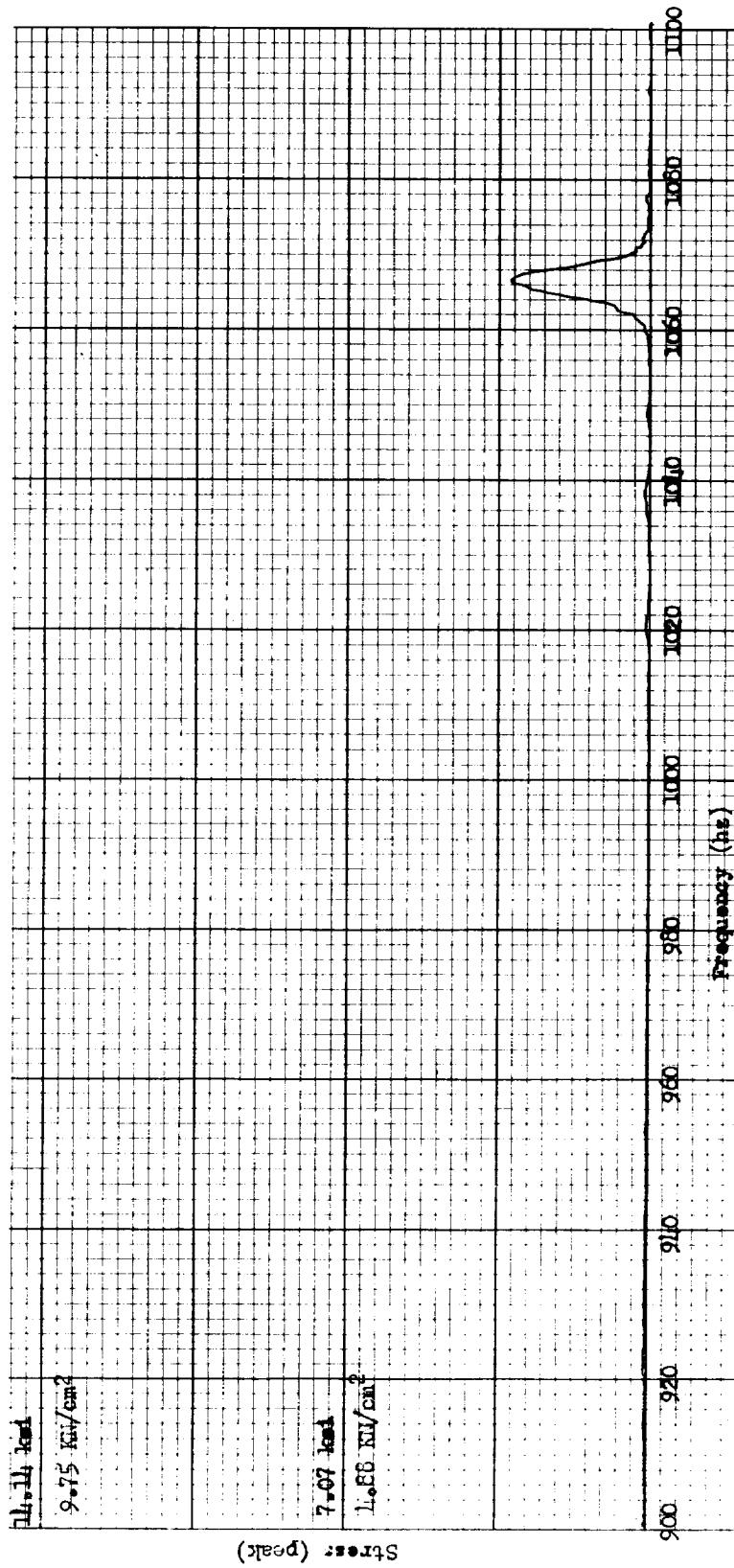
Figure 11. — Continued.

83

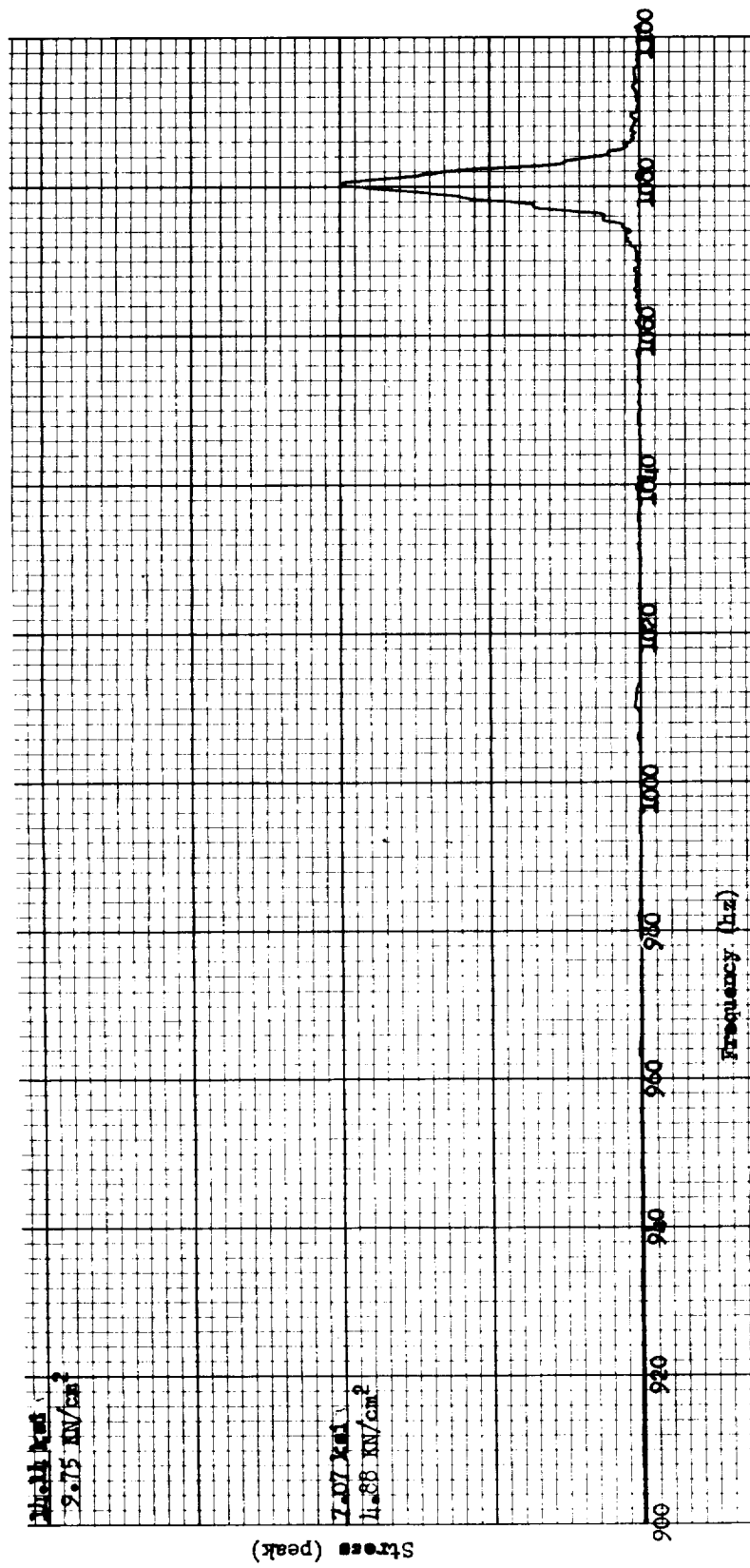(f) Strain gage 109, ASMT; flutter; analog reading 53.
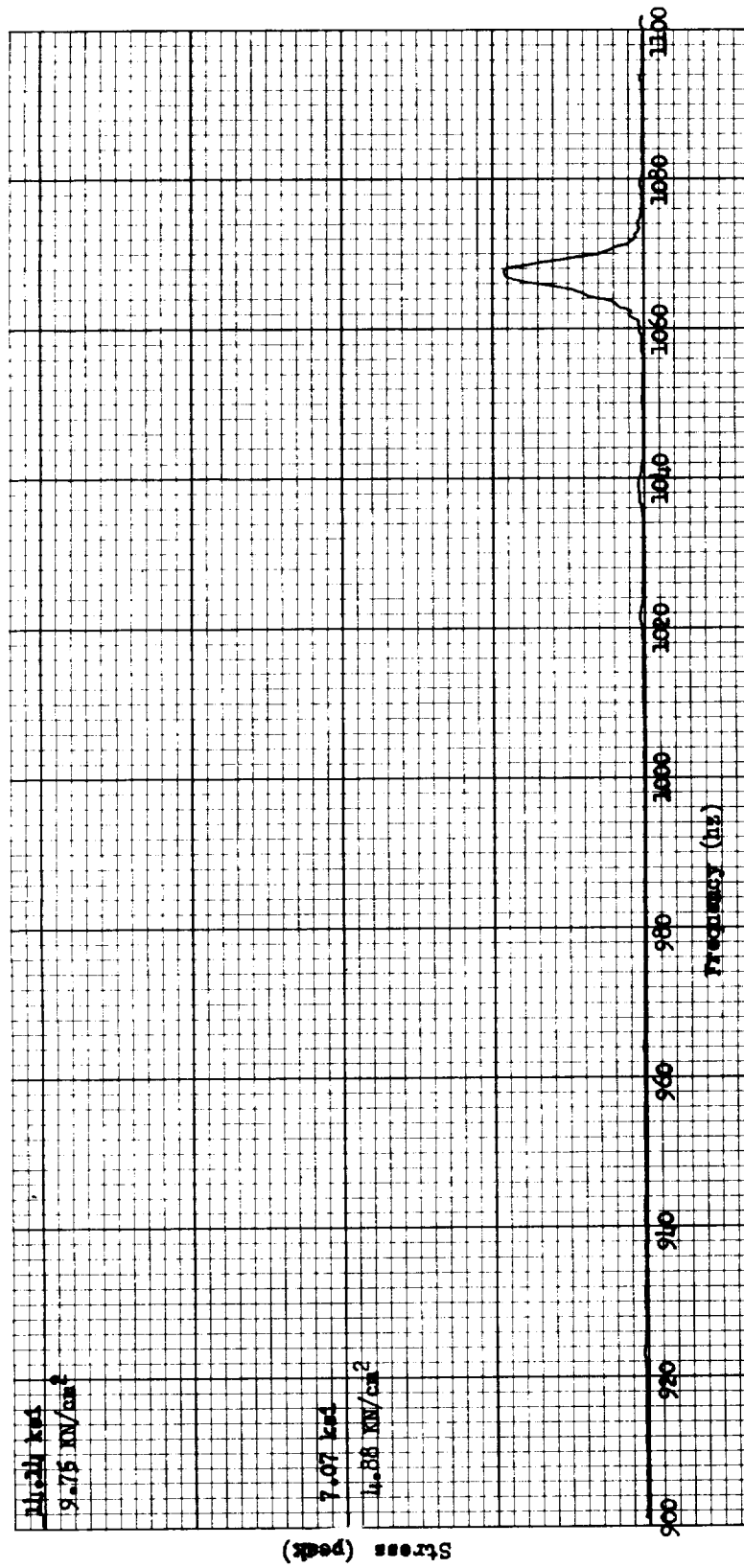
Figure 11. – Continued.

84

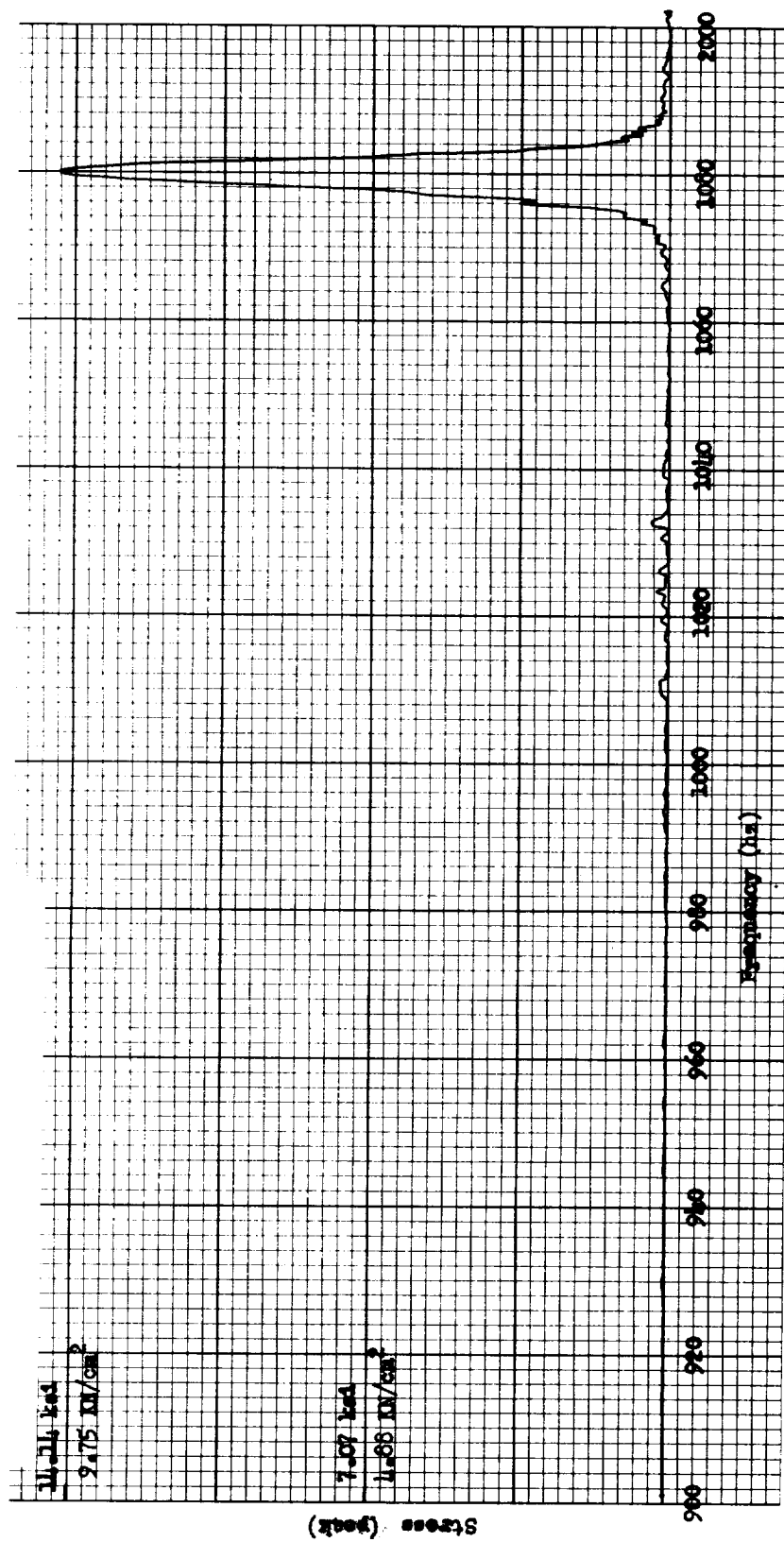(g) Strain gage 113, ASMT; flutter; analog reading 53.
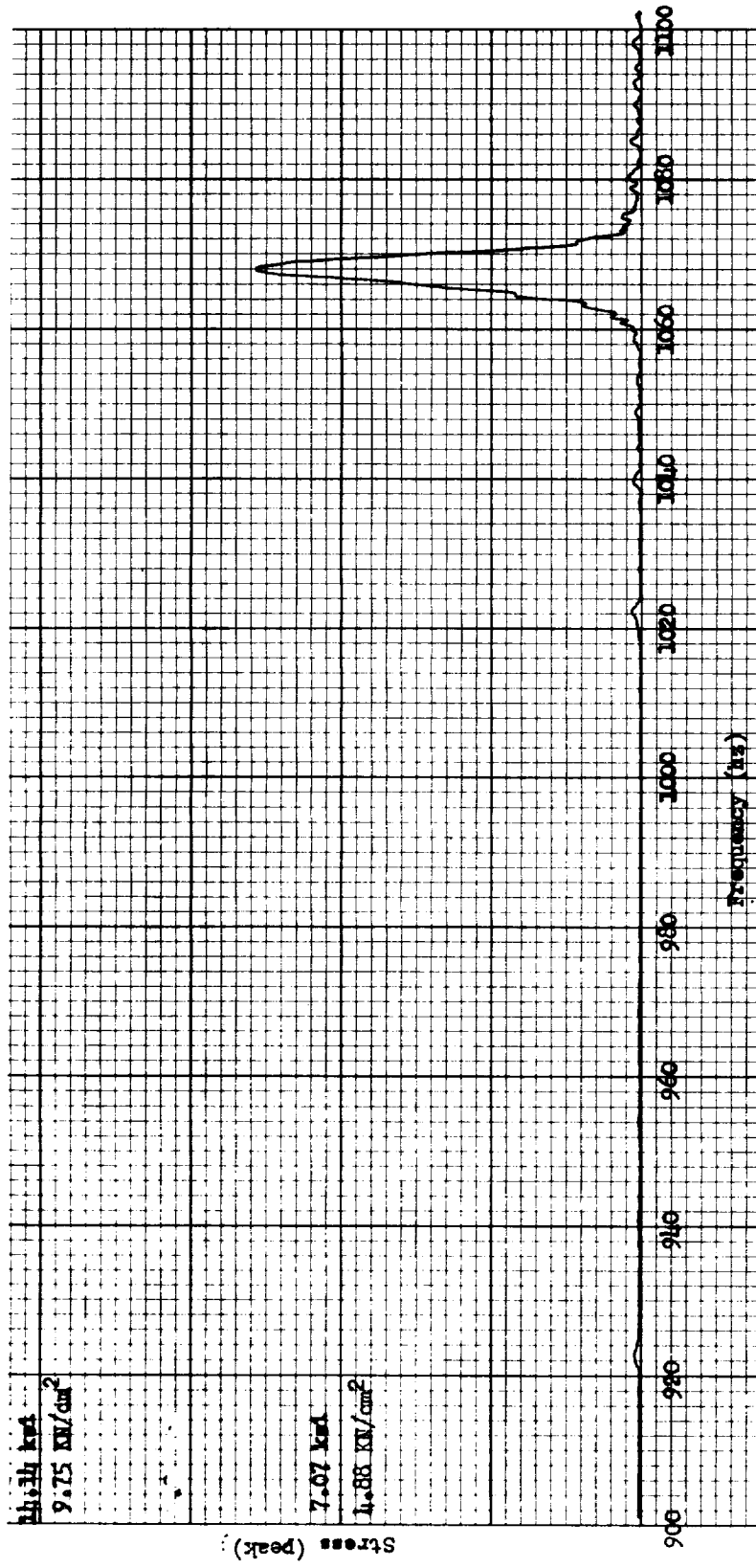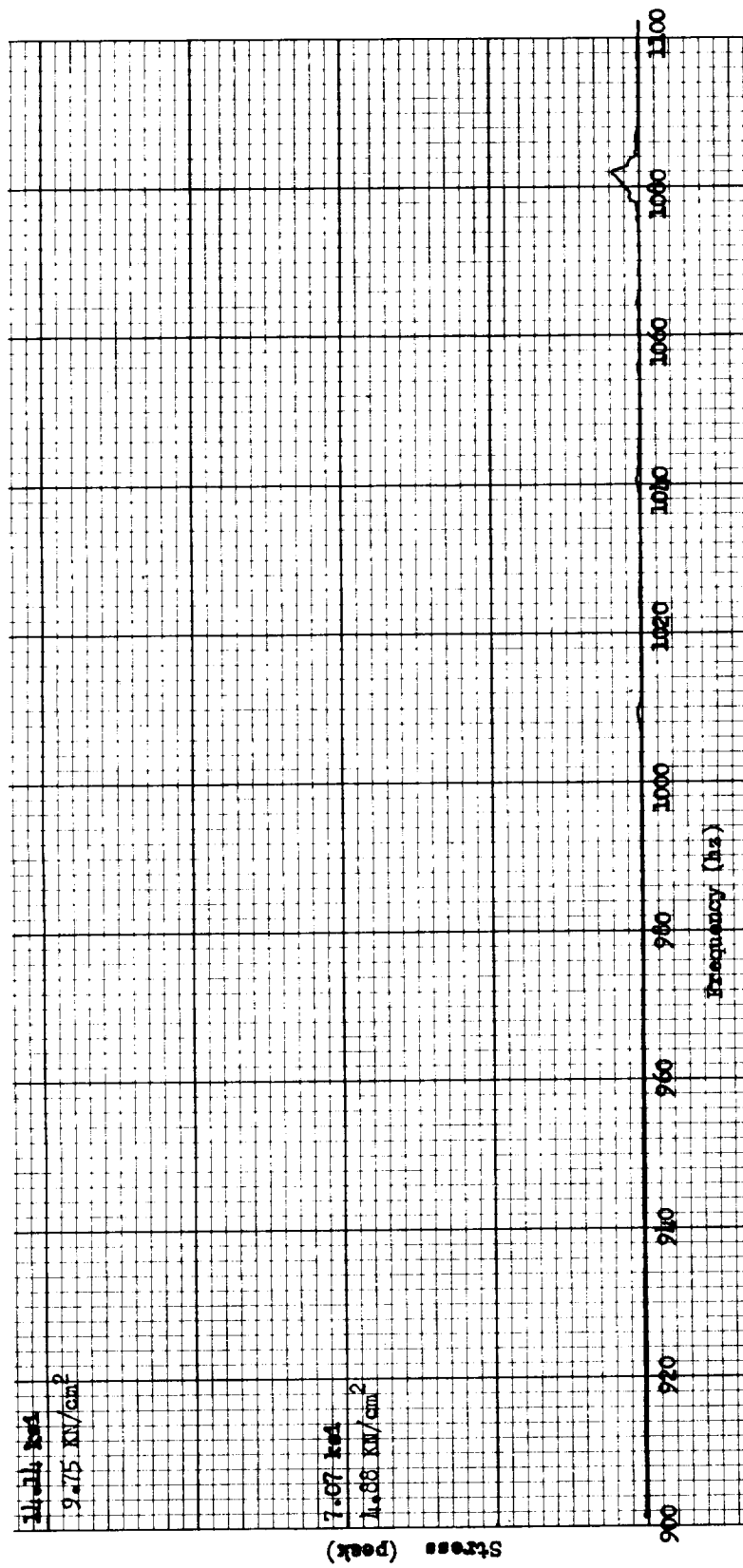
Figure 11. - Continued.

85

(h) Strain gage 116, ASTE; flutter; analog reading 53.
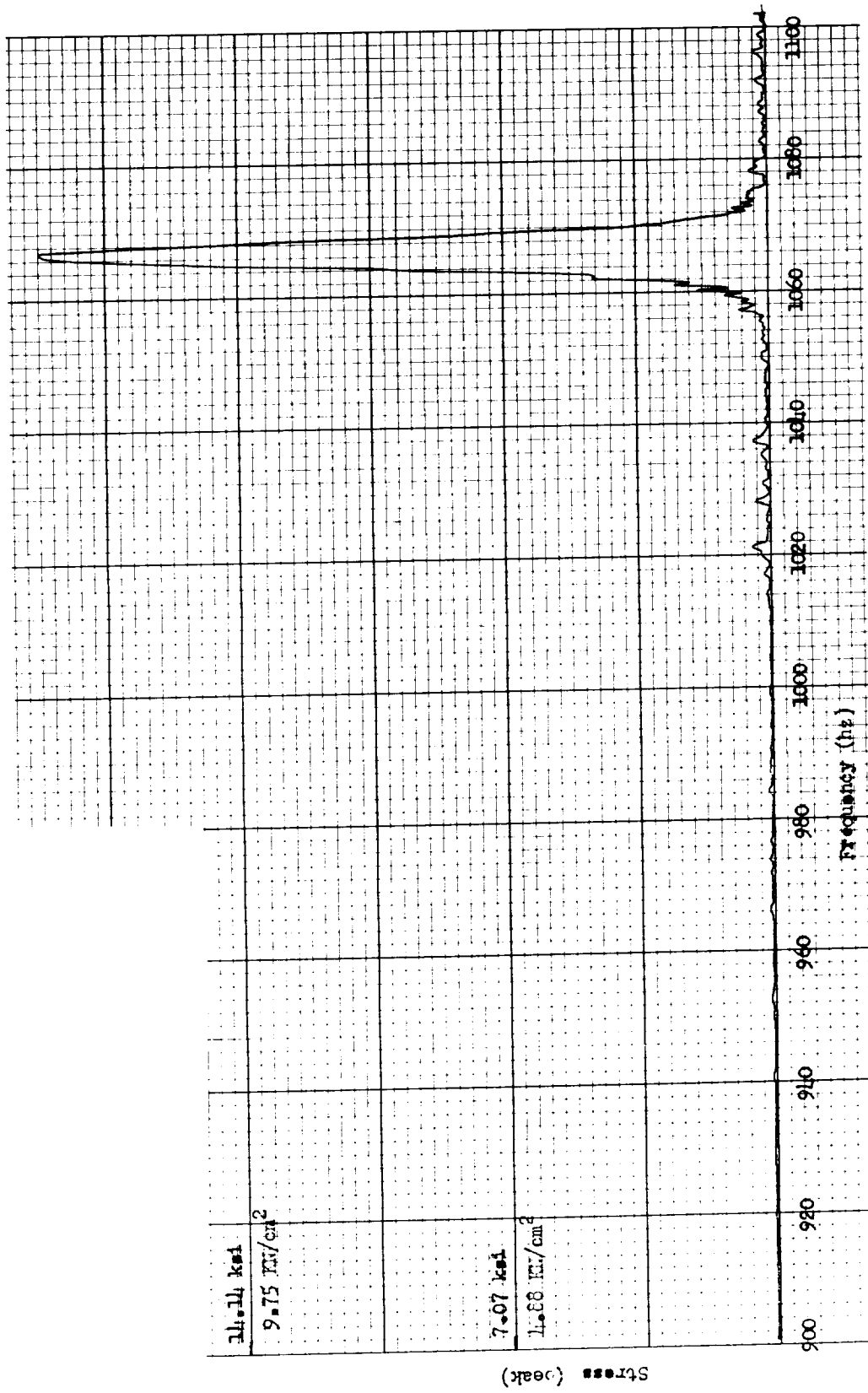
Figure 11. - Continued.

86

(i) Strain gage 117, ASTE; flutter; analog reading 53.

Figure 11. – Continued.

87

(j) Strain gage 122, SHRD-CX; flutter; analog reading 53.

Figure 11. – Continued.

88

Frequency (Hz)

Stress (peak)
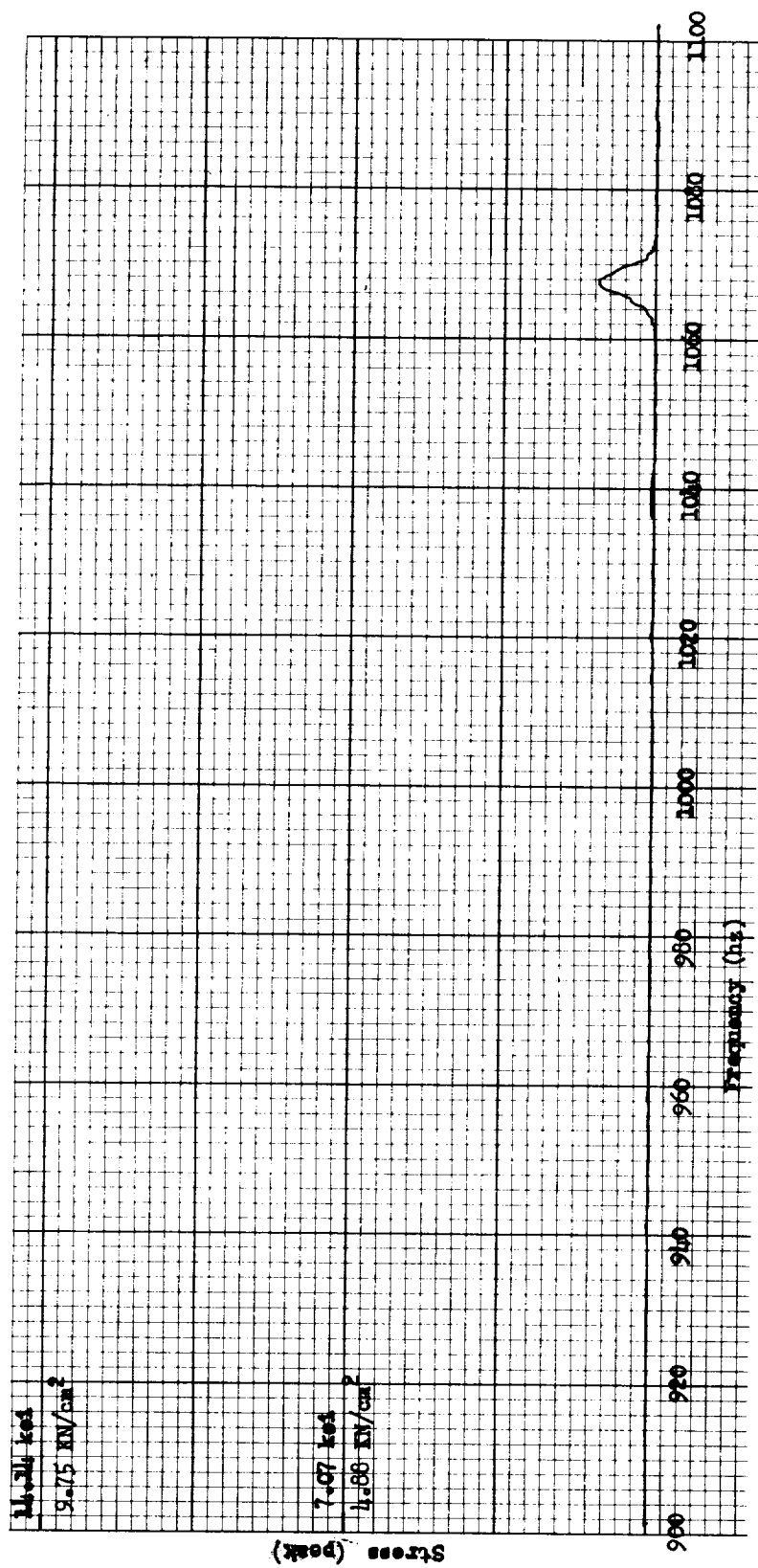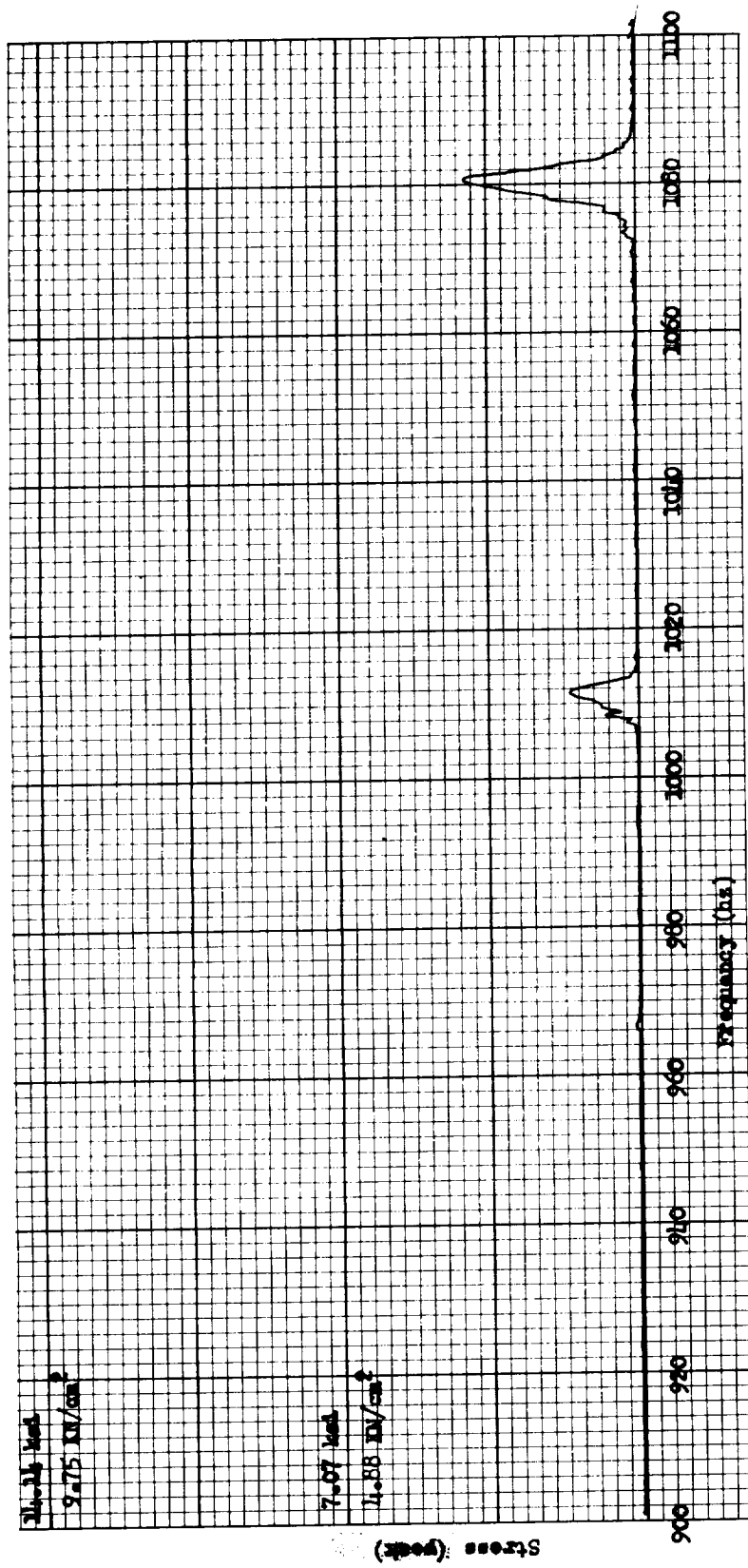
(k) Strain gage 103, TIP; flutter; analog reading 54.

Figure 11. - Continued.
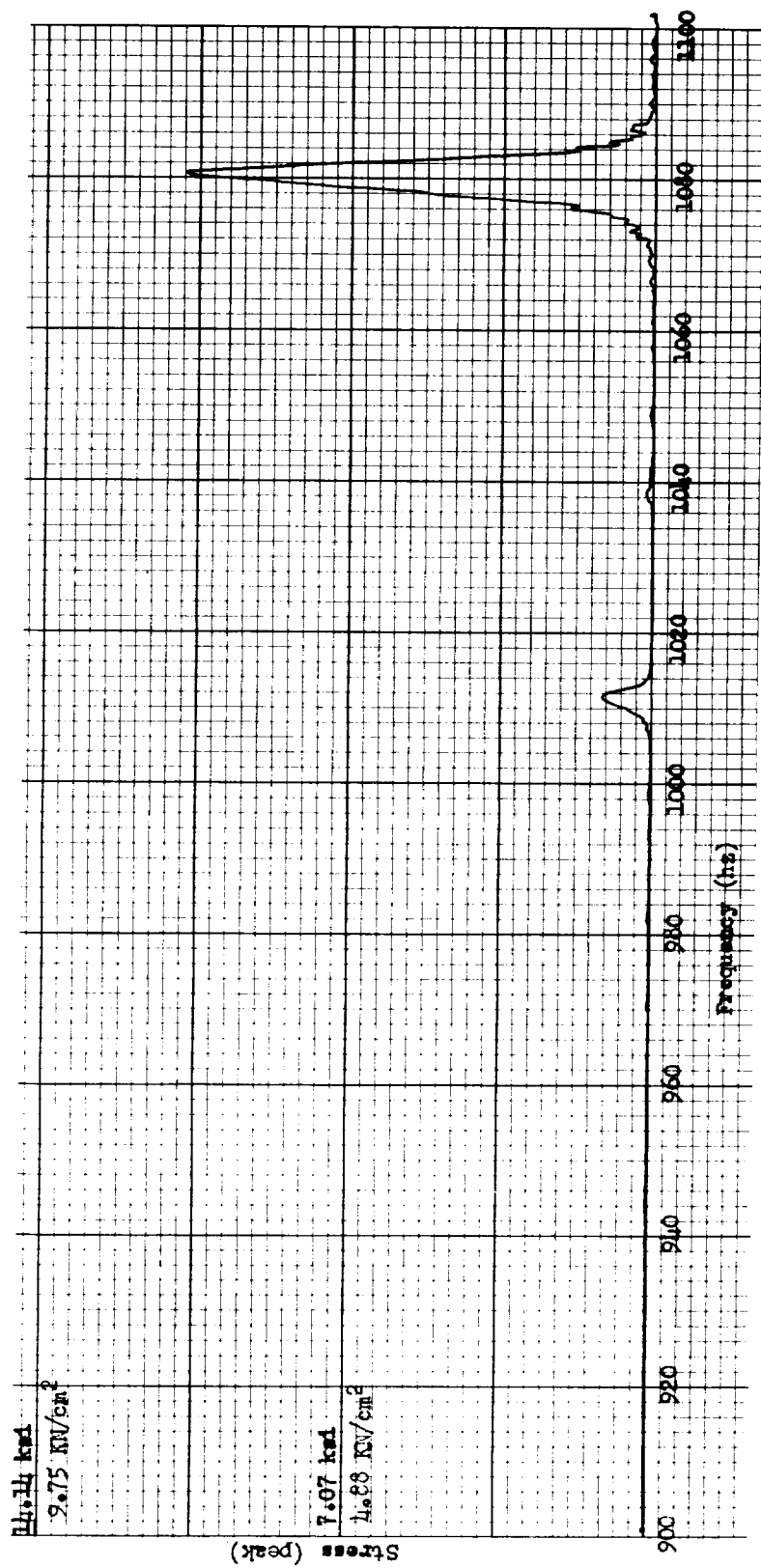
(ℓ) Strain gage 104, TIP; flutter; analog reading 54.

Figure 11. – Continued.
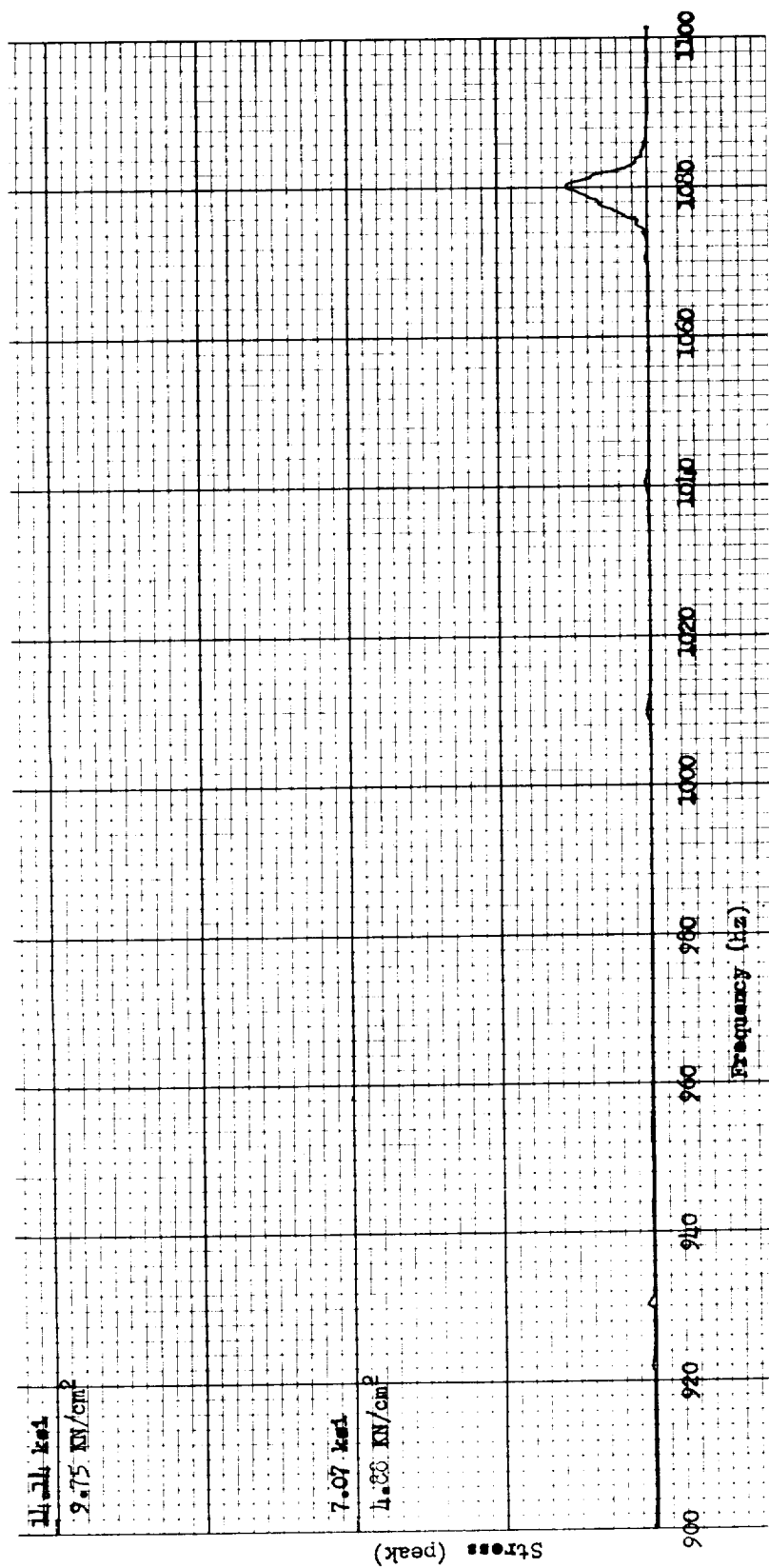
(m) Strain gage 109, ASMT; flutter; analog reading 54.

Figure 11. – Continued.

91
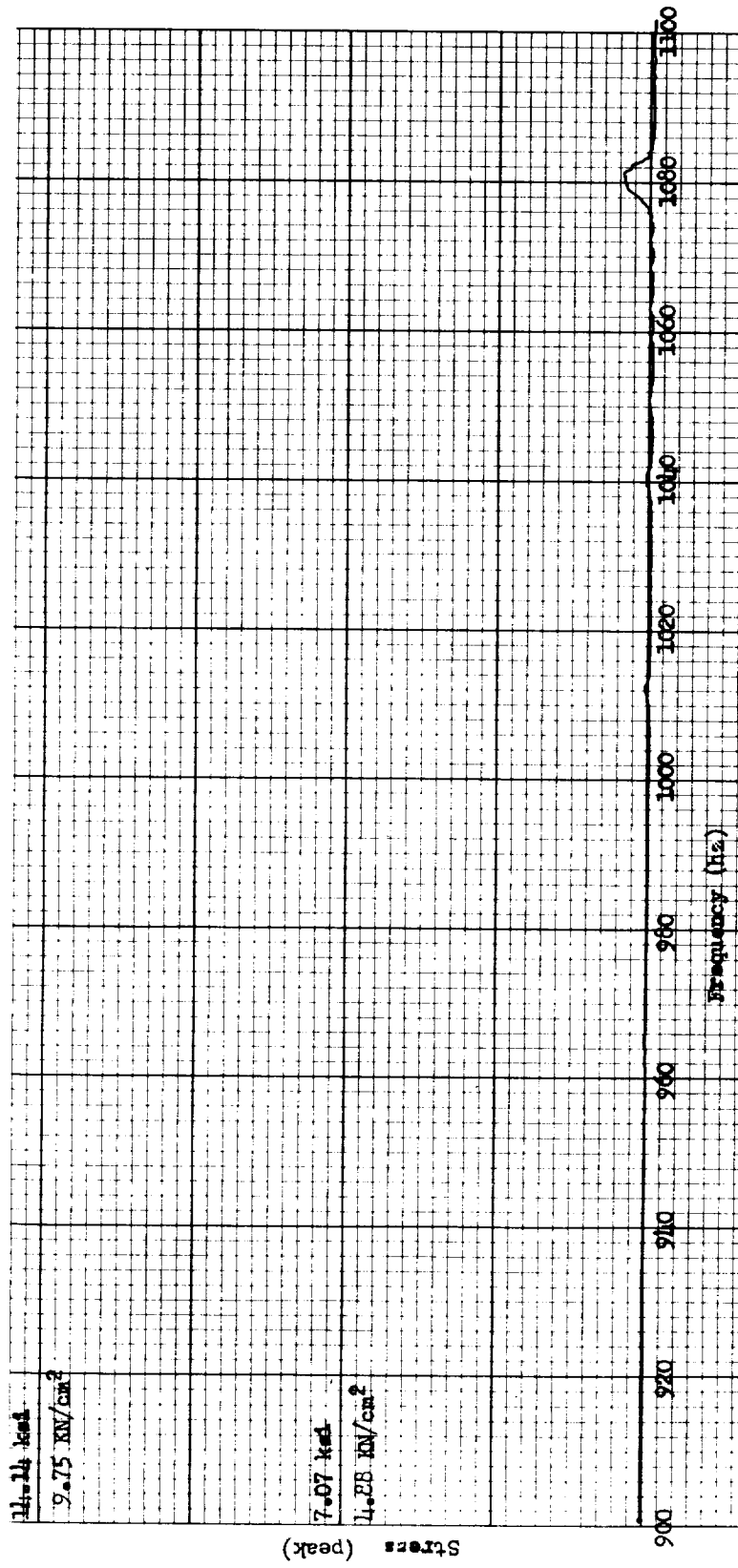
(n) Strain gage 113, ASMT; flutter; analog reading 54.

Figure 11. – Continued.

92

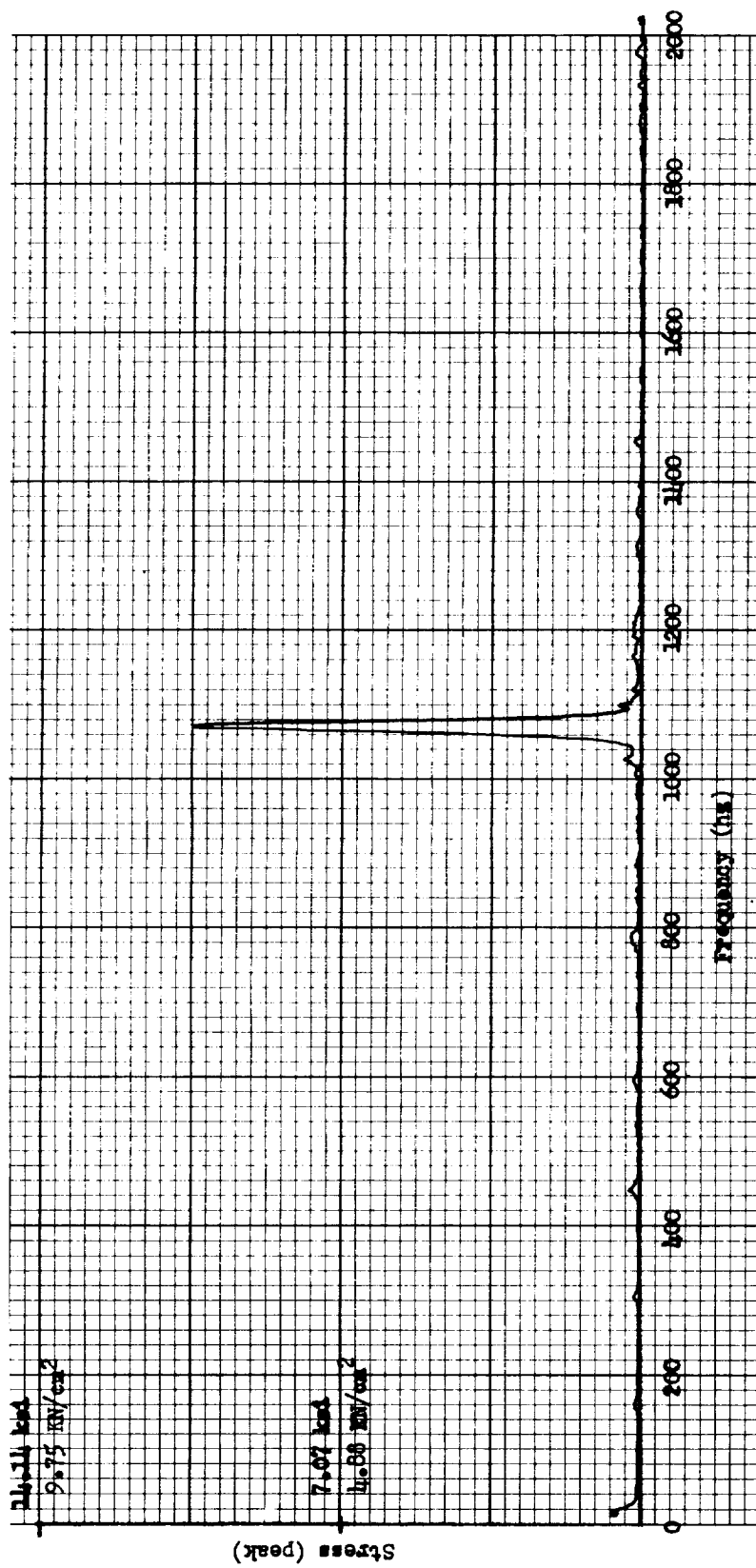(o) Strain gage 116, ASTE; flutter; analog reading 54.

Figure 11. – Continued.

93

(p) Strain gage 117, ASTE; flutter; analog reading 54.
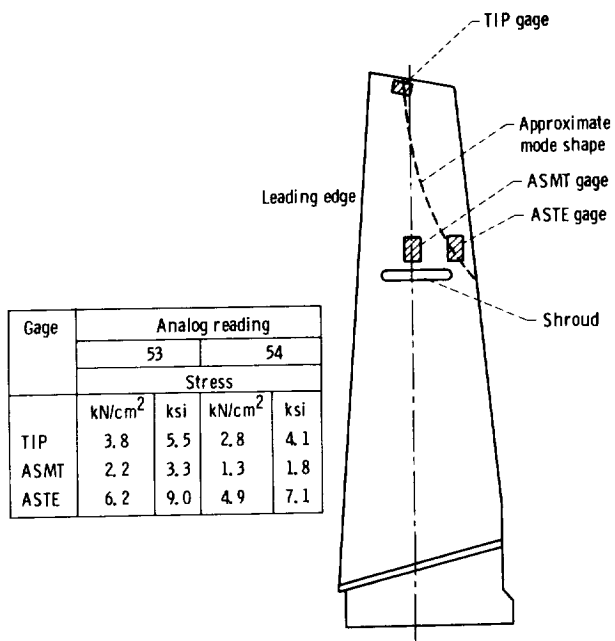
Figure 11. - Continued.

94

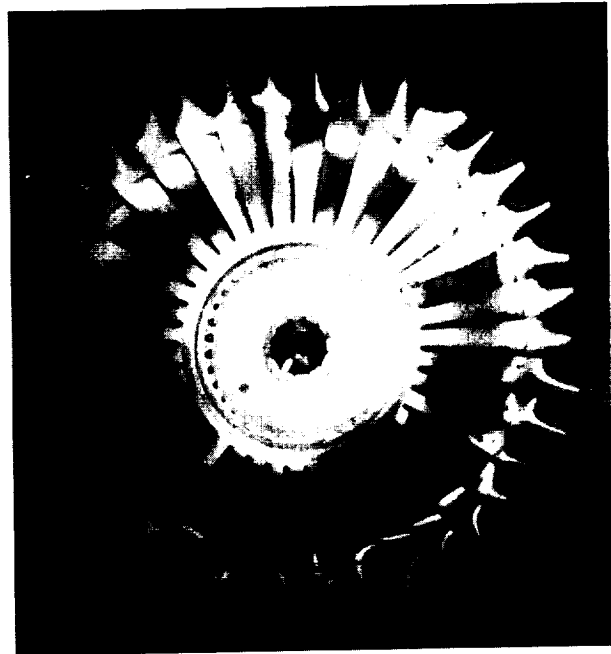(q) Strain gage 122, SHRD-CX; flutter; analog reading 54.

Figure 11. – Continued.

95

(r) Strain gage 117, ASTE; flutter; analog reading 53.

Figure 11. – Concluded.

96

Gage	Analog reading			
	53		54	
	Stress			
	kN/cm^2	ksi	kN/cm^2	ksi
TIP	3.8	5.5	2.8	4.1
ASMT	2.2	3.3	1.3	1.8
ASTE	6.2	9.0	4.9	7.1

(a) Flutter vibratory stress amplitude and distribution.

(b) Holograph of rotor assembly in forced flutter excitation.

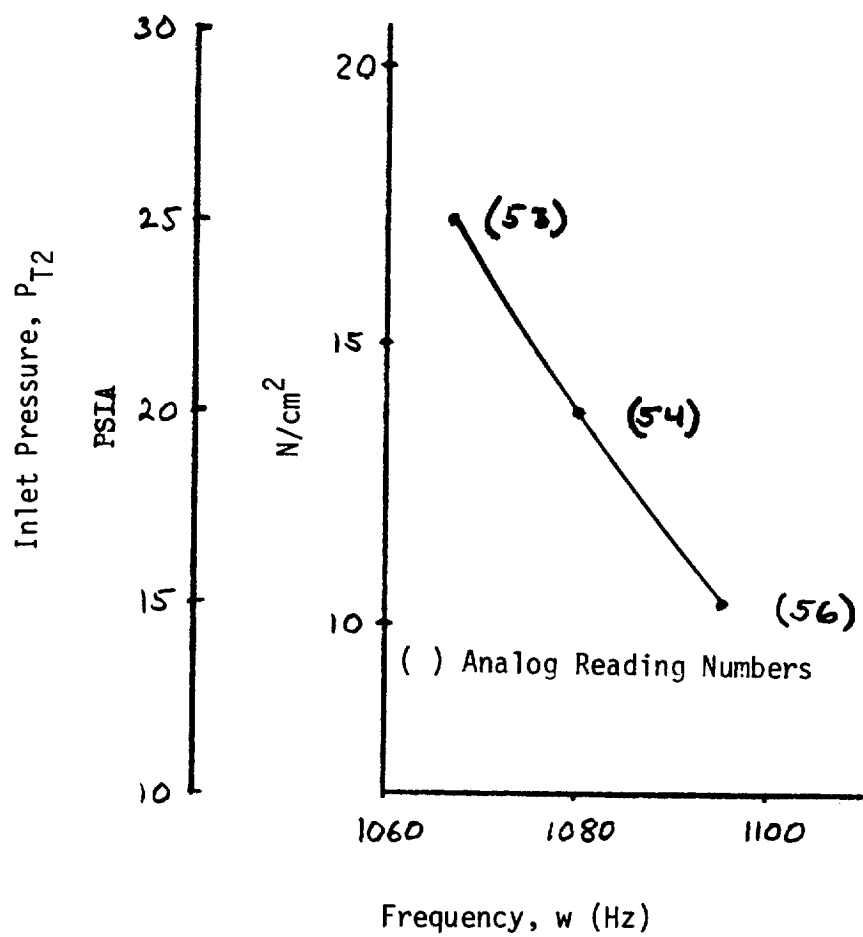Figure 12. - Flutter mode characteristics for fan first-stage rotor.

Figure 13. - Effect of inlet pressure on blade flutter frequency of fan first-stage rotor. Strain gage 117, ASTE.